

A Longitudinal Aerodynamic Data Repeatability Study for a Commercial Transport Model Test in the National Transonic Facility

R. A. Wahls and J. B. Adcock
Langley Research Center • Hampton, Virginia

D. P. Witkowski and F. L. Wright
Boeing Commercial Airplane Company • Seattle, Washington

The use of trademarks or names of manufacturers in this report is for accurate reporting and does not constitute an official endorsement, either expressed or implied, of such products or manufacturers by the National Aeronautics and Space Administration.

Available electronically at the following URL address: <http://techreports.larc.nasa.gov/ltrs/ltrs.html>

Printed copies available from the following:

NASA Center for AeroSpace Information
800 Elkridge Landing Road
Linthicum Heights, MD 21090-2934
(301) 621-0390

National Technical Information Service (NTIS)
5285 Port Royal Road
Springfield, VA 22161-2171
(703) 487-4650

Abstract

A high Reynolds number investigation of a commercial transport model was conducted in the National Transonic Facility (NTF) at Langley Research Center. This investigation was part of a cooperative effort to test a 0.03-scale model of a Boeing 767 airplane in the NTF over a Mach number range of 0.70 to 0.86 and a Reynolds number range of 2.38 to 40.0×10^6 based on the mean aerodynamic chord. One of several specific objectives of the current investigation was to evaluate the level of data repeatability attainable in the NTF. Data repeatability studies were performed at a Mach number of 0.80 with Reynolds numbers of 2.38, 4.45, and 40.0×10^6 and also at a Mach number of 0.70 with a Reynolds number of 40.0×10^6 . Many test procedures and data corrections are addressed in this report, but the data presented do not include corrections for wall interference, model support interference, or model aeroelastic effects. Application of corrections for these three effects would not affect the results of this study because the corrections are systematic in nature and are more appropriately classified as sources of bias error. The repeatability of the longitudinal stability-axis force and moment data has been assessed. Coefficients of lift, drag, and pitching moment are shown to repeat well within the pretest goals of ± 0.005 , ± 0.0001 , and ± 0.001 , respectively, at a 95-percent confidence level over both short- and near-term periods.

Introduction

Every field of study must contend with the issue of error or uncertainty analysis to some degree. Accordingly, the data obtained and used in a given analysis must be evaluated and the quality documented. Data evaluation includes the broad category of uncertainty analysis and can extend from simple observations to complex theoretical analysis of errors and comparisons with fundamental principles. Documentation of the evaluation, whether simple or complex, is no less important than the evaluation itself because potential users of the results of a particular analysis must have a basis with which to judge usefulness to their situations. The need for such analysis and documentation practices in aerodynamic research and development, whether experimental or computational, is well documented. (See refs. 1–6 for examples.) This report is presented in the spirit of that general philosophy.

This report documents a study of data repeatability in the National Transonic Facility (NTF) at Langley Research Center performed during a recent high Reynolds number test of a commercial transport model. The investigation is part of a cooperative effort between Langley, Ames Research Center, and the Boeing Commercial Airplane Company. The program involves tests on a 0.03-scale model of a Boeing 767 airplane at three facilities: the NTF, the 11- by 11-foot transonic leg of the Ames Unitary Plan Wind Tunnel, and the Boeing Transonic Wind Tunnel. The primary purposes of the overall program are the comparison of data and data reduction processes from each facility, the acquisition of full-scale Reynolds number data in the NTF to study

Reynolds number effects and scaling, and the comparison of wind tunnel data with available flight data.

Data repeatability during prior tests of this and other models in the NTF has typically been described in some form relative to the observed data scatter, but those descriptions have not included a consistent mathematical measure of the scatter or an indication of how much confidence may be placed in the data based on the observed scatter. Statistical analysis provides an approach to address these issues. Statistically meaningful data sample sizes have been lacking during past tests in the NTF because each cryogenic test condition requires the use of gaseous nitrogen as the test medium and subsequent repeat tests of that condition are considerably more expensive than typical conditions in other facilities. In addition, the number of polars per test at the NTF is less than typical compared with other facilities because of liquid nitrogen production and storage limitations. As such, each repeat test condition at the NTF represents a larger percentage of an overall test plan. Researchers must choose whether to investigate a wider range of test conditions and configurations or to investigate repeatability more fully. The usual choice is the former. The test of the 767 airplane model on which this report is based placed more than the usual emphasis on the investigation of repeatability. The priority to assess data repeatability during this investigation was due to mixed results from previous tests of this model in the NTF. (See ref. 7.) Particular attention was directed toward drag repeatability.

In addition to better establishment of the repeatability level, the other primary objectives of this investigation were to obtain data for tunnel-to-tunnel

correlation at low Reynolds numbers; to decouple Reynolds number and static aeroelastic effects; and to obtain refined, high Reynolds number drag measurements for eventual comparison with flight data. Only the analysis pertaining to the repeatability assessment is presented in this report. Repeat test conditions were chosen such that the remainder of the test objectives would be met. The focus of the investigation was on the longitudinal aerodynamic characteristics of the model. The repeatability analysis herein emphasizes stability-axis longitudinal force and moment characteristics, but it also addresses body-axis longitudinal force and moment characteristics, the angle of attack, and the flow conditions. The repeat conditions were at the cruise Mach number of 0.80 with Reynolds numbers of 2.38, 4.45, and 40.0×10^6 based on the mean aerodynamic chord and also at a Mach number of 0.70 with a Reynolds number of 40.0×10^6 . The Reynolds number range includes those obtained in the atmospheric conditions of the Boeing facility (2.38×10^6), in the Ames facility pressurized to 2 atm in air (4.45×10^6), and at the cruise flight condition (40.0×10^6). The maximum angle of attack was limited to 3.5° for high Reynolds number conditions that can only be obtained in the cryogenic mode of operation. This limitation was imposed because of adverse model and support system dynamics encountered during previous investigations (refs. 7 and 8) near initial buffet at the full-scale Reynolds number in the Mach number range of interest herein. Full-scale cruise conditions were obtained with tunnel conditions of 63.1 psia total pressure and -250°F total temperature.

Symbols

All dimensional values are given in U.S. Customary Units.

AR	aspect ratio
B_X	bias estimate for parameter X
b	wing span, in.
CI	confidence interval
C_A	axial-force coefficient, $\frac{\text{Axial force}}{qS}$
C_D	drag coefficient, $\frac{\text{Drag}}{qS}$
$C_{D,sf}$	drag coefficient due to skin friction plus overspeed
C_i	least squares coefficients, $i = 0, 1, 2, \dots, K$
C_L	lift coefficient, $\frac{\text{Lift}}{qS}$
C_m	pitching-moment coefficient, referenced to $0.25\bar{c}$, $\frac{\text{Pitching moment}}{qS\bar{c}}$

C_N	normal-force coefficient, $\frac{\text{Normal force}}{qS}$
\bar{c}	wing mean aerodynamic chord, in.
K	order of least squares polynomial regression equation
M	free-stream Mach number
M_{ref}	reference Mach number based on static pressure measured in plenum
N	number of data points in sample
P_X	precision estimate for parameter X
PI	prediction interval
p_t	total pressure, psia
p_s	static pressure, psia
Q	data density term
q	free-stream dynamic pressure, psf
$R_{\bar{c}}$	Reynolds number based on \bar{c}
S	wing reference area, ft^2
SE	standard error
s	sample standard deviation
T_{bal}	balance temperature, $^\circ\text{F}$
T_{grad}	temperature gradient across balance from front to rear, $^\circ\text{F}$
T_t	total temperature, $^\circ\text{F}$
t	value of t distribution dependent upon $\tilde{\alpha}$ and ν
U_X	uncertainty estimate for parameter X
X	generic parameter
X_{best}	best estimate for parameter X
X_i	value of parameter X for i th data point
X_{true}	true value for parameter X
Y	generic parameter
Y_i	value of parameter Y for i th data point
\bar{Y}	arithmetic mean for N values of parameter Y
\hat{Y}	curve-fit-based best estimate of parameter Y
α	onboard body angle of attack, deg
$\tilde{\alpha}$	term representative of confidence level, used to determine t value
β	true bias error
ϵ_i	true precision error for i th data point
ν	degrees of freedom
δ_i	true error for i th data point

δ_T horizontal-tail angle, positive trailing edge down, deg

Abbreviations:

NTF National Transonic Facility

rpm revolutions per minute

RSA regression statistical analysis

SVSA single-variable statistical analysis

Model configuration notation:

W wing, one piece

B body (fuselage)

M nacelle struts, one per side

N nacelles, one per side

T wing flap track fairings, three per side

H = δ_T horizontal tail at angle δ_T (positive trailing edge down), deg

Background Statistical Information

Because measurements of any property contain some degree of uncertainty, any parameter derived from a measurement also must contain some degree of uncertainty. Therefore, the question is how closely does the measured or subsequently derived parameter agree with its true value? The difference is the true error

$$X_{\text{true}} = X_i + \delta_i \quad (1)$$

where X_i is the measured value, δ_i is the true error for measurement i , and X_{true} is the true value for the parameter of interest. The true values X_{true} and δ_i are never known; the task of an uncertainty analysis is to quantify these values by estimation.

The true error of a measurement has two components as follows:

$$\delta_i = \beta + \varepsilon_i \quad (2)$$

where the true error δ_i for measurement i comprises the true bias error β and a true precision error ε_i for measurement i . The true bias error is considered systematic or fixed. The determination of the true bias error can be made only if the true value of the measured property is known. Reference 5 provides a good discussion of the classification of various types of bias errors. Briefly, biases can be large or small, each with some combination of known and unknown sign and magnitude. In general, large biases are assumed to be eliminated in a well-controlled experiment by some means, such as by the calibration of an instrument. Small biases, however, typically remain and form the bias error. The primary difficulty in determining the bias error arises from the fact that both the sign and magnitude are difficult to define

without a known true value with which to compare. If the true value were known, the true bias error would be determined as the difference between the mean of the population of measured values and the true value. Because the population is typically infinite in size, reality dictates that experimenters work with a finite sample of the population.

Unlike the true bias error, the true precision error does not rely on a knowledge of the true value; it does, however, depend on the true mean value of the population. The true precision error is the random component of the true error and is often referred to as the repeatability error (as is the case throughout this report). The true precision error represents the difference between a measured value and the mean of the population of measured values. The random nature of the precision error lends itself to estimation by statistical analysis and is easier to quantify mathematically than the bias error. Such quantification of a precision error estimate is discussed in the section, "Method of Repeatability Analysis."

Uncertainty Analysis

The result of the uncertainty analysis is the determination of an interval within which the experimenter can state with a specified level of confidence that the true value lies. That is,

$$X_{\text{best}} \pm U_X \quad (3)$$

where X_{best} is usually the mean value of the sample measurements and U_X is the uncertainty in the measurements of parameter X stated with a specified level of confidence. The uncertainty U_X is a combination of both bias and precision error estimates (B_X and P_X , respectively) as shown below in its sum-of-squares form:

$$U_X^2 = B_X^2 + P_X^2 \quad (4)$$

As described above, estimation of the absolute uncertainty including biases is difficult and is outside the scope of this report. As such, in the remainder of this report the authors concentrate on the estimation of the precision (repeatability) error only.

Method of Repeatability Analysis

This section describes the approach taken to quantify data repeatability in this investigation. The quantification takes the form of an estimate of the precision error and is stated with a specified level of confidence. The approach builds on the use of simple statistics as used for analysis of a single variable and extends such statistical concepts to the multiple linear regression problem. As described next, the approach is based on estimating the data mean and representing the data scatter about the estimated mean. The combination of probability and statistical

concepts provides an approach to establish a level of confidence. The primary underlying assumptions for all statistical analyses to follow are that the data scatter is random and that the random scatter can be represented by a normal (Gaussian) distribution. Background and further details on much of the following discussion can be found in many statistics textbooks. Several such texts are references 9–11.

Single-Variable Statistical Analysis

The most common situation applicable for statistical analysis involves the quantification of the random scatter of a single parameter. The method used to analyze such a problem is referred to herein as single-variable statistical analysis (SVSA). This method uses well-defined, relatively simple statistical parameters to quantify random scatter. The quantification of total pressure repeatability during a test run is an example of a problem appropriate for the use of the SVSA approach.

Estimation of the data mean. The most fundamental statistic for the SVSA approach, or any other statistical approach for that matter, is a best estimate of the data mean. This statistic is simply the arithmetic mean defined in its usual form for a parameter Y as

$$\bar{Y} = \frac{\sum_{i=1}^N Y_i}{N} \quad (5)$$

where Y_i is the i th data point and N is the data sample size. Once determined, the data scatter about the best estimate of the data mean can be assessed.

Measures of repeatability. The most fundamental statistic to describe data scatter is the standard deviation. Because an experimenter typically deals with only a finite data sample rather than an entire population, the true mean is not known and the true standard deviation can only be estimated. The sample standard deviation s , which is used as an estimate of the true standard deviation, is defined as

$$s = \left[\frac{\sum_{i=1}^N (Y_i - \bar{Y})^2}{N - 1} \right]^{1/2} \quad (6)$$

The confidence and prediction intervals, both of which depend on the sample standard deviation, are two additional measures of repeatability. The confidence interval is related to the location of the true mean, whereas the prediction interval is related to the probability that a single future observation will fall within a cer-

tain interval about the estimated mean. The confidence interval is defined as

$$CI = \pm t_{\tilde{\alpha}/2, v} \times s \times \frac{1}{\sqrt{N}} \quad (7)$$

where $t_{\tilde{\alpha}/2, v}$ is the value of the t distribution for a specified level of confidence and number of degrees of freedom and N is the data sample size. The t distribution is a modified normal distribution in which the size of the data sample, represented by $v = N - 1$ degrees of freedom, is taken into account. The t value is also related to the specified level of confidence as defined through $\tilde{\alpha}$ by the relationship

$$\text{Percent confidence} = (1 - \tilde{\alpha}) \times 100 \quad (8)$$

The t value is tabulated (ref. 9) as a function of $\tilde{\alpha}$ and v . In a similar manner, the prediction interval is defined as

$$PI = \pm t_{\tilde{\alpha}/2, v} \times s \quad (9)$$

The confidence interval, as defined, can be interpreted as the bounds about the estimated mean that encompass the true mean value, with a chance of $100(1 - \tilde{\alpha})$ percent. The prediction interval, as defined, can be interpreted as the bounds about the estimated mean that will contain any single future observation with a probability of $100(1 - \tilde{\alpha})$ percent. Thus, the prediction interval characterizes the data scatter.

Multivariable Statistical Analysis

Normal data analysis procedures in which only two variables are involved usually begin with a curve fit to the data. Curve fitting can be done by eye and provides a rough idea as to the relationship between the variables. Unfortunately, because the fit is subjective, the selected relationship may not be the one chosen by the original analyst or by some other analyst in the future. In addition, some measure is needed of how well the curve represents the data. The method of least squares (refs. 9–11) provides a consistent method to obtain a mathematical curve fit to a set of data and, in combination with probability and statistical concepts, allows researchers to quantify how well the resulting estimate represents the data with a specified level of confidence.

In terms of wind tunnel data, least squares curves are determined by relating two variables obtained during a test run. If two or more runs are obtained that in theory are identical (same model configuration and flow conditions), the repeatability of the dependent variable can be assessed as a function of the independent variable. A common approach is to represent each individual run analytically and assess repeatability by interrogating each resulting analytic model at a constant value

of the independent variable and comparing the corresponding estimates of the dependent variable. This approach is in effect the SVSA method described earlier after the analytic representations of each run are evaluated at a chosen value of the independent variable. In this approach, the repeatability assessment is directly related to the set of analytic representations but only indirectly to the actual data points.

An alternate approach is applied here where a single best estimate curve fit is determined based on all data from a set of identical test runs. This approach is referred to herein as regression statistical analysis (RSA) as it relies on the extension of simple statistics to the multiple linear regression problem. Repeatability is assessed by the amount of scatter about the single best estimate least squares curve fit (best estimate of the data sample mean) and remains directly related to the actual data points. The extensions to the statistical parameters described above for the SVSA approach are described below for the RSA approach. This approach requires the additional assumption that random variance of the dependent variable is constant over the range of the independent variable.

Estimation of the data mean. For the RSA approach, the estimate of the mean is represented by an analytic equation that is determined to be the best model for the relationships observed in the data. The true functional relationship may include dependence on more than one independent variable or on powers thereof. The estimated mean is dependent on the functional relationship specified and is a best estimate for the specified functional relationship in the context of the method of least squares. Application of the RSA approach in this report is based on the assumption that the functional relationship between any two variables can be adequately represented by a polynomial regression equation of order K ; the chosen value of K is dependent on the relationship between the variables of interest and its selection is described further herein. The polynomial regression equation of order K has a general form as follows:

$$\hat{Y}(X) = C_0 + C_1X + C_2X^2 + C_3X^3 + \dots + C_KX^K \quad (10)$$

where X is the independent variable; \hat{Y} is the resulting best estimate of the dependent variable; and the least squares constant coefficients are C_0, C_1, \dots, C_K . The over-specified system of N equations can be written in condensed matrix notation as

$$\mathbf{X}_{N \times (K+1)} \mathbf{C}_{(K+1) \times 1} = \mathbf{Y}_{N \times 1} \quad (11)$$

where each equation is of the form

$$Y_i = C_0 + C_1X_i + C_2X_i^2 + C_3X_i^3 + \dots + C_KX_i^K \quad (12)$$

The parameters X_i and Y_i are the measured values of the independent and dependent variables, respectively, for the i th data point. Equation (11) is solved for the $K+1$ constant coefficients by the method of least squares; the result is a mathematical model in the form of equation (10) that is used as an estimate of the mean.

The selection of the order of the polynomial regression model K has a direct effect on the quality of the estimate of the mean. That selection, however, can be somewhat subjective. The approach used for the selection of K in the present investigation was twofold as follows. For each estimate of mean required, several values of K were evaluated by inspection of the data scatter about the resulting estimate; the standard error, which is defined in equation (14), is the statistical parameter used in the evaluation. In addition, selection of the order of the polynomial regression model is subject to the following guideline:

$$K \leq \sqrt{N} - 1 \quad (13)$$

This guideline is described as a useful rule of thumb (ref. 12) and provides a criterion to limit the maximum order of the polynomial model.

Measures of repeatability. When an estimate of the data mean $\hat{Y}(X)$ has been determined, a measure of the data scatter about the mean can be applied. The fundamental measure of the scatter about an estimated mean in the RSA approach is the standard error SE , which is defined as

$$SE = \left[\frac{\sum_{i=1}^N (Y_i - \hat{Y}_i)^2}{N - K - 1} \right]^{1/2} \quad (14)$$

where \hat{Y}_i is the estimated value of Y that corresponds to the dependent variable X_i of the i th data point. In effect, the standard error is an extension of the sample standard deviation defined in equation (6) to the multiple linear regression problem.

The concepts of the confidence and prediction intervals described in the SVSA approach can be extended as well. In the RSA approach, the confidence interval CI is defined as

$$CI(X_0) = \pm t_{\tilde{\alpha}/2, v} \times SE \times Q(X_0) \quad (15)$$

and the prediction interval PI is defined as

$$PI(X_0) = \pm t_{\tilde{\alpha}/2, v} \times SE \times \sqrt{1 + Q(X_0)^2} \quad (16)$$

As in the SVSA approach, $t_{\alpha/2, \nu}$ is the value of the t distribution for a specified level of confidence and the number of degrees of freedom; the difference in the RSA approach is the definition of the degrees of freedom ($\nu = N - K - 1$) where the order of the polynomial regression equation K is taken into account. The term $Q(X_0)$ is defined as

$$Q(X_0) = \sqrt{\mathbf{X}_0^T (\mathbf{X}^T \mathbf{X})^{-1} \mathbf{X}_0} \quad (17)$$

where the independent variable of interest is represented in vector form as

$$\mathbf{X}_0^T = \begin{bmatrix} 1 & X_0 & X_0^2 & \dots & X_0^K \end{bmatrix}_{1 \times (K+1)} \quad (18)$$

and the matrix \mathbf{X} is that used in equation (11). The term $Q(X_0)$ is a measure of data density in the neighborhood of the independent variable of interest X_0 and accounts for data density such that highly populated regions of the data sample may have narrower confidence and prediction intervals than sparsely populated regions. The effect of this term is observed in the data that follow.

Interpretation of the confidence and prediction intervals is the same as that described for the SVSA approach. The primary difference in application with the RSA approach is that the intervals define bounds about a least squares-based estimate of the mean, rather than about a simple arithmetic mean. In addition, the defined bounds of the RSA approach are functions of the independent variable rather than a constant interval that is valid over the range of the independent variable.

Interpretation of Confidence Level

Both the confidence and prediction intervals are associated with a user-specified level of confidence, which is stated as a percentage and is based on the numerical probability that an event will occur. In the present context, the events of interest are that the true mean value falls within the confidence interval and that a single future observation falls within the prediction interval. An understanding of what a given confidence level implies is useful. One useful tool is the relationship between odds and the confidence level where, for example, 9-to-1 odds are equivalent to a 90-percent confidence level. A subjective relationship between the confidence level and an appropriate adjective that describes the probability of an event is given in reference 13 as

75% to 90% confidence levelFairly probable
 90% to 95% confidence levelHighly probable
 95% to 100% confidence level Extremely probable

Researchers can define their own hierarchies of confidence level descriptors; the one presented here is simply an example.

Timescales for Repeatability Analysis

Three timescales are defined in this paper to classify a given repeatability sample—short, near, and long term. The timescales relate to both the period and circumstances in which data are collected. A short-term repeatability sample describes data variability over a relatively short period with minimal change in circumstance. Examples of the short-term time frame with respect to wind tunnel tests are within a single polar and repeat Mach number polars within a Mach number series. A near-term repeatability sample describes data variability when a given configuration is retested during a single tunnel entry and at least one other configuration is tested in between. A long-term repeatability sample describes the data variability from entry to entry for a given model. Obviously, the potential for the introduction of biases, particularly model-related biases, increases when going from short- to long-term comparisons. The present investigation includes many examples of short-term repeatability and presents a near-term sample. The near-term sample was acquired across a significant break in the cryogenic tests and, in some respects, warrants classification of the sample as long term.

Experimental Apparatus and Procedures

Facility Description

The NTF (ref. 14) is a unique national facility that provides full-scale (high) Reynolds number tests of vehicles (such as commercial transport airplanes) designed to fly in and through the transonic speed regime. The facility provides a test environment for a scale model that is similar to that of the full-scale airplane in flight; that is, the Mach and chord Reynolds numbers are identical in the tunnel and full-scale flight environments. The NTF is a conventional closed-circuit fan-driven wind tunnel that is capable of operating at elevated pressures and cryogenic temperatures to obtain high Reynolds numbers. The test section is 8.2 by 8.2 by 25 ft and has a slotted floor and ceiling. The test-section floor and ceiling divergence angles, the reentry flap angles, and the step height for slot flow reentry are adjustable by remote control. In addition, turbulence is reduced by four damping screens in the settling chamber and a contraction ratio of 15:1 from the settling chamber to the nozzle throat. Fan-noise effects are minimized by an acoustic treatment both upstream and downstream of the fan.

The NTF has an operating pressure range of approximately 15 to 125 psia, a temperature range of -320°

to 150°F, and a Mach number range of 0.2 to 1.2. The maximum Reynolds number per foot is 146×10^6 at Mach 1. The test gas may be either dry air or nitrogen. When the tunnel is operated cryogenically, heat is removed by the evaporation of liquid nitrogen, which is sprayed into the tunnel circuit upstream of the fan. During this operational mode, venting is necessary to maintain a constant total pressure. When air is the test gas, heat is removed from the system by a water-cooled heat exchanger at the upstream end of the settling chamber. (See ref. 15 for further tunnel details.)

A detailed assessment of the dynamic flow quality in the NTF is reported in reference 16. Fluctuating static pressures were measured on the test-section sidewall opposite a 10° cone fairing over the end of a standard model support system. The root mean square of the fluctuating component of static pressure nondimensionalized by the free-stream dynamic pressure is approximately 0.0084 at low Reynolds numbers in the ambient air environment and approximately 0.0095 at high Reynolds numbers in the cryogenic nitrogen environment; each of these results is for a Mach number of approximately 0.80.

Model Description

The model is a 0.03-scale representation of the Boeing 767 production airplane. The model is shown in figure 1 mounted in the NTF test section; the pertinent model geometry is given in figure 2. The model was designed and constructed specifically for tests in the cryogenic, pressurized conditions of the NTF, where dynamic pressures reached approximately 2700 psf during this investigation. The model was built of maraging steel with a surface finish of 10μ in. (root mean square). The general wing contour tolerance was ± 0.003 in.; the wing leading-edge tolerance was ± 0.0015 in.

The model, which contains separable components, allows tests of multiple configurations. The wing component, which includes the wing-body fairing, does not include the wing vortex generators that are found on full-scale production airplanes. (See ref. 7.) The body (fuselage) design incorporated a nonmetric upper swept strut support system. (See fig. 1.) The upper swept strut support is intended to minimize support interference in the horizontal-tail region and is integrated into the body with a shape that approximates the airplane vertical tail. However, because greater structural strength was required, the strut integration was thicker than the true vertical tail loft.

Other model components include flow-through nacelles, which simulate a JT9D-7R4 engine installation, nacelle struts, wing flap track fairings, and a horizontal tail. The horizontal-tail incidence can be set at nominal

angles of -3° , -1° , 0° , and 1° . Configurations are defined herein with the component notation described in the symbols list. For example, WB indicates a wing-body configuration.

Instrumentation

Aerodynamic force and moment data were obtained with an internal, six-component, strain gauge balance. The quoted accuracy of the balance (stated in terms of the worst outlying point during the calibration) is ± 0.5 percent of the maximum design loads; design loads for the balance and the data acquisition system resolution of the channels used to read the balance output are given in table 1. An internal, heated accelerometer package was used to measure the onboard angle of attack; quoted accuracy of the package under smooth wind tunnel operating conditions is $\pm 0.01^\circ$ (ref. 17), and the data acquisition system resolution of the package output is 0.0021° . Model pressure measurements were obtained using 5-psid barocells, each with a quoted accuracy of ± 0.01 psi (worst case). Model pressure measurements were limited to three internal body locations chosen to assess flow into and out of the aft-body cavity. The three pressure measurements near the upper swept strut seal were made without tubes bridging the balance.

The primary measured flow variables of interest include both the total and static pressures and the total temperature. Mach number, Reynolds number, and dynamic pressure are calculated from these measured quantities. Briefly, static pressure is measured by a set of gauges with full-scale ranges of 150, 100, 50, 30, and 15 psia. Each gauge has a quoted accuracy of ± 0.01 percent of full scale (worst case). An autorange system allows the most sensitive gauge to be used. An identical system is used to measure the total pressure, except that a 15-psia gauge is omitted. Total temperature is measured by a platinum-resistance temperature probe mounted in the reservoir section of the tunnel near the screens. This measurement has an accuracy of approximately $\pm 0.1^\circ\text{F}$ (worst case). A complete description of these measurements and subsequent calculations is given in reference 18.

Data Corrections

Information on the various instrumentation devices, the data acquisition and control computers, and the data reduction algorithms for the different measurement systems is provided in reference 18. Standard balance, angle-of-attack, and tunnel parameter corrections have been applied. An additional part of data reduction at the NTF is balance temperature compensation. The temperature compensation methods are designed to correct balance output due to thermal loads and are discussed in

references 18 and 19. A model-specific correction has been applied to the drag data to account for the internal drag of the flow-through nacelles and is based on unpublished nacelle calibration data obtained by Boeing. The data herein have not been corrected for model aeroelastics, wall interference, or model support interference. Application of corrections for these three effects would not affect the results of this study as the corrections are systematic in nature and are more appropriately classified as sources of bias error.

The free-stream Mach number is corrected based on clear-tunnel calibrations that correlate tunnel centerline static pressure measurements with the reference static pressures measured in the plenum. Table 2 contains the free-stream Mach number corrections applied for the repeat conditions studied herein. As indicated in table 2, the corrections are functions of both Mach and Reynolds numbers.

The angle of attack was corrected for flow angularity (upflow) by measurement of both upright and inverted model force data for a given configuration; in particular, the C_N - α offset method was used. The flow angularity was evaluated at the beginning of each polar series and when the flow-field total temperature was changed. This approach was taken based on the assumption that flow angularity is primarily a function of cold soaking (time) and total temperature. Flow angularity was assessed 20 times during this investigation, all at $M = 0.80$; the observed variation of flow angularity is discussed later.

Empty-tunnel calibrations allow tunnel wall angles to be set so as to reduce pressure gradients and buoyancy effects in the test section. However, tunnel wall angles were set at a nominal angle (0°) before the investigation and remained fixed throughout the test because wall actuation is currently problematical at cryogenic conditions. Buoyancy drag corrections based on the empty-tunnel calibrations were about 0.0001 (in coefficient form) or less throughout the investigation. The model and the support system introduce pressure gradients and buoyancy effects that could not be accounted for during the empty-tunnel calibration of the wall angles. Corrections to the data for such effects have not as yet been determined. The solid blockage ratio for the WB configuration at an angle of attack of 0° is 0.55 percent; this value is sufficiently low to minimize blockage effects, based on conventional criteria. Buoyancy corrections, based on the empty-tunnel calibrations, have been applied to the data.

Strut Seal

The upper swept strut support requires a seal at the junction of the strut and the upper aft body of the model. The seal, which prevents airflow into and out of the aft-

body cavity, was designed specifically for use in the NTF environment. This seal is made of polyester fiber filler material in an elastic nylon wrap that was stiffened with thin pieces of DuPont Mylar¹. Tests without the seal have shown drag and pitching-moment shifts relative to tests with a seal in place.

Previous experience (ref. 7) indicates that force and moment data repeatability can be adversely affected by deterioration of the upper swept strut seal. Modifications to the seal during the investigation described in reference 7 improved data repeatability to an acceptable level ($\Delta C_L = \pm 0.0015$, $\Delta C_D = \pm 0.0002$, and $\Delta C_m = \pm 0.001$). In reference 7, repeatability was not quantified because a meaningful data sample size was lacking; instead, the repeatability quote is a more subjective representation of the observed range of a given parameter at constant conditions. Three modified seals were used during the present investigation. The aft-body cavity was instrumented with three static pressure orifices that monitored airflow within the cavity caused by seal leakage. In general, no significant leakage was observed with any seal configuration; one exception is described herein in which the seal was damaged during a Mach number series. The seal was not used during tests at $R_{\bar{c}} = 2.38 \times 10^6$ to allow a direct comparison with data obtained in the Boeing Transonic Wind Tunnel.

Transition

Boundary-layer transition was fixed by distributing epoxy disks (ref. 20) at specified locations on the model surface. The distributed disk method minimizes variations in the trip distributions and height and allows the trip to be easily inspected, repaired, or duplicated. However, the initial application of the distributed disks is more time consuming than a corresponding application of the more traditional grit trip method. Transition trip disks were applied to the upper and lower surfaces of the wing and horizontal tail, the internal and external surfaces of the nacelles, the nacelle struts, and the nose of the body for tests at low Reynolds numbers ($R_{\bar{c}} = 2.38$ and 4.45×10^6). Table 3 provides the sizes and locations of the transition trip disks for the conditions at $R_{\bar{c}} = 2.38$ and 4.45×10^6 . The two patterns differ only in the disk height on the wing surfaces. The transition trip disks were removed from the wing, horizontal tail, and external nacelle surfaces for the high Reynolds number test conditions ($R_{\bar{c}} \geq 21.1 \times 10^6$). A comparison of trip-on and trip-off configurations at $R_{\bar{c}} = 21.1 \times 10^6$ (ref. 7) indicates that boundary-layer transition did occur at or near the 10-percent local chord location of the trip.

¹Mylar is a registered trademark of E. I. du Pont de Nemours & Company.

Test Approach

Repeatability Goals

The primary data of interest for this investigation are the longitudinal stability-axis coefficients of lift, drag, and pitching moment. Goals for the repeatability of these coefficients were based on the needs of industry and the information contained in reference 2. The repeatability goals for these coefficients are given as confidence intervals about an estimated mean (least squares curve-fit representation) as

$$\Delta C_L \dots\dots\dots \pm 0.005$$

$$\Delta C_D \dots\dots\dots \pm 0.0001$$

$$\Delta C_m \dots\dots\dots \pm 0.001$$

and are stated at the 95-percent confidence level, which indicates a high to extreme probability that the true mean value lies within the prescribed interval in the absence of bias.

Repeated Test Conditions

Equation (15) shows three factors that can affect the size of the confidence interval for a specified confidence level—the standard error, the data sample size, and the data sample distribution. The data sample sizes and data sample distributions, unlike the standard error, are under the direct control of the investigator and are chosen based on the goals of a given investigation. The data sample distribution is typically chosen to define the polar shape over a specified range and is often concentrated in regions of particular interest. Thus, the data sample size becomes the primary factor affecting the size of the confidence interval for a specified level of confidence. Figure 3 indicates how the data sample size affects the size of the confidence interval for a specified level of confidence, assuming that the standard error remains constant as N varies; figure 3 is based on the SVSA definition of the confidence interval given in equation (7). One implication of figure 3 is that for constant data scatter (s , the sample standard deviation), increasing N decreases the size of the confidence interval for a specified confidence level. Figure 3 indicates that a confidence interval equal to the sample standard deviation can be attained at a 95-percent confidence level with a sample size of approximately 6. Based on this result, the importance of drag repeatability, and the expectation that the standard deviation of the drag-coefficient data would be approximately ± 0.0001 (equal to the confidence interval goal), 6 polars per repeated test condition were performed in an attempt to meet the stated confidence interval goal at a 95-percent confidence level. Note that this result depends on s such that if s were smaller, N could also decrease while maintaining a 95-percent confidence level in the

desired confidence interval. As is shown later, the data scatter was less than anticipated and the number of repeat polars per test condition was reduced during the investigation. Table 4 summarizes the repeated test conditions, including the number of polars actually performed and the sample size used with the RSA approach; table 4 also assigns a group number to each repeated test condition to facilitate the discussion below.

Results and Discussion

The purpose of this report is to quantify and document the data repeatability obtained during a recent high Reynolds number investigation of a Boeing 767 model in the NTF. The approach is to quantify repeatability using the RSA statistical method described earlier. The statistical analysis of the force and moment coefficient repeatability is discussed first and is followed by a discussion of several factors that may contribute to nonrepeatability through either bias or precision errors.

The maximum angle of attack was limited to 3.5° for high Reynolds number test conditions because of previous encounters with adverse model and support system dynamics in the cryogenic mode of operation; the majority of the data obtained lies within the range $\alpha = -2^\circ$ to 3° . Previous experience (ref. 7) indicates that the flow over this range is well behaved, thus reducing the potential for unsteady, separated flow phenomena that could affect repeatability. Although data were obtained over a larger angle-of-attack range for low Reynolds numbers (air mode of operation), repeatability was examined over a range consistent with the high Reynolds number data. As such, the analysis below is based on data taken in the range $\alpha = -2^\circ$ to 3° for all repeated test conditions.

Force and Moment Repeatability

The longitudinal stability-axis coefficients of lift, drag, and pitching moment are of primary interest in this investigation. The drag coefficient is of particular interest in this investigation because a major goal was the acquisition of refined drag measurements for eventual comparison with flight data. Specific repeatability goals were established before the experiment as outlined earlier. The data are graphically presented as residual plots of the force and moment coefficients, where the residual of a parameter Y is defined as

$$\Delta Y = Y_i - \hat{Y} \quad (19)$$

Selection of polynomial regression model order K.

The process used to select an appropriate value of K has been outlined. The rule of thumb (eq. (13)) is evaluated based on the data sample sizes provided in table 4; the guideline indicates that maximum values of K should

be in the range of 3 to 5. The final value of K is chosen based on a survey of the standard error (eq. (14)) that results from curve fits over a range of K and on an examination of residuals. The random data scatter in the residual plots validates the polynomial regression model relative to the assumption of random data scatter. Figures 4 and 5 show the results of this process for the longitudinal stability- and body-axis coefficients, respectively. The value of K was varied from 0 to 8 in each case; extending the range to 8, which is beyond the recommended maximum just identified, is simply for demonstration purposes. The standard errors for low-order fits are often very large and are not always shown in figures 4 and 5. Based on examination of these figures, a single value of K was selected for each functional relationship modeled. The selected values of K are summarized in table 5 and the two exceptions are noted. The results shown in figures 4(b) and 5(b) for the pitching-moment data of groups 11 and 12 indicate a significant reduction in the standard error when K was increased from 3 to 5; the increased order also served to make the data scatter of the residuals significantly more random. Although the selection remains somewhat subjective, an interesting note is that the air-mode groups generally benefit from a slightly higher order model than do the cryogenic-mode groups. As a result, the order of the air-mode regression models typically defined the final choice of K for the cryogenic-mode models.

Short-term analysis—cryogenic mode. Groups 1–7 were obtained in the cryogenic mode of operation, they varied in size from three to six polars, and they totaled 20 to 40 data points. Repeated polars were generally obtained during a Mach number series in which the Mach number was alternately set at 0.70 and 0.80. Figure 6 shows the 95-percent confidence and prediction intervals and the residuals of the lift, drag, and pitching-moment coefficients as defined in equation (19) for groups 1–7. Note that both the confidence and prediction intervals are functions of the independent variable. The magnitude of the prediction interval is nearly constant except near the outer bounds of the data range, whereas the confidence interval varies more throughout. The variability observed for both confidence and prediction intervals is a result of dependence on the data density term Q . (See eq. (17).) In regions of high data density, the confidence interval becomes more narrow; the widening of both prediction and confidence intervals at the outer bounds is directly related to this effect as well, an effect that reflects the intuitive result that the mean value of the dependent parameter is known with more confidence where the data are concentrated. Table 6 provides a summary of the 95-percent confidence and prediction intervals over the range of data $\alpha = -2^\circ$ to 3° ; the generalized data presented in table 6 are simply averages of the confidence

and prediction intervals computed at the independent variable for each data point. Clearly, in each case the repeatability goals as specified on the confidence interval for coefficients of lift, drag, and pitching moment were satisfied.

Groups 1 and 5 were unique in that a single polar from each group (run 28 in group 1 and run 29 in group 5) was obtained two days after the other five in that respective group. In addition, the tunnel environment was purged of nitrogen and warmed to ambient temperature during the off day. The significant time difference and tunnel cycling could allow these two groups to be subdivided and classified as near-term timescale situations; as such, the potential was greater for less repeatable data within the two groups. The results indicate that the repeatability within groups 1 and 5 is essentially the same as for the other short-term, cryogenic-mode groups.

Figure 7 shows the residuals of the longitudinal body-axis force and moment coefficients for groups 1–7. The results are similar to those presented for the longitudinal stability-axis coefficients. Table 7 provides a summary of these data; note the very small differences in the results given in table 6 for the drag coefficient compared with the axial-force coefficient results.

Short-term analysis—air mode. Groups 8–13 were obtained in the air mode of operation and each was formed from three polars. Repeated polars were obtained during a Mach number series and followed the pattern $M = 0.80, 0.86, 0.84, 0.82, 0.80, 0.78, 0.75, 0.70,$ and 0.80 . Figure 8 shows the 95-percent confidence and prediction intervals and the residuals of the lift, drag, and pitching-moment coefficients for groups 8–13; figure 9 presents the longitudinal body-axis coefficients. As with the cryogenic-mode data, the repeatability in the air mode is very good and generally within the pretest goals. Tables 6 and 7 contain the summarized results for the stability- and body-axis coefficients, respectively.

The drag-coefficient (and axial-force coefficient) confidence and prediction intervals for group 8 are noteworthy because they are significantly larger than those of the other air- and cryogenic-mode groups; figures 8(a) and 9(a) show the drag- and axial-force coefficient data, respectively, for group 8. The figures reveal that a single run (run 113) has a lower drag level by roughly 2.5 to 3 drag counts compared with the other two polars in the group. This disparity was probably due to the strut seal partially tearing loose during the Mach number series. (Seal damage was discovered when the model was inspected after the Mach number series.) As a result, some seal stuffing was lost and part of the seal cover protruded into the flow field and shifted the drag to a higher level. This error is classified as a bias and invalidates the

statistical analysis because it violates the assumption that all errors are random. However, the shift is explainable to an acceptable degree such that the nonbiased polar could be used with confidence and the biased polars disregarded during the aerodynamic analysis phase of the investigation. The identification of this bias error demonstrates an extra advantage of the residual analysis beyond its use in quantifying precision.

Near-term analysis. Groups 2 and 3 can be combined to form a data set that is suitable for near-term repeatability analysis. The acquisition of the two data groups was separated by 15 days during which the tunnel was purged, multiple large changes were made in tunnel temperature and pressure, and multiple model changes were made during the low Reynolds number, air-mode portion of the investigation. The comparison of two short-term groups acquired in such a manner demonstrates the near-term repeatability of the force and moment data across a break in the cryogenic tests.

Figures 10 and 11 show the residuals and the 95-percent confidence and prediction intervals for longitudinal stability- and body-axis force and moment coefficients, respectively; average values for the intervals are included in tables 6 and 7. As with the short-term results, the near-term results demonstrate levels of repeatability within the pretest goals of the investigation. In addition, the residual analysis clearly shows a small shift in the pitching-moment coefficient of approximately 0.002 across the break in the cryogenic tests. This shift is probably due to the use of two different strut seals; past experience (ref. 7) has shown the pitching-moment coefficient to be sensitive to seal quality, particularly for the tail-on configurations. As discussed previously, the bias error technically invalidates the statistical analysis; however, the magnitude of the bias is small and explainable and was not particularly significant during the aerodynamic analysis phase of the investigation. This case is another example of the utility of residual plots in detecting bias errors.

Contributing Factors to Nonrepeatability

The data demonstrate excellent force and moment coefficient repeatability, particularly in relation to the complex wind tunnel test environment in general and the NTF in particular. A seemingly endless list of possible sources for bias and precision errors could be generated. For the sake of brevity, only several possible sources are discussed here. Highlighting several potential sources of error demonstrates the detail required to achieve the level of repeatability demonstrated in this investigation.

Balance accuracy. Accuracy and repeatability represent two distinct areas of interest that relate to the quality of any measurement. A given measurement may be highly accurate, yet other factors within a system may inhibit repeatability. On the other hand, a series of measurements of the same parameter may be highly repeatable, but the accuracy compared with the true value may be poor. A comparison is useful, however, of the balance measurement accuracy bands with the stated repeatability goals. Figure 12 shows the accuracy bands for the normal force, axial force, and pitching moment in coefficient form; figure 12 includes curves for the quoted accuracy (table 1) and two additional, tighter accuracy bands for reference. Figure 12 highlights two points as follows. First, the balance used in this investigation and all balances designed for use in the NTF yield significantly more accurate coefficients at the high dynamic pressure conditions. Second, the repeatability goals set forth and satisfied herein are generally within the quoted accuracy bands of the balance measurements. As shown in figure 12, the exception occurs on the normal-force coefficient at dynamic pressures above approximately 2368 psf; note that the results given in table 7 show confidence intervals on the normal-force coefficient to be approximately one order of magnitude lower than the stated goal. Thus, the confidence in the accuracy of a repeatable measurement due to some unknown measurement bias may be more of an issue than the repeatability of the measurement itself.

Note that the form of the balance accuracy quote has changed since the last calibration of the balance used during this investigation. (See ref. 21.) Previously, the accuracy quote was stated in terms of the worst outlying point during the calibration, as in this report. This form of quotation is generally overly conservative. Balance accuracies are currently quoted based on a 95-percent confidence level and yield a more realistic assessment; the revised form of the quotation aligns the balance accuracy assessment more closely with the method of repeatability assessment used herein. Reference 21 shows calibration results for other cryogenic balances used in the NTF that indicate a consistent improvement from 0.5 percent of the maximum design loads previously quoted to a quote in the range of 0.1 to 0.3 percent.

Balance temperature gradient effect. References 18 and 19 discuss the balance temperature compensation algorithm used in the data reduction process at the NTF. In effect, all balance output is corrected to a reference temperature (295 K) based on pretest temperature cycling of the balance. During the pretest temperature cycling as well as during the test in both air and cryogenic modes of operation, a temperature gradient will

often occur across the balance. Reference 19 presents data indicating a direct effect of the temperature gradients on the balance output. The temperature compensation algorithm is not a function of the temperature gradient, which, in effect, means that the temperature compensation algorithm assumes a zero temperature gradient across the balance. As a result, operational practice includes time to drive the balance toward thermal equilibrium, meaning to some temperature near the flow temperature with a minimal gradient of 10° to 15°F, before the test condition is set and the data are collected. This operational practice is used if the highest quality force data are required, and experience has shown that the temperature gradient generally moves toward zero as the test condition is set and data collection begins.

Figure 13 shows the variation of the balance temperature and the temperature gradient across the balance for each group of repeat data. The balance temperature presented is measured in the middle of the balance and the gradient is defined as the temperature difference from the front to the rear of the balance. The temperature compensation algorithm accounts for the variations observed in the balance temperature within a given group; the variations in temperature gradient are potential sources for error, as a correction for this effect is not applied. Because of the time given to condition the balance, however, the maximum magnitude of the gradient is a relatively small 8°F and does not adversely affect the force and moment coefficient repeatability. The gradients generally move toward zero over time. Also, cold test conditions tend toward negative front-to-rear gradients, whereas the warm test conditions have positive gradients; this situation is attributed to the fact that the front portion of the balance adjusts more rapidly to the flow condition than the rear, sting-connected portion of the balance.

Angle of attack. The determination of the angle of attack has a direct effect on the calculation of the lift and drag coefficients:

$$\left. \begin{aligned} C_D &= C_N \sin \alpha + C_A \cos \alpha \\ C_L &= C_N \cos \alpha - C_A \sin \alpha \end{aligned} \right\} \quad (20)$$

The direct effect of angle-of-attack errors on the calculation of C_L and C_D can be estimated as

$$\left. \begin{aligned} \Delta C_D &= C_L \Delta \alpha (\pi/180) \\ \Delta C_L &= -C_D \Delta \alpha (\pi/180) \end{aligned} \right\} \quad (21)$$

Equations (21) show that the effect of $\Delta \alpha$ on the drag coefficient is much more significant than that on the lift

coefficient relative to the repeatability goals. Figure 14 shows the effect of angle-of-attack errors on the drag coefficient for a range of lift coefficients; an error of 0.01° in the angle of attack is shown to affect the drag coefficient by approximately 0.8 drag counts at the cruise lift coefficient of 0.45.

The determination of the angle of attack can be affected by several factors. The first and foremost factor is the measurement itself. The primary measurement is taken from an onboard accelerometer package that, as stated previously, has a quoted accuracy of 0.01°. This quoted accuracy is based on calibrations performed under controlled, laboratory conditions at ambient temperature rather than in an actual wind-on test environment. One potential factor that affects the onboard angle-of-attack measurement in the wind-on environment is the model and support system dynamics; model and support system dynamics can be sufficiently large, particularly at high load conditions, to introduce significant centrifugal forces that cause incorrect (biased) angle-of-attack measurements. (See ref. 17.)

The flow angularity in the test section is another important factor affecting the determination of the angle of attack. If the flow angularity were known to be constant, it could be assessed once and applied to data for all configurations and test conditions. In reality, however, the flow angularity should not be assumed to be constant. This fact is especially true when an error of only 0.01° can affect the drag data significantly relative to the repeatability goals. Flow angularity was assessed more frequently than normal during this investigation, all at a nominal Mach number of 0.80. The variation of the flow angularity throughout the investigation is given in figure 15. The mean upflow was 0.131° with a standard deviation of 0.011°. Note the large variation of more than 0.05° on a single day of tests that encompassed a wide range of operating conditions and the shift of 0.015° for the repeated flow condition assessment. No definite conclusions can be drawn as to the variability of flow angularity from these data.

Figure 16 presents residual plots and the accompanying statistical intervals for the angle of attack; these data were obtained by representing the angle of attack as a function of the normal-force coefficient with a third-order polynomial regression model and applying the RSA approach. The residual plots demonstrate the characteristics of random variation, thereby validating the use of statistics to quantify repeatability. Average values of the 95-percent confidence and prediction intervals are presented in table 8. The scatter in the angle-of-attack measurement, as quantified by the prediction interval, is approximately $\pm 0.02^\circ$ to the 95-percent confidence level;

confidence in the mean value is approximately $\pm 0.005^\circ$ at a 95-percent confidence level. Although the repeatability is very good, this analysis does not address possible biases that may affect the absolute accuracy of the angle-of-attack measurement such as possible model and support system dynamics as mentioned earlier.

Flow conditions. The repeatability of the flow conditions has a direct influence on the repeatability of the aerodynamic data. The measured flow parameters are total pressure, total temperature, and static pressure from which the primary flow parameters of interest are calculated—namely, the Reynolds number, the Mach number, and the dynamic pressure. The repeatability of these flow parameters is summarized in table 9 where the mean, sample standard deviation, and 95-percent prediction interval are given for each parameter for the combined short-term groups of polars; figure 17 shows the variations from polar to polar within each combined short-term group. Table 10 presents the variation expected due to pure instrument uncertainty for the four repeated flow conditions included in this investigation; the uncertainty of the measured quantities is that described herein and in reference 18, and the uncertainty of the calculated quantities is based on the propagation of uncertainty equations given by Rind. (See ref. 3.)

The measured quantities p_t , p_s , and T_t are shown in figures 17(a), 17(b), and 17(c), respectively. The repeatability of these quantities is at least somewhat indicative of the flow condition control in addition to the accuracy of the measurement instruments. The maximum standard deviation of total pressure within any single polar is less than 0.04 psia and less than 0.06 psia for any group of polars. No distinct difference is apparent between the cryogenic- (groups 1–7) and the air-mode groups (groups 8–13). The trends for static pressure and total temperature, however, show more scatter in the air mode than in the cryogenic mode. The increased scatter in the air mode is not truly significant, as the primary flow parameters (figs. 17(d), 17(e), and 17(f)) are less sensitive to these parameters in the air mode. The maximum standard deviation of static pressure within any single cryogenic-mode polar is less than 0.07 psia and less than 0.09 psia for any cryogenic-mode group. The maximum standard deviation for static pressure in the air mode is less than 0.02 psia within a polar and less than 0.03 psia within a group. The maximum standard deviation of total temperature within any single cryogenic-mode polar is less than 0.8°F and less than 0.6°F for any cryogenic-mode group. The maximum standard deviation for total temperature in the air mode is less than 1.4°F within a polar and less than 1.6°F within a group.

The potential effects of the primary flow parameters on the drag data are now addressed. The effect of

Reynolds number variations has been assessed based solely on predicted variations in the skin-friction drag coefficient $C_{D,sf}$. Skin-friction drag-coefficient estimates were made by using an equivalent flat-plate drag plus overspeed factors that were based on the wetted areas of the model components. Figure 18 shows the predicted Reynolds number variation that would cause a shift of 0.1 drag count (0.00001) in the drag-coefficient data at $M = 0.80$. Table 9 and figure 17(d) show very good Reynolds number repeatability based on this strict criterion. Note, however, that cryogenic-mode groups 1 and 5 show greater scatter than all others; this scatter is attributed to the fact that a single polar in each group was obtained at a slightly lower mean total temperature and on a separate day (table 4) than the others within that group.

The key concerning Mach number variations is the drag-divergence Mach number, which can be defined as the Mach number at which the drag-rise rate $\Delta C_D/\Delta M$ reaches 0.1. This criterion implies that deviations of about $\Delta M = 0.001$ near the drag-divergence Mach number will cause a drag-coefficient shift of about one drag count. The drag-divergence Mach number varies from configuration to configuration and decreases with increasing lift. The general implication is that Mach number control becomes more important with both increasing Mach number and increasing lift. Data from reference 7 indicate that the repeat conditions herein are below drag divergence for the primary lift range examined ($\alpha \leq 3.0^\circ$); however, increased drag data scatter with increasing lift may be partially due to Mach number variations, particularly for the test conditions at $M = 0.80$. Table 9 and figure 17(e) show the 95-percent prediction intervals to be about 0.002 and 0.001 for the cryogenic and air modes of operation, respectively.

The dynamic pressure variations shown in table 9 are judged to be negligible compared with the potential effects of Mach and Reynolds number variations. This judgment is based on data presented in reference 7 in which the dynamic pressure was varied over a large range. In addition, the effect of dynamic pressure due to pure instrument uncertainty (table 10) on the calculation of the force and moment coefficients is also negligible.

Combined force and pressure tests. Another significant source of nonrepeatability in the NTF may appear when force and pressure tests are combined. Balance repeatability can be adversely affected by pressure tubes that bridge the balance in such a way as to cause fouling; nonrepeatability can result when the tubes contract and expand over the wide temperature range encountered. The investigation described herein was conducted as a force test only to eliminate this situation as a potential source of nonrepeatability. Note that the three pressure

measurements near the upper swept strut seal were made without tubes bridging the balance.

Summary of Results

A high Reynolds number investigation of a 0.03-scale model of the Boeing 767 airplane has been conducted in the National Transonic Facility (NTF) at Langley Research Center; this investigation was part of a cooperative effort to test this model at the NTF and two other transonic wind tunnels. The model was tested over a Mach number range of 0.70 to 0.86 and a Reynolds number range of 2.38 to 40.0×10^6 based on the mean aerodynamic chord. The present report focuses on a study of data repeatability during this investigation. Two statistical and probability-based approaches are outlined and provide the means to quantify data repeatability in a consistent, mathematical manner. The results are summarized as follows:

1. Excellent force and moment coefficient repeatability was demonstrated in both air and cryogenic modes of operation over short-term periods.
2. Excellent force and moment coefficient repeatability was demonstrated across a 15-day break in the cryogenic tests. The two cryogenic repeat series were separated by 81 runs of tests in air, multiple model changes, multiple large changes in tunnel total temperature and total pressure, and tunnel volume exchanges of air for nitrogen and vice versa.
3. Repeatability results for both short- and near-term time spans were within the stated pretest goals for the confidence interval of ± 0.005 , ± 0.0001 , and ± 0.001 with a 95-percent confidence level for the coefficients of lift, drag, and pitching moment, respectively. The repeat series which did not meet these goals could be explained by the introduction of a bias that violates the primary requirement of randomness and invalidates the statistical analysis. The use of residual plots, however, was a key factor in identifying biases.
4. Force and moment coefficient repeatability was insensitive to the balance thermal gradients of $\pm 8^\circ\text{F}$ experienced during data acquisition.
5. Repeatability assessments herein are based on data acquired over a limited range of angle of attack ($\alpha = -2^\circ$ to 3°) and without onboard pressure instrumentation.
6. Repeatability of the angle of attack, which was quantified by the prediction interval as a function of the normal-force coefficient, is approximately $\pm 0.02^\circ$ to the 95-percent confidence level; confidence in each mean value of the angle of attack is approximately $\pm 0.005^\circ$ at a 95-percent confidence level.

7. Repeatability of the flow conditions was sufficient to preclude an adverse effect on the force and moment coefficient data repeatability. However, instances occurred when a flow parameter varied very little within a polar, but the mean value was offset from the other polars within a group due to a set point bias. Likewise, instances occurred when the set point for a flow parameter was highly repeatable, but specific polars within a group exhibited more variation than the others.

NASA Langley Research Center
Hampton, VA 23681-0001
May 15, 1995

References

1. Anon.: *Aerodynamic Data Accuracy and Quality: Requirements and Capabilities in Wind Tunnel Testing*. AGARD-CP-429, 1988. (Available from DTIC as AD A202 496.)
2. Steinle, F.; Stanewsky, E.; and Dietz, R. O.: *Wind Tunnel Flow Quality and Data Accuracy Requirements*. AGARD-AR-184, 1982. (Available from DTIC as AD A129 881.)
3. Rind, Emanuel: *Instrument Error Analysis as It Applies to Wind-Tunnel Testing*. NASA TP-1572, 1979.
4. Brown, Clinton E.; and Chen, Chaun Fang: *An Analysis of Performance Estimation Methods for Aircraft*. NASA CR-921, 1967.
5. Abernethy, R. B.: Precision and Propagation of Error. *Thrust and Drag: Its Prediction and Verification*, Eugene E. Covert, ed., AIAA, 1985, pp. 281–330.
6. Roache, P. J.: Need for Control of Numerical Accuracy. *J. Spacecr. & Rockets*, vol. 27, no. 2, Mar.–Apr. 1990, pp. 98–102.
7. Wahls, Richard A.; Gloss, Blair B.; Flechner, Stuart G.; Johnson, William G., Jr.; Wright, F. L.; Nelson, C. P.; Nelson, R. S.; Elzey, M. B.; and Hergert, D. W.: *A High Reynolds Number Investigation of a Commercial Transport Model in the National Transonic Facility*. NASA TM-4418, 1993.
8. Young, Clarence P., Jr.; Hergert, Dennis W.; Butler, Thomas W.; and Herring, Fred M.: Buffet Test in the National Transonic Facility. AIAA-92-4032, July 1992.
9. Walpole, Ronald E.; and Myers, Raymond H.: *Probability and Statistics for Engineers and Scientists*. Third ed., Macmillan Publ. Co., 1972.
10. Draper, N. R.; and Smith, H.: *Applied Regression Analysis*. John Wiley & Sons, Inc., 1966.
11. Coleman, Hugh W.; and Steele, W. Glenn, Jr.: *Experimentation and Uncertainty Analysis for Engineers*. John Wiley & Sons, Inc., 1989.

12. MIDAP Study Group: *Guide to In-Flight Thrust Measurement of Turbojets and Fan Engines*. AGARD-AG-237, 1979. (Available from DTIC as AD A065 939.)
13. Simon, Leslie E.: *An Engineers' Manual of Statistical Methods*. John Wiley & Sons, Inc., 1941, p. 43.
14. Gloss, B. B.: Current Status and Some Future Test Directions for the US National Transonic Facility. *Wind Tunnels and Wind Tunnel Test Techniques*, R. Aeronaut. Soc., 1992, pp. 3.1–3.7.
15. Fuller, Dennis E.: *Guide for Users of the National Transonic Facility*. NASA TM-83124, 1981.
16. Igoe, William B.: Analysis of Fluctuating Static Pressure Measurements in a Large High Reynolds Number Transonic Cryogenic Wind Tunnel. Ph.D. Diss., George Washington Univ., May 1993.
17. Finley, Tom D.; and Tcheng, Ping: Model Attitude Measurements at NASA Langley Research Center. AIAA-92-0763, 1992.
18. Foster, Jean M.; and Adcock, Jerry B.: *User's Guide for the National Transonic Facility Data System*. NASA TM-100511, 1987.
19. Williams, M. Susan: Experience With Strain Gage Balances for Cryogenic Wind Tunnels. *Special Course on Advances in Cryogenic Wind Tunnel Technology*, AGARD-R-774, 1989, pp. 18-1–18-14. (Available from DTIC as AD A217 716.)
20. Chan, Y. Y.: *Comparison of Boundary Layer Trips of Disk and Grit Types on Airfoil Performance at Transonic Speeds*. NAE-AN-56 (NRC-29908), National Aeronautical Establ. (Ottawa, Ontario), Dec. 1988.
21. Ferris, Alice T.: *An Improved Method for Determining Force Balance Calibration Accuracy*. ISA 93-092, 1993.

Table 1. Force and Moment Measurement Characteristics

Measurement	Full-scale (FS) design limit	Balance accuracy ^a ±0.5% FS	Data acquisition resolution
Normal force, lb	6 500	±32.5	0.398
Axial force, lb	400	±2.0	.048
Pitching moment, in-lb	13 000	±65.0	1.151
Rolling moment, in-lb	9 000	±45.0	.803
Yawing moment, in-lb	6 500	±32.5	.723
Side force, lb	4 000	±20.0	.255

^aQuoted balance accuracy (stated in terms of worst outlying point during calibration).

Table 2. Mach Number Corrections for Repeated Test Conditions Based on Mach Number Calibrations as Function of Reynolds Number

$$[M = M_{\text{ref}} + \Delta M]$$

$R_{\bar{c}}$	M	ΔM
40.0×10^6	0.80	-0.0037
40.0	.70	-.0032
4.45	.80	-.0025
2.38	.80	-.0025

Table 3. Transition Disk Size and Distribution

[Disk spacing = 0.1 in. from center to center; disk diameters = 0.0455 in.]

Component	Location	Disk height, in. for—	
		$R_{\bar{c}} = 2.38 \times 10^6$	$R_{\bar{c}} = 4.45 \times 10^6$
Body	1 in. aft of nose	0.0060	0.0060
Nacelles:			
Cowl inside	^a 0.5 in. aft of hilite	0.0045	0.0045
Cowl outside	0.5 in. aft of hilite	0.0050	0.0050
Primary inside	0.5 in. aft of hilite	0.0050	0.0050
Primary outside	0.5 in. aft of hilite	0.0050	0.0050
Bifurcation	0.5 in. aft of hilite	0.0050	0.0050
Nacelle struts	1 in. aft of leading edge	0.0040	0.0040
Horizontal tail:			
Upper surface	25-percent local chord	0.0045	0.0045
Lower surface	25-percent local chord	0.0045	0.0045
Wing:			
Upper surface	10-percent local chord	0.0060	0.0045
Lower surface	10-percent local chord	0.0060	0.0045

^aHilite—leading edge of nacelle components.

Table 4. Short-Term Repeat Configurations and Test Conditions

Group	$R_{\bar{c}}$	M	q , psf	Configuration	Upper swept strut seal ^a	Repeat polars ^b	Sample size	Date
1	40.0×10^6	0.80	2661	WBMNT	1	^c 5+1	40	1-13-92
2				WBMNTH = -1	1	4	28	^d 1-15-92
3				WBMNTH = -1	3	6	40	^d 1-16-92
4				WBMNTH = +1	3	4	36	2-3-92
5	40.0×10^6	0.70	2426	WBMNT	1	^c 5+1	40	1-13-92
6				WBMNTH = -1	1	4	29	1-15-92
7				WBMNTH = +1	3	3	20	1-16-92
8	4.45×10^6	0.80	1237	WBMNTH = -1	2	3	37	1-29-92
9				WBMNT	3	3	39	1-29-92
10				WBMNTH = +1	3	3	42	1-30-92
11	2.38×10^6	0.80	653	WB	Out	3	40	1-22-92
12				WBMNT	Out	3	40	1-24-92
13				WBMNTH = 0	Out	3	39	1-24-92

^aSeal number if on, otherwise seal out.

^bDoes not include inverted polars.

^cFive polars on 1-13-92, 1 polar on 1-15-92: combine for short-term analysis.

^dCombine for near-term analysis.

Table 5. Selected Order of Polynomial Regression Model

Dependent variable	Independent variable	Order of polynomial regression model K
C_D	C_L	4
C_m	C_L	^a 3
C_L	α	3
C_A	C_N	4
C_m	C_N	^a 3
C_N	α	3
α	C_N	3

^aGroups 11 and 12 used $K = 5$.

Table 6. Confidence and Prediction Intervals at 95-Percent Confidence Level for Longitudinal Stability-Axis Coefficients

[Values averaged over range of data. Repeatability goals stated for confidence interval at 95-percent confidence level: $\Delta C_D = \pm 1.0 \times 10^{-4}$; $\Delta C_L = \pm 5.0 \times 10^{-3}$; $\Delta C_m = \pm 1.0 \times 10^{-3}$]

Group	R_c	M	ΔC_D		ΔC_L		ΔC_m		
			CI	PI	CI	PI	CI	PI	
1	40.0×10^6	0.80	$\pm 0.5 \times 10^{-4}$	$\pm 1.5 \times 10^{-4}$	$\pm 0.6 \times 10^{-3}$	$\pm 2.0 \times 10^{-3}$	$\pm 0.2 \times 10^{-3}$	$\pm 0.8 \times 10^{-3}$	
2	↓	↓	±.3	±.9	±.7	±2.0	±.2	±.5	
3			±.3	±1.0	±.7	±2.4	±.1	±.5	
4			±.4	±1.2	±.7	±2.2	±.1	±.4	
5			.70	±.2	±.7	±.5	±1.6	±.2	±.6
6			.70	±.3	±.7	±.5	±1.5	±.1	±.3
7			.70	±.3	±.7	±.6	±1.5	±.2	±.4
8			4.45	.80	±1.1	±3.2	±.5	±1.7	±.3
9	4.45	↓	±.4	±1.2	±.6	±2.1	±.5	±1.8	
10	4.45		±.3	±.9	±.6	±2.0	±.1	±.5	
11	2.38		±.4	±1.3	±.7	±2.4	±.1	±.3	
12	2.38		±.6	±1.7	±.5	±1.7	±.1	±.3	
13	2.38		±.4	±1.1	±.6	±2.0	±.2	±.6	
2 & 3	40.0	0.80	±.2	±1.0	±.5	±2.1	±.4	±1.8	

Table 7. Confidence and Prediction Intervals at 95-Percent Confidence Level for Longitudinal Body-Axis Coefficients

[Values averaged over range of data. Repeatability goals stated for confidence interval at 95-percent confidence level: $\Delta C_D = \pm 1.0 \times 10^{-4}$; $\Delta C_L = \pm 5.0 \times 10^{-3}$; $\Delta C_m = \pm 1.0 \times 10^{-3}$]

Group	$R_{\bar{c}}$	M	ΔC_A		ΔC_N		ΔC_m		
			CI	PI	CI	PI	CI	PI	
1	40.0×10^6	0.80	$\pm 0.4 \times 10^{-4}$	$\pm 1.2 \times 10^{-4}$	$\pm 0.6 \times 10^{-3}$	$\pm 2.0 \times 10^{-3}$	$\pm 0.2 \times 10^{-3}$	$\pm 0.8 \times 10^{-3}$	
2	↓	↓	±.4	±1.1	±.7	±2.0	±.2	±.5	
3			±.4	±1.3	±.7	±2.4	±.1	±.5	
4			±.5	±1.6	±.7	±2.2	±.1	±.4	
5			.70	±.2	±.8	±.5	±1.6	±.2	±.6
6			.70	±.2	±.6	±.5	±1.5	±.1	±.3
7			.70	±.3	±.7	±.6	±1.5	±.2	±.4
8			4.45	.80	±1.1	±3.6	±.5	±1.7	±.3
9	4.45	↓	±.5	±1.5	±.6	±2.1	±.5	±1.8	
10	4.45		±.5	±1.5	±.6	±2.0	±.2	±.5	
11	2.38		±.5	±1.7	±.7	±2.4	±.1	±.3	
12	2.38		±.7	±2.1	±.5	±1.7	±.1	±.3	
13	2.38		±.4	±1.3	±.6	±2.0	±.2	±.6	
2 & 3	40.0	.80	±0.3	±1.2	±0.5	±2.1	±.4	±1.8	

Table 8. Confidence and Prediction Intervals at 95-Percent Confidence Level for Angle of Attack

[Values averaged over range of data]

Group	R_c	M	$\Delta\alpha$, deg		
			CI	PI	
1	40.0×10^6	0.80	± 0.005	± 0.018	
2	↓	↓	± 0.006	± 0.016	
3		↓	± 0.006	± 0.020	
4		↓	± 0.005	± 0.018	
5		↓	.70	± 0.005	± 0.017
6		↓	.70	± 0.005	± 0.014
7		↓	.70	± 0.006	± 0.014
8		4.45	.80	± 0.004	± 0.014
9		4.45	↓	± 0.005	± 0.019
10		4.45	↓	± 0.005	± 0.017
11		2.38	↓	± 0.006	± 0.022
12		2.38	↓	± 0.005	± 0.016
13		2.38	↓	± 0.005	± 0.017
2 & 3		40.0	.80	± 0.004	± 0.017

Table 9. Flow Condition Repeatability

Group	Measure	P_t , psia	P_s , psia	T_t , °F	R_c	M	q , psf
1	Mean	63.078	41.310	-250.05	39.984×10^6	0.7998	2659.2
	s	.013	.032	.46	$.126 \times 10^6$.0007	3.1
	95% PI	± 0.026	± 0.064	± 0.94	$\pm 0.255 \times 10^6$	± 0.0015	± 6.2
2	Mean	63.112	41.341	-250.57	40.149×10^6	0.7996	2659.7
	s	.029	.037	.11	$.047 \times 10^6$.0010	4.8
	95% PI	± 0.059	± 0.077	± 0.22	$\pm 0.097 \times 10^6$	± 0.0021	± 9.9
3	Mean	63.087	41.321	-250.59	40.140×10^6	0.7997	2659.0
	s	.007	.032	.17	$.050 \times 10^6$.0007	2.9
	95% PI	± 0.014	± 0.064	± 0.35	$\pm 0.102 \times 10^6$	± 0.0015	± 5.9
4	Mean	63.104	41.308	-250.76	40.217×10^6	0.8003	2662.1
	s	.033	.041	.12	$.056 \times 10^6$.0011	5.1
	95% PI	± 0.067	± 0.083	± 0.24	$\pm 0.114 \times 10^6$	± 0.0022	± 10.3
5	Mean	68.416	49.260	-249.88	39.959×10^6	0.6999	2426.1
	s	.025	.043	.46	$.145 \times 10^6$.0008	3.5
	95% PI	± 0.050	± 0.088	± 0.93	$\pm 0.293 \times 10^6$	± 0.0016	± 7.0
6	Mean	68.432	49.271	-250.90	40.260×10^6	0.7000	2426.5
	s	.019	.027	.16	$.056 \times 10^6$.0007	3.9
	95% PI	± 0.038	± 0.055	± 0.34	$\pm 0.114 \times 10^6$	± 0.0015	± 8.0
7	Mean	68.327	49.165	-250.78	40.192×10^6	0.7007	2426.1
	s	.053	.089	.16	$.058 \times 10^6$.0013	4.6
	95% PI	± 0.111	± 0.186	± 0.34	$\pm 0.122 \times 10^6$	± 0.0026	± 9.7
8	Mean	29.188	19.077	120.55	4.445×10^6	0.8008	1237.7
	s	.011	.017	.90	$.008 \times 10^6$.0010	2.0
	95% PI	± 0.024	± 0.035	± 1.82	$\pm 0.016 \times 10^6$	± 0.0020	± 4.1
9	Mean	29.180	19.086	120.72	4.441×10^6	0.8000	1236.1
	s	.010	.010	1.10	$.010 \times 10^6$.0004	.9
	95% PI	± 0.020	± 0.020	± 2.24	$\pm 0.020 \times 10^6$	± 0.0009	± 1.9
10	Mean	29.182	19.084	119.66	4.452×10^6	0.8002	1236.4
	s	.014	.013	1.51	$.013 \times 10^6$.0005	1.2
	95% PI	± 0.027	± 0.026	± 3.04	$\pm 0.027 \times 10^6$	± 0.0011	± 2.3
11	Mean	15.595	10.201	120.68	2.373×10^6	0.8002	660.5
	s	.032	.018	.69	$.008 \times 10^6$.0004	1.7
	95% PI	± 0.064	± 0.036	± 1.39	$\pm 0.017 \times 10^6$	± 0.0008	± 3.4
12	Mean	15.600	10.204	119.82	2.378×10^6	0.8003	660.8
	s	.024	.017	.40	$.005 \times 10^6$.0004	1.1
	95% PI	± 0.049	± 0.034	± 0.81	$\pm 0.009 \times 10^6$	± 0.0009	± 2.1
13	Mean	15.600	10.201	120.68	2.374×10^6	0.8005	661.1
	s	.033	.022	1.06	$.007 \times 10^6$.0004	1.4
	95% PI	± 0.067	± 0.045	± 2.14	$\pm 0.014 \times 10^6$	± 0.0009	± 2.9

Table 10. Flow Condition Uncertainty Based on Quoted Instrument Uncertainty

p_t , psia	p_s , psia	T_t , °F	R_C , 10^6	M	q , psf
63.10 ± 0.010	41.30 ± 0.005	-250.0 ± 0.1	40.00 ± 0.031	0.800 ± 0.0002	2661 ± 1.4
68.40 ± 0.010	49.30 ± 0.005	-250.0 ± 0.1	40.00 ± 0.031	0.700 ± 0.0002	2426 ± 1.4
29.20 ± 0.003	19.10 ± 0.003	120.0 ± 0.1	4.45 ± 0.001	0.800 ± 0.0002	1236 ± 0.6
15.60 ± 0.003	10.20 ± 0.0015	120.0 ± 0.1	2.38 ± 0.001	0.800 ± 0.0002	660 ± 0.4



Figure 1. Model in NTF test section.

L-87-4167

Wing area (S) = 2.745 ft²
Wing span (b) = 55.8 in.
Wing aspect ratio (AR) = 7.877
Mean aerodynamic chord (\bar{c}) = 7.124 in.
Sweep back $c/4$ = 31.5°
Taper ratio = 0.267
Model scale = 0.03

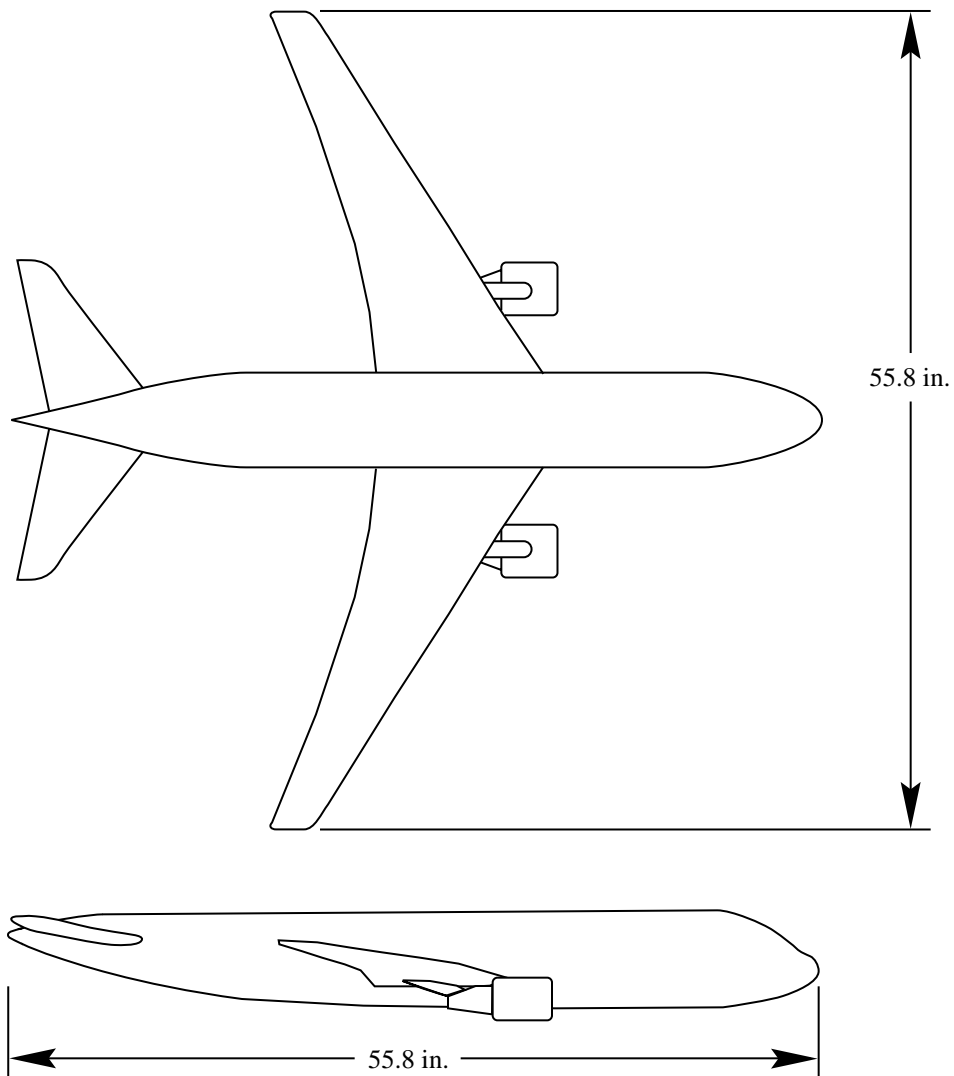


Figure 2. Model geometry.

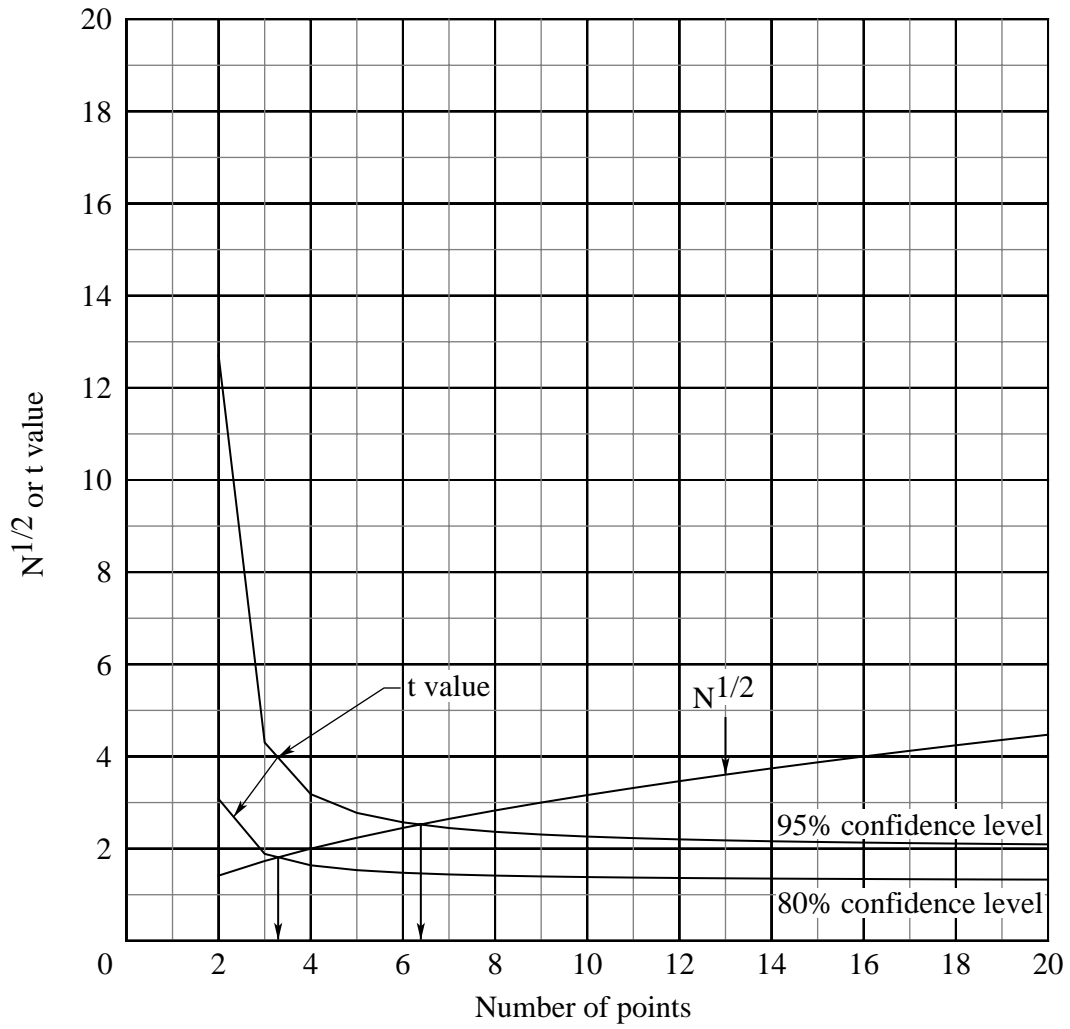
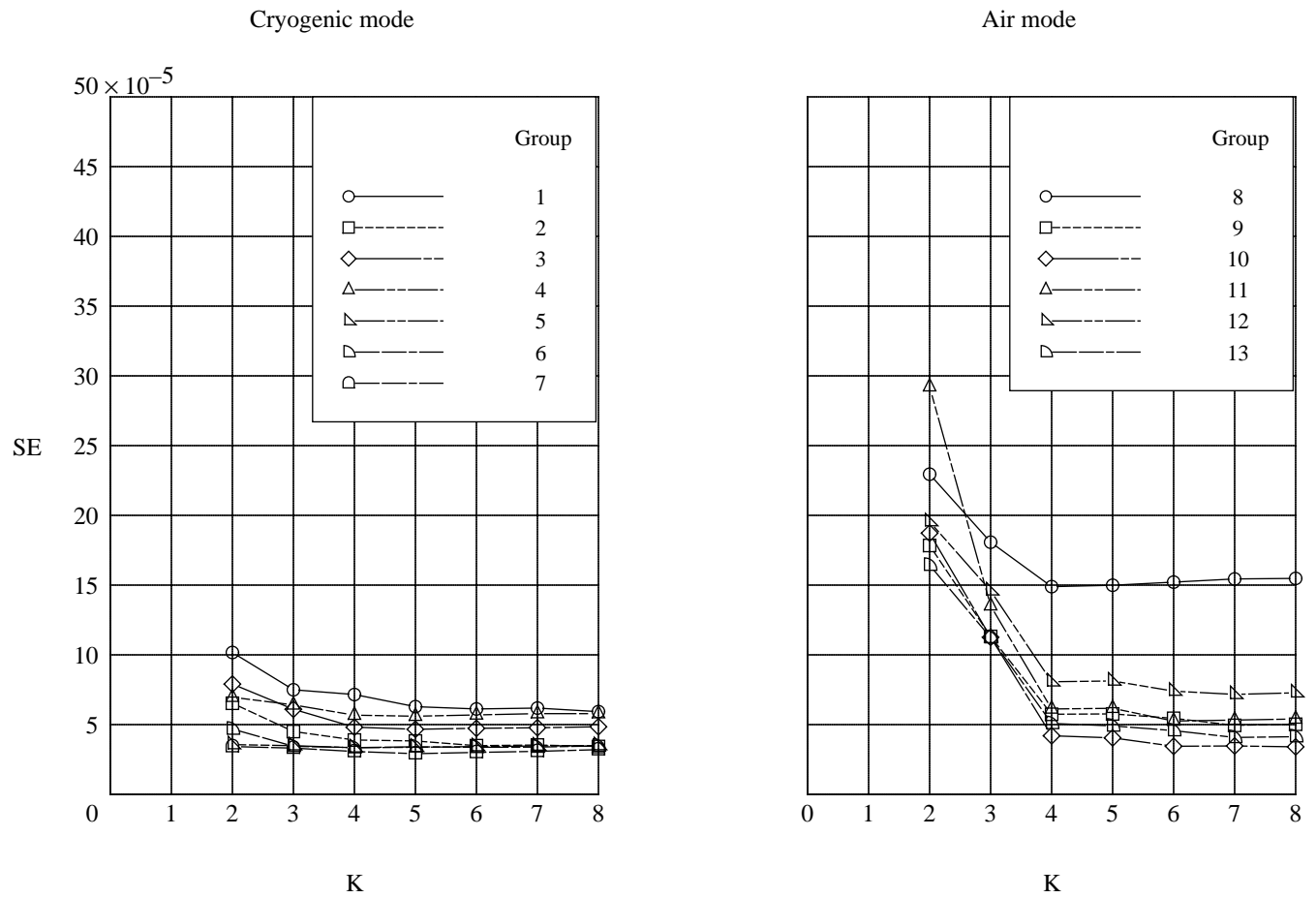
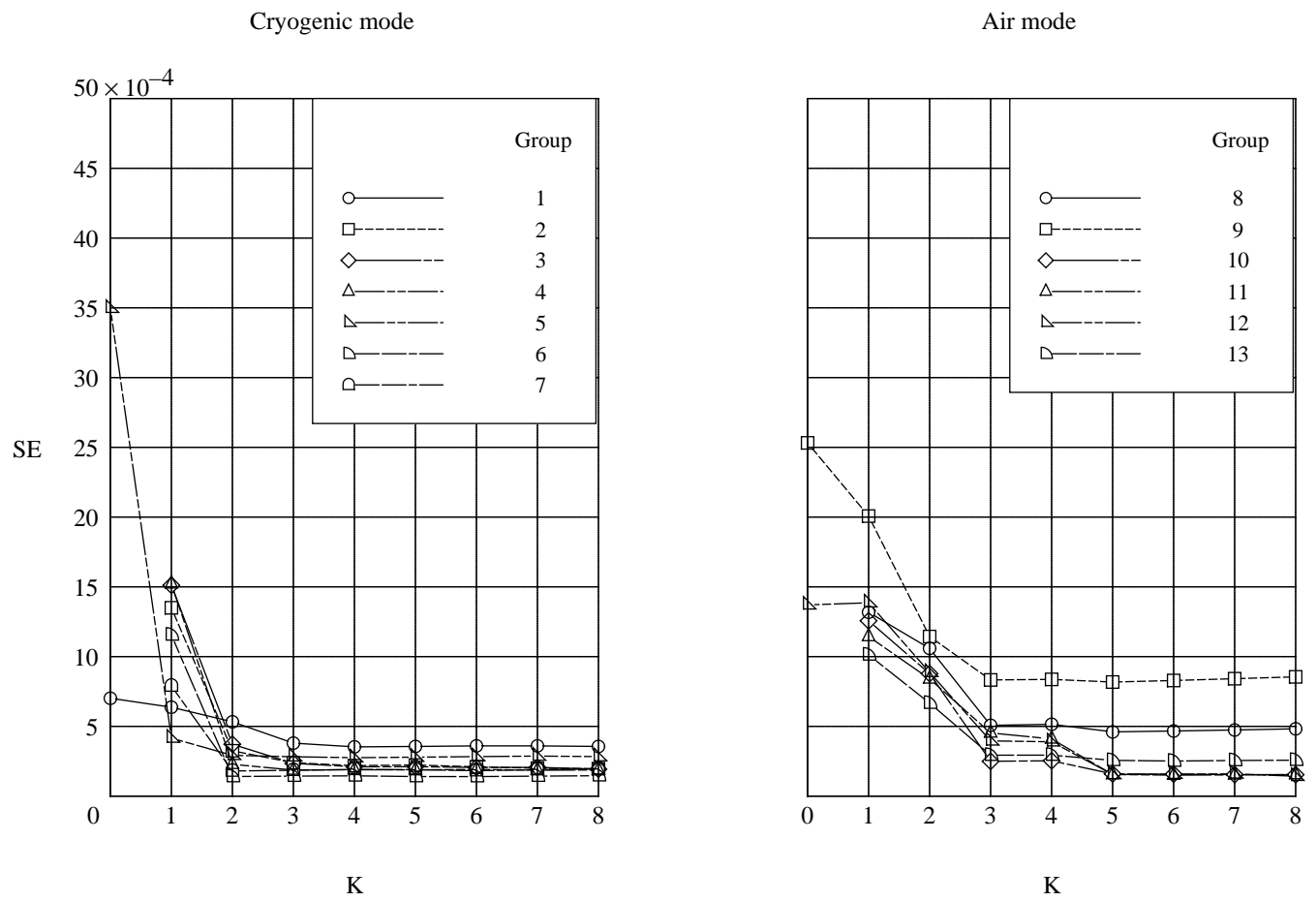


Figure 3. Variation of $N^{1/2}$ and t value with data sample size N .



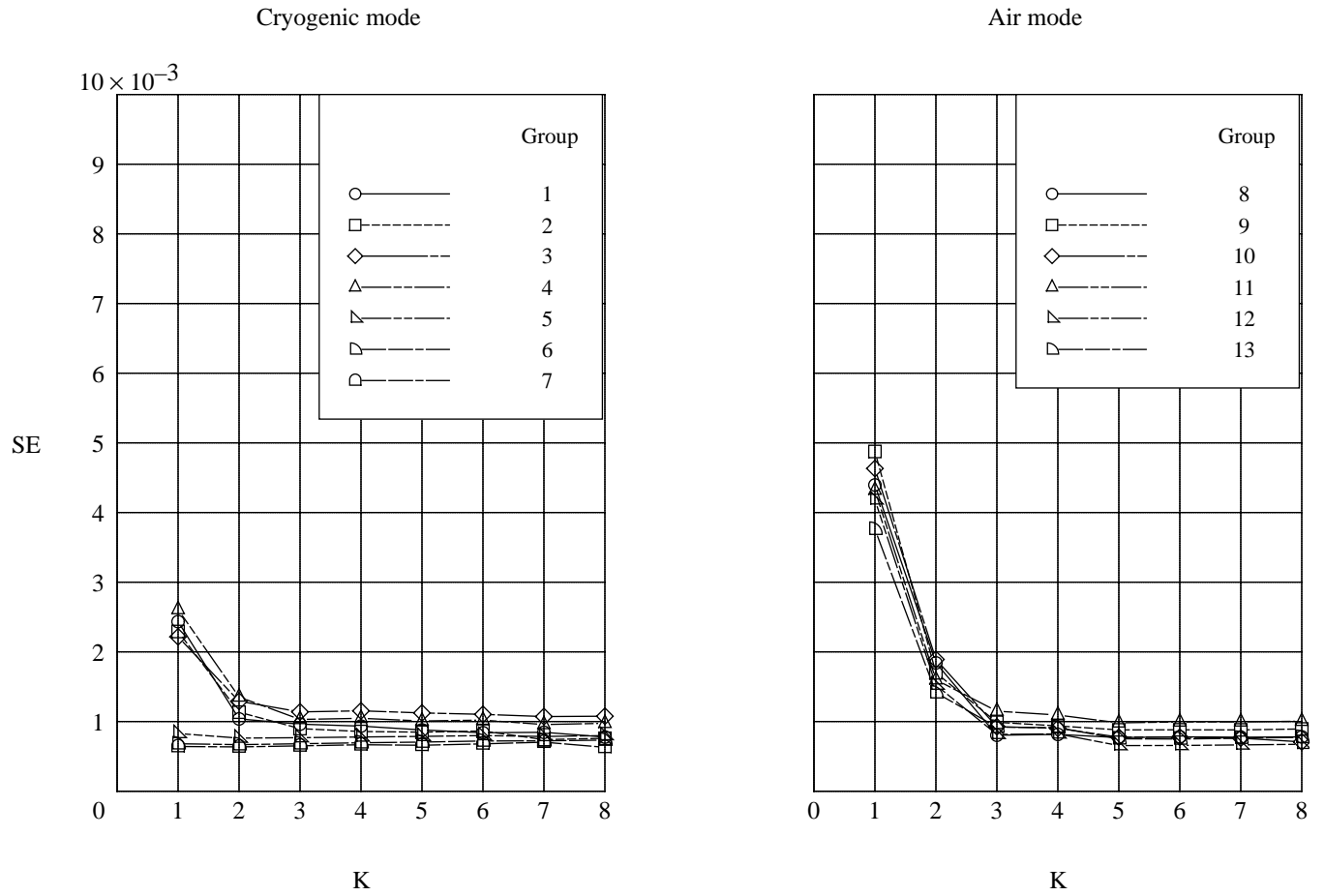
(a) C_D evaluated as a function of C_L .

Figure 4. Variation of standard error of longitudinal stability-axis coefficients as a function of order of polynomial regression model.



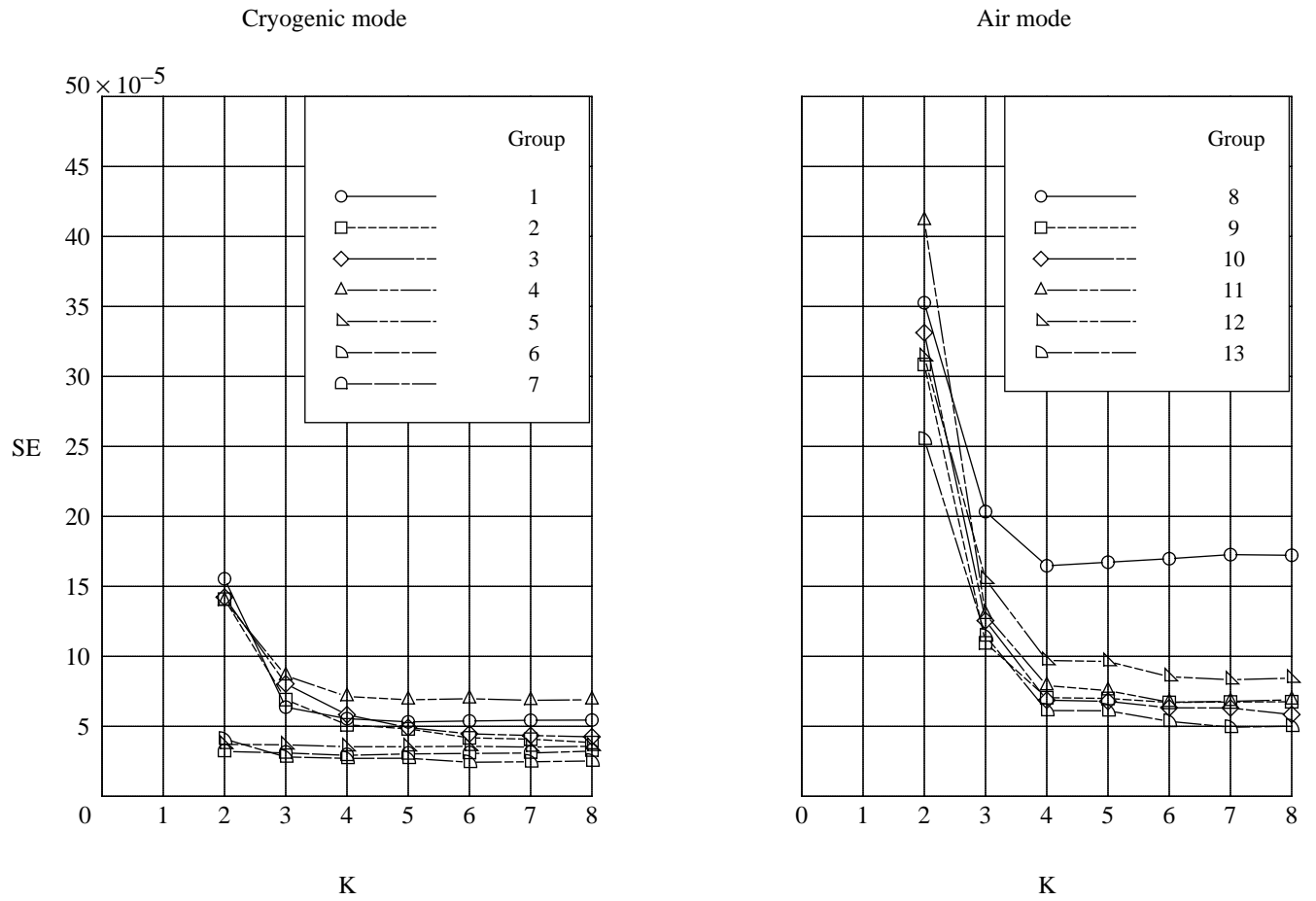
(b) C_m evaluated as a function of C_L .

Figure 4. Continued.



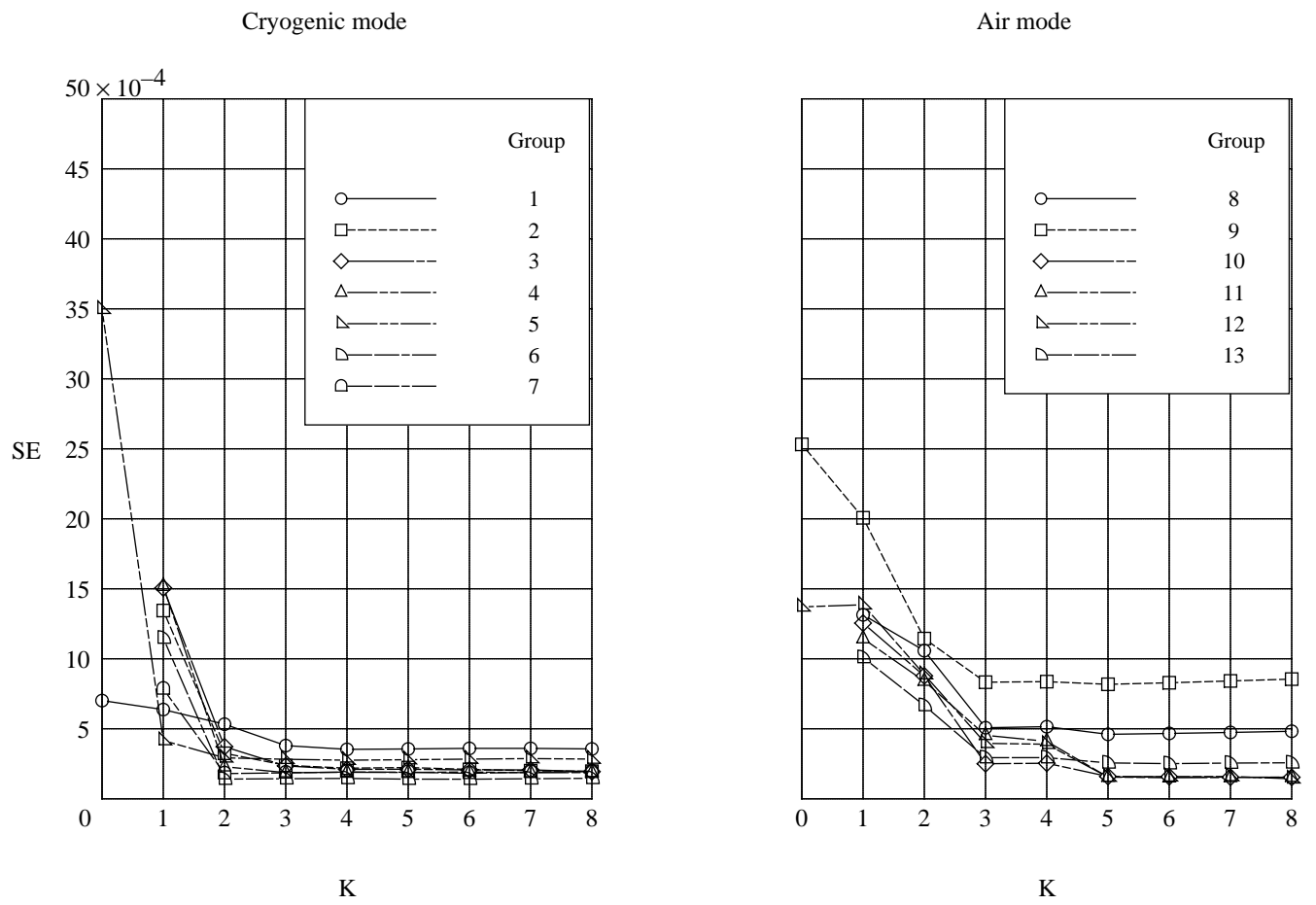
(c) C_L evaluated as a function of α .

Figure 4. Concluded.



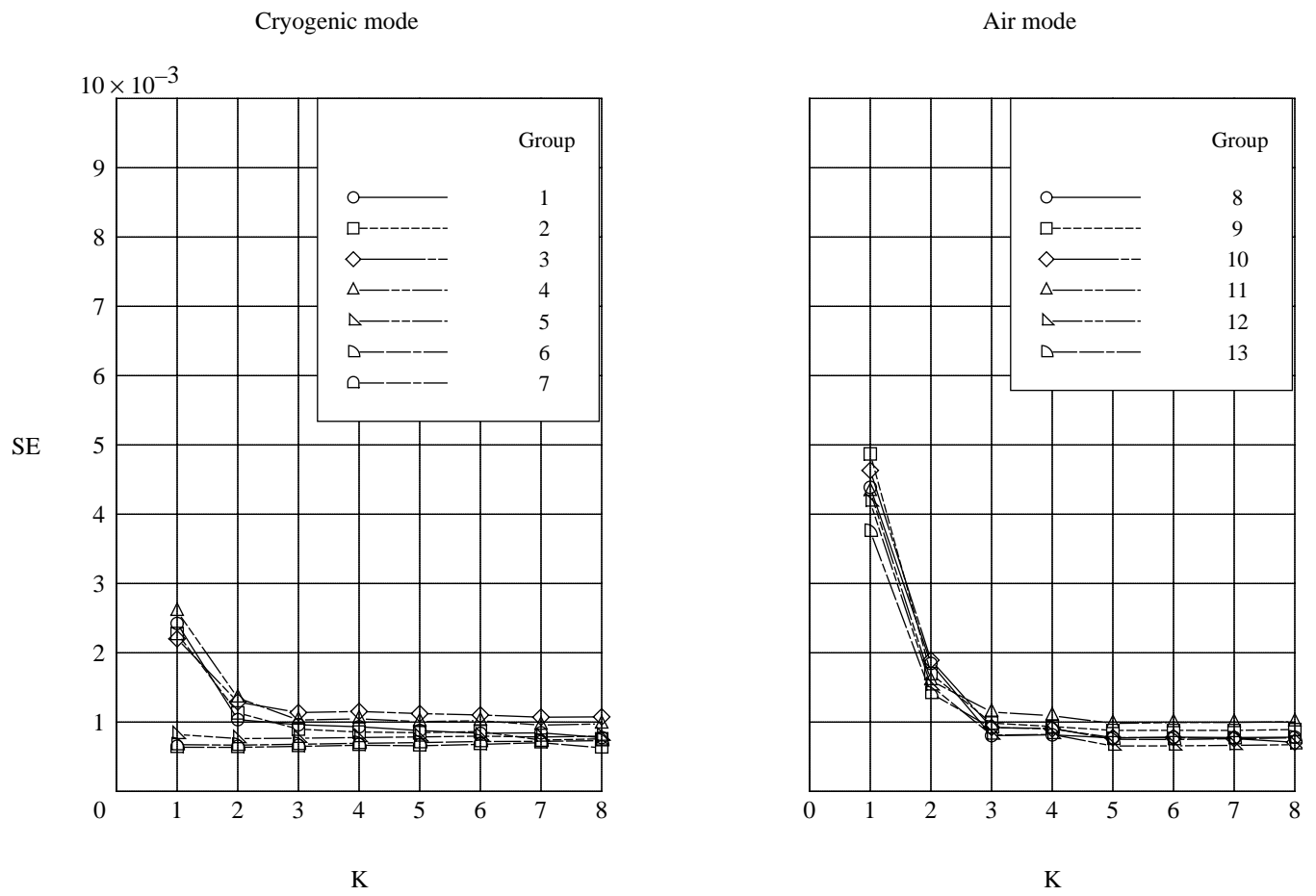
(a) C_A evaluated as a function of C_N .

Figure 5. Variation of standard error of longitudinal body-axis coefficients as a function of order of polynomial regression model.



(b) C_m evaluated as a function of C_N .

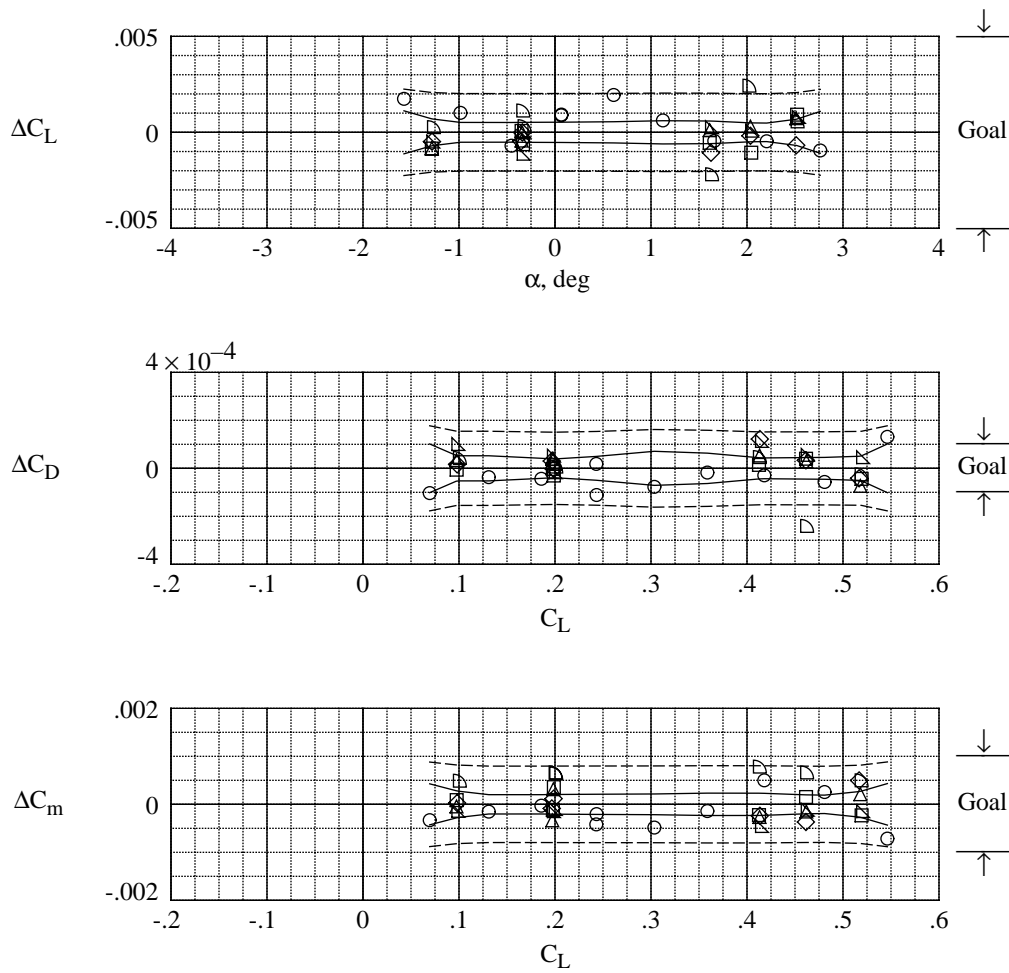
Figure 5. Continued.



(c) C_N evaluated as a function of α .

Figure 5. Concluded.

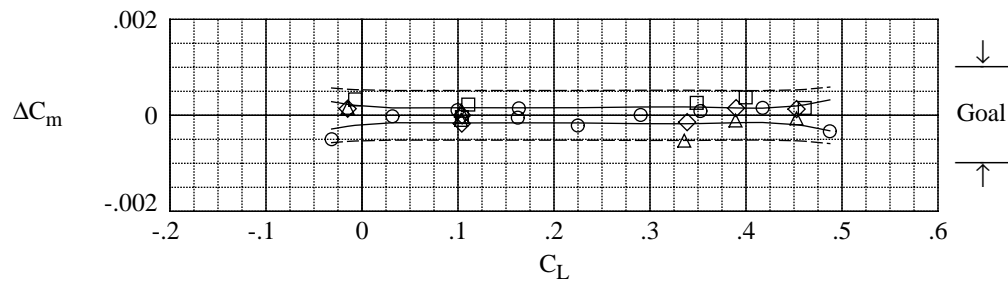
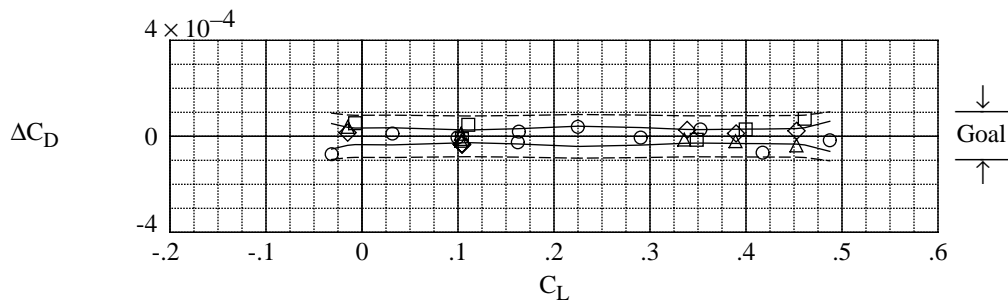
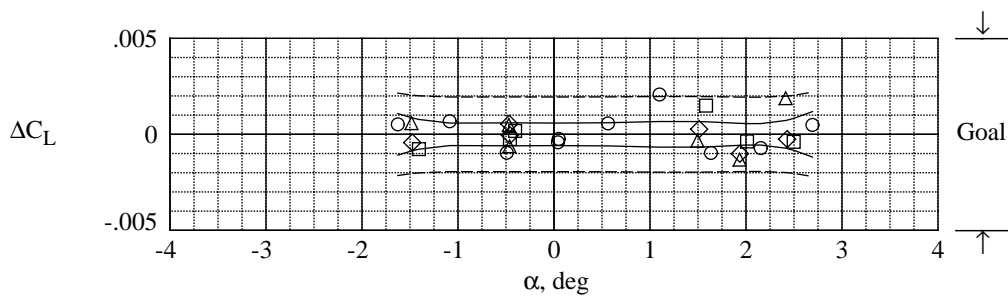
	Run	$R_{\bar{c}}$	M	q, psf
○	14	39.92×10^6	0.800	2660
□	16	39.93	.799	2658
◇	18	39.95	.799	2658
△	20	39.93	.800	2660
▽	22	39.96	.800	2661
▷	28	40.27	.800	2658
—	95% confidence interval			
- - -	95% prediction interval			



(a) Group 1.

Figure 6. Statistical results of C_L , C_D , and C_m short-term repeat data acquired in cryogenic mode.

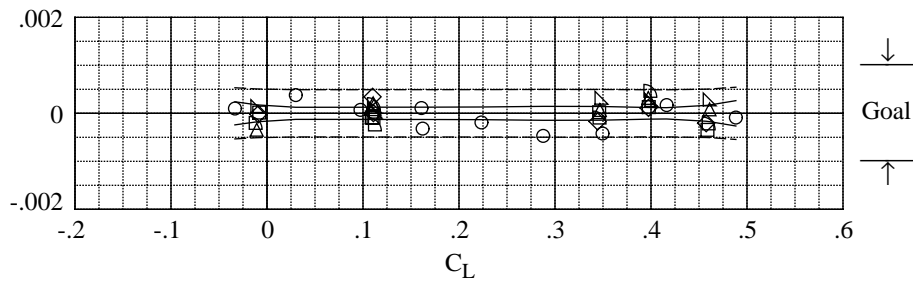
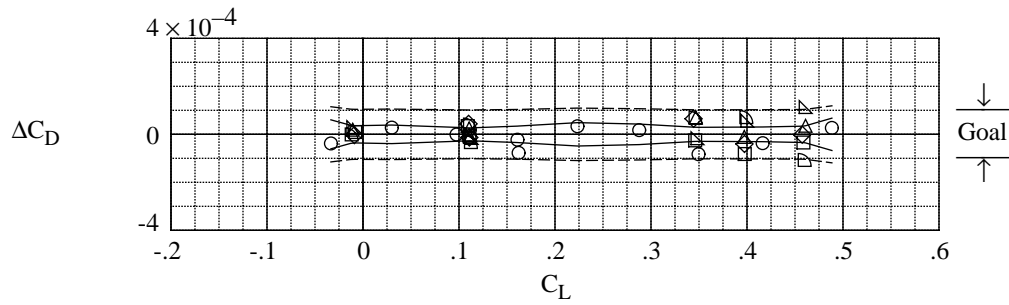
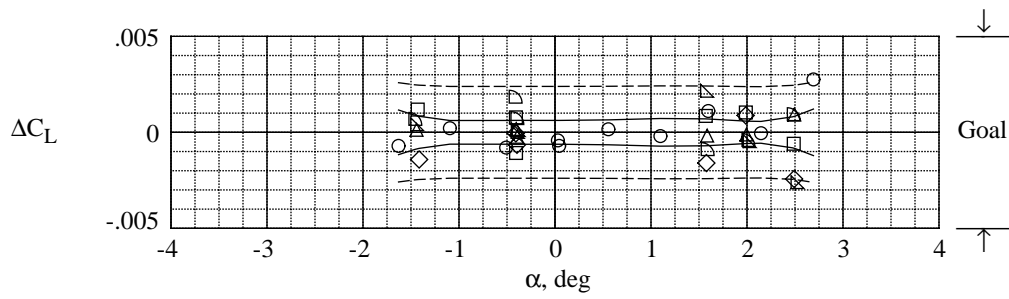
	Run	$R_{\bar{c}}$	M	q, psf
○	44	40.17×10^6	0.800	2662
□	46	40.18	.800	2664
◇	48	40.11	.799	2656
△	50	40.12	.799	2656
—	95% confidence interval			
- - -	95% prediction interval			



(b) Group 2.

Figure 6. Continued.

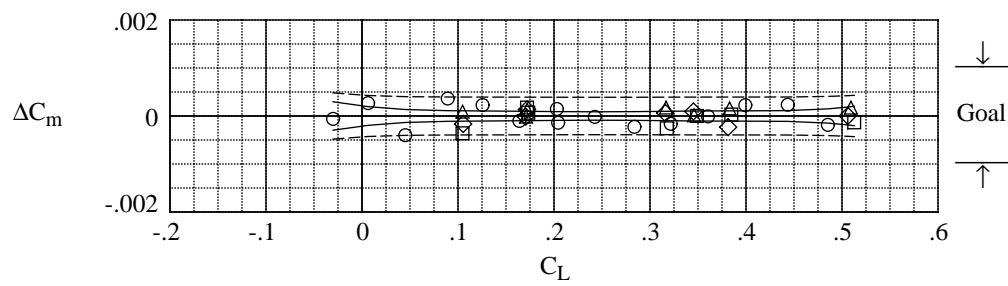
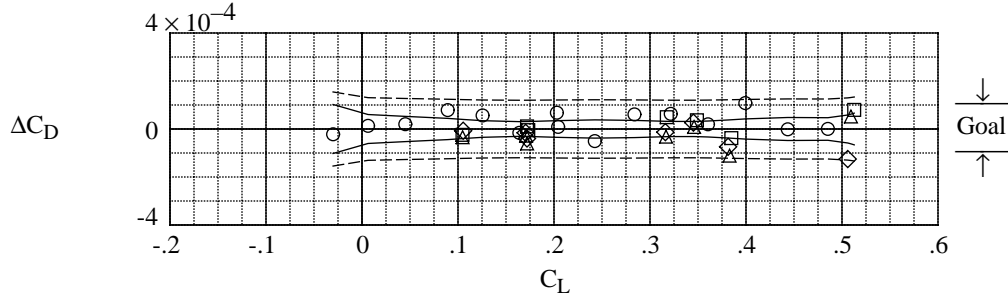
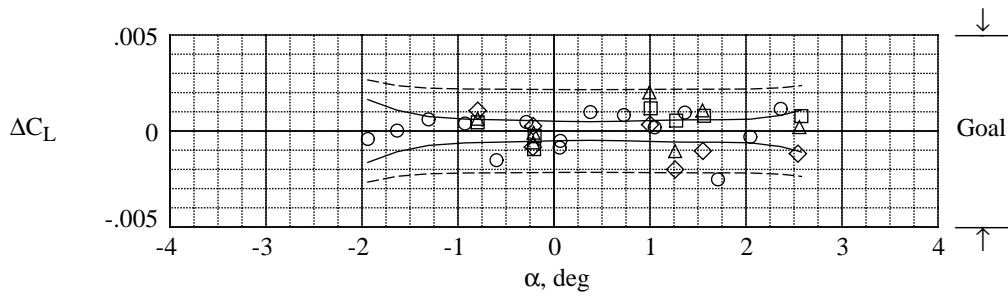
	Run	$R_{\bar{c}}$	M	q, psf
○	147	40.12×10^6	0.800	2659
□	148	40.17	.800	2659
◇	149	40.14	.799	2658
△	150	40.12	.800	2659
▽	151	40.16	.800	2661
▷	152	40.14	.800	2659
—	95% confidence interval			
- - -	95% prediction interval			



(c) Group 3.

Figure 6. Continued.

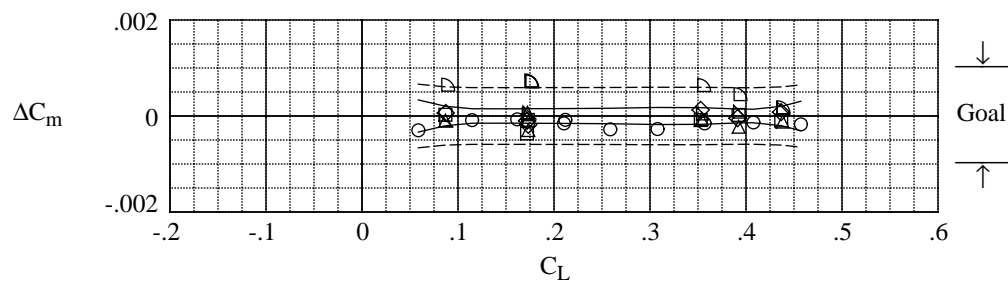
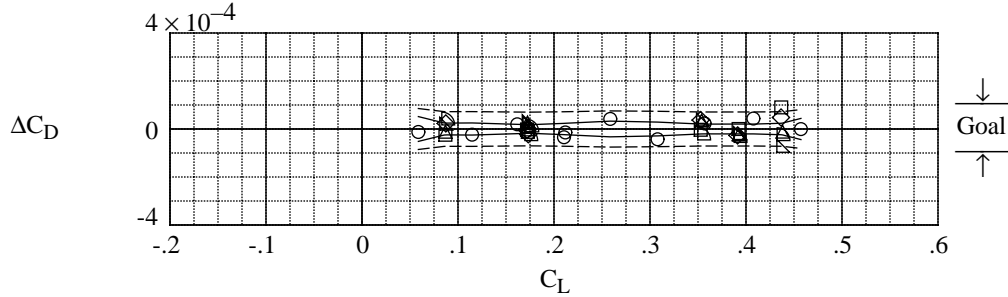
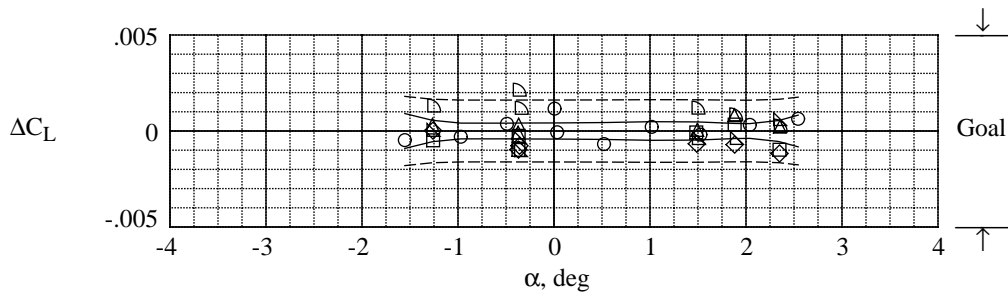
	Run	R_c	M	q, psf
○	156	40.25×10^6	0.801	2666
□	158	40.21	.801	2662
◇	160	40.14	.799	2656
△	162	40.23	.800	2661
—	95% confidence interval			
- - -	95% prediction interval			



(d) Group 4.

Figure 6. Continued.

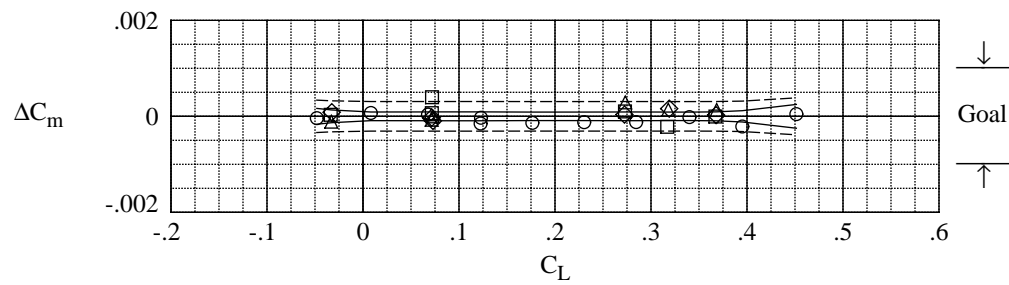
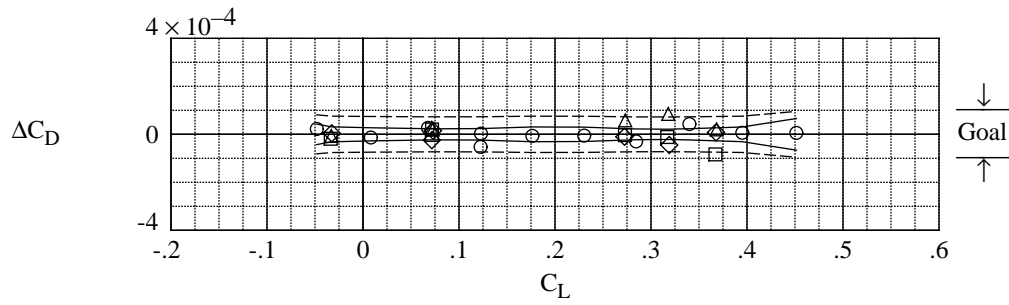
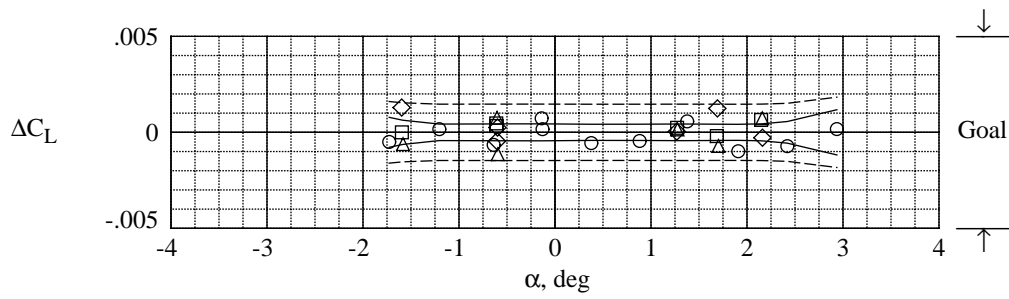
	Run	R_c	M	q, psf
○	15	39.89×10^6	.700	2426
□	17	39.90	.700	2426
◇	19	39.91	.699	2424
△	21	39.92	.700	2428
▴	23	39.91	.699	2422
▾	29	40.28	.701	2430
—	95% confidence interval			
- - -	95% prediction interval			



(e) Group 5.

Figure 6. Continued.

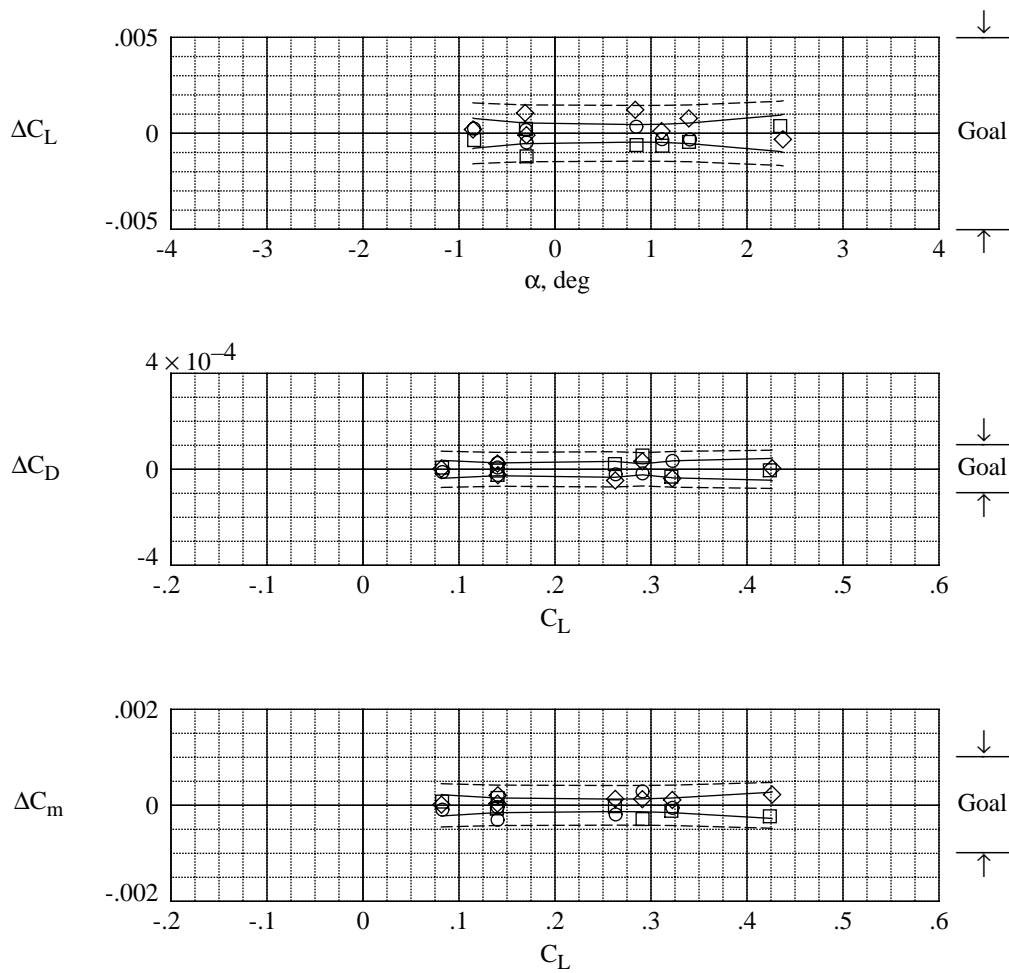
	Run	$R_{\bar{c}}$	M	q, psf
○	45	40.24×10^6	0.699	2423
□	47	40.25	.700	2428
◇	49	40.26	.700	2429
△	51	40.31	.700	2429
—	95% confidence interval			
- - -	95% prediction interval			



(f) Group 6.

Figure 6. Continued.

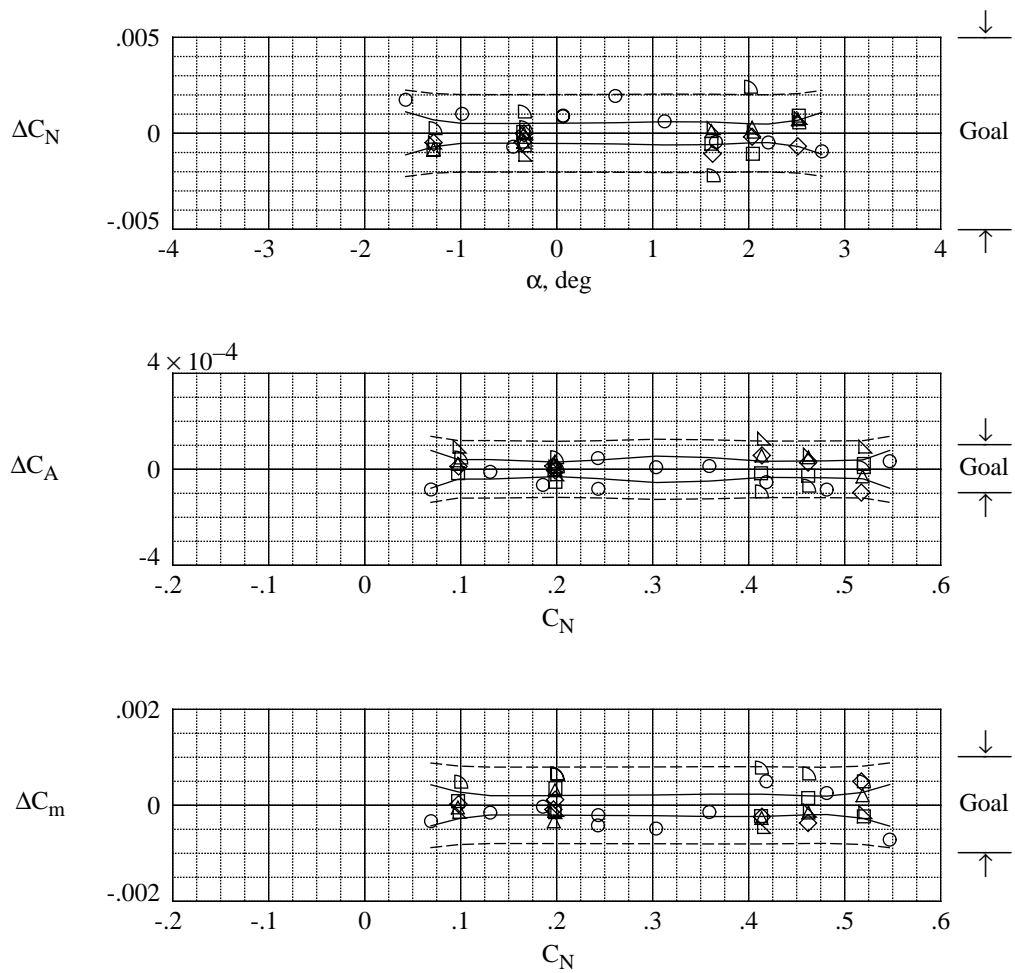
	Run	$R_{\bar{c}}$	M	q, psf
○	157	40.20×10^6	0.700	2424
□	159	40.16	.700	2423
◇	161	40.22	.702	2431
—	95% confidence interval			
- - -	95% prediction interval			



(g) Group 7.

Figure 6. Concluded.

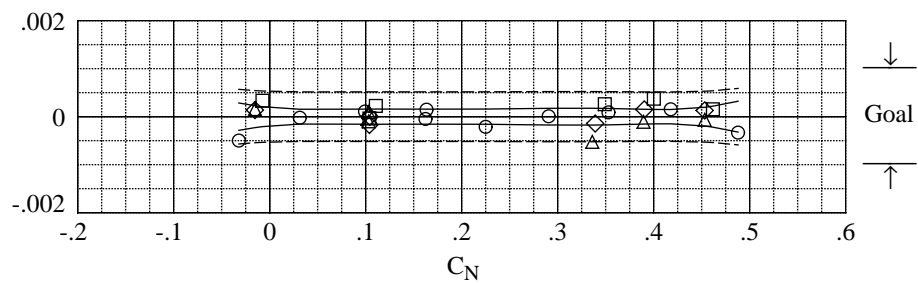
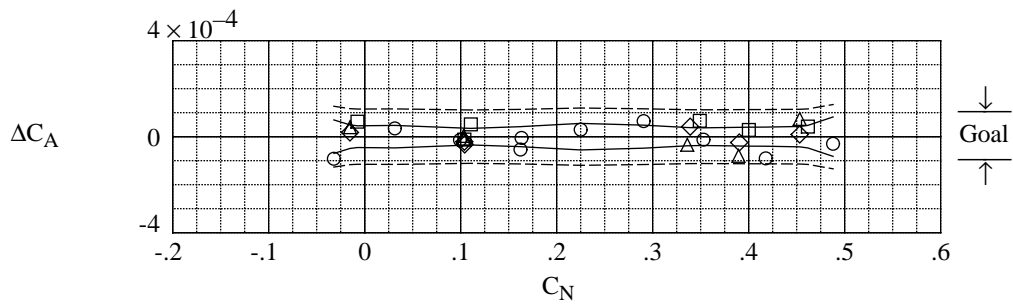
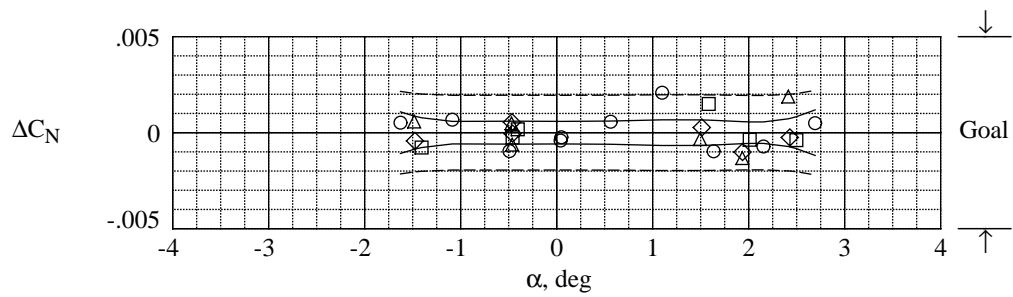
	Run	$R_{\bar{c}}$	M	q, psf
○	14	39.92×10^6	0.800	2660
□	16	39.93	.799	2658
◇	18	39.95	.799	2658
△	20	39.93	.800	2660
▽	22	39.96	.800	2661
▷	28	40.27	.800	2658
—	95% confidence interval			
- - -	95% prediction interval			



(a) Group 1.

Figure 7. Statistical results of C_N , C_A , and C_m short-term repeat data acquired in cryogenic mode.

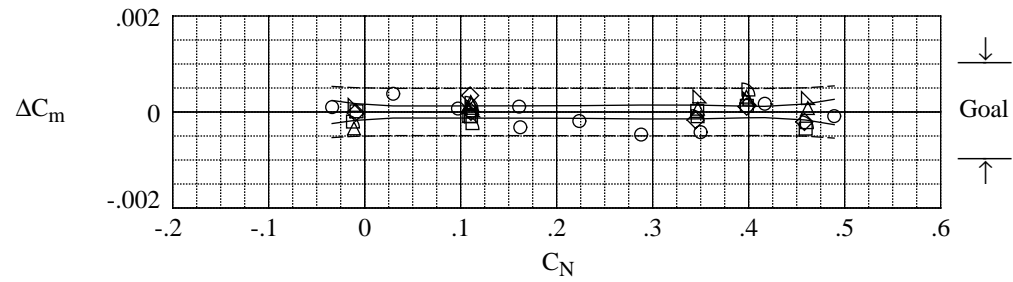
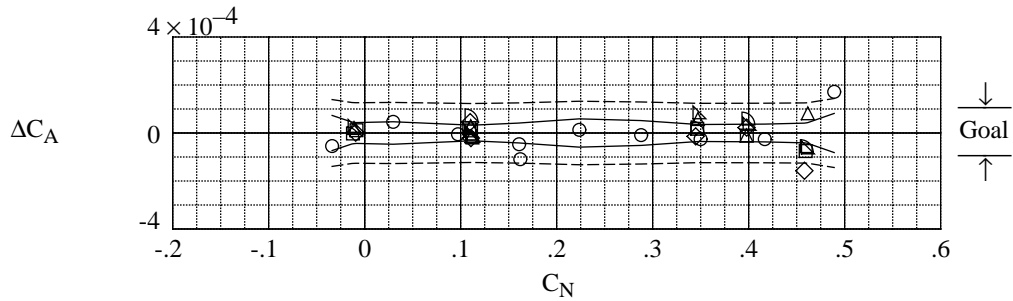
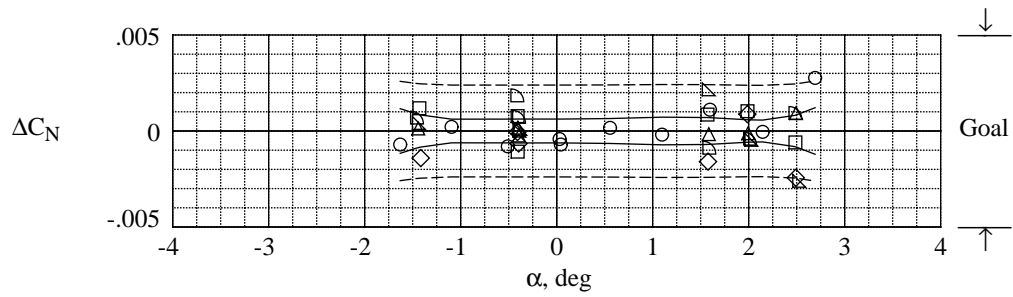
	Run	$R_{\bar{c}}$	M	q, psf
○	44	40.17×10^6	0.800	2662
□	46	40.18	.800	2664
◇	48	40.11	.799	2656
△	50	40.12	.799	2656
—	95% confidence interval			
- - -	95% prediction interval			



(b) Group 2.

Figure 7. Continued.

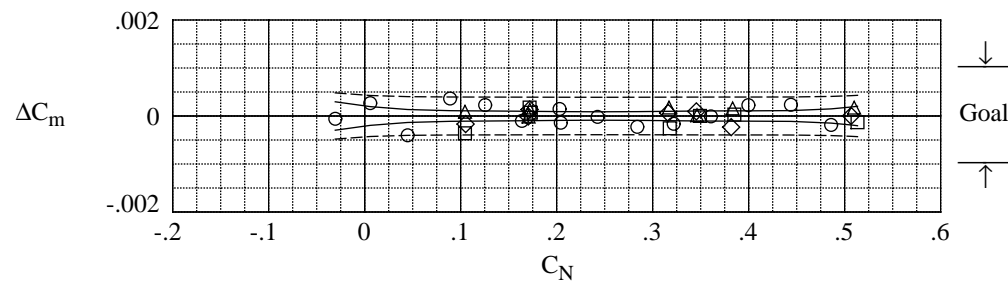
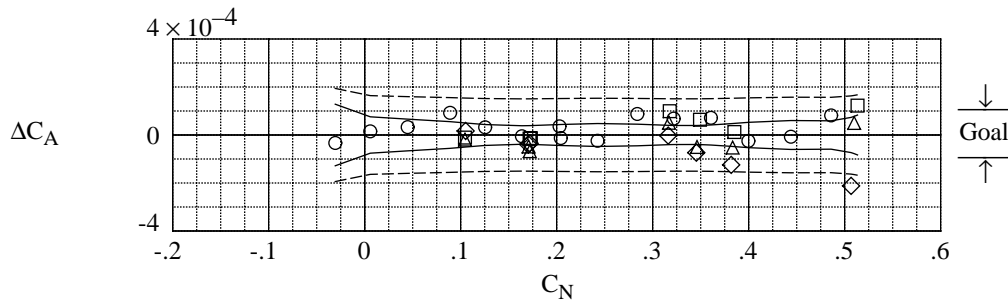
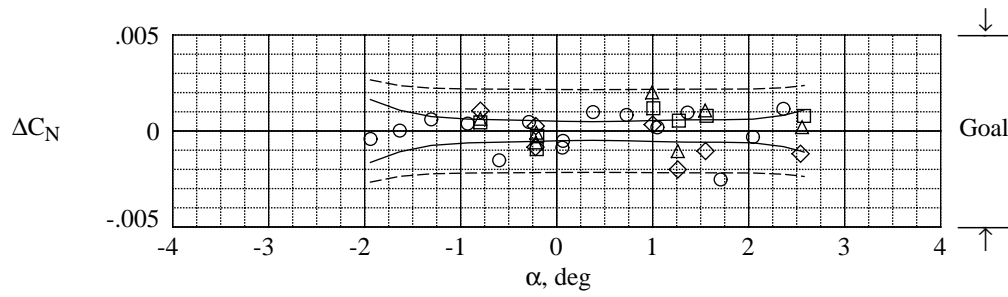
	Run	$R_{\bar{c}}$	M	q, psf
○	147	40.12×10^6	0.800	2659
□	148	40.17	.800	2659
◇	149	40.14	.799	2658
△	150	40.12	.800	2659
▽	151	40.16	.800	2661
▷	152	40.14	.800	2659
—	95% confidence interval			
- - -	95% prediction interval			



(c) Group 3.

Figure 7. Continued.

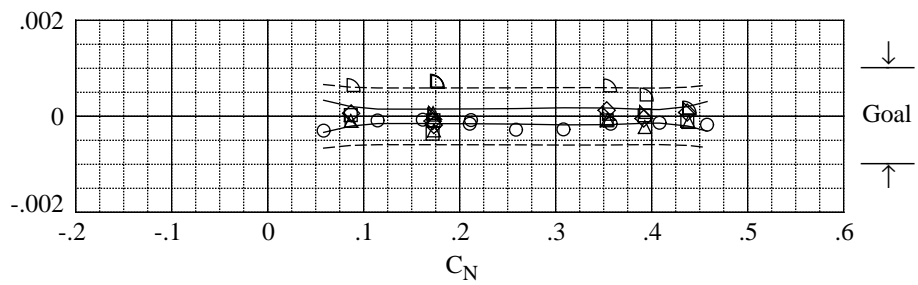
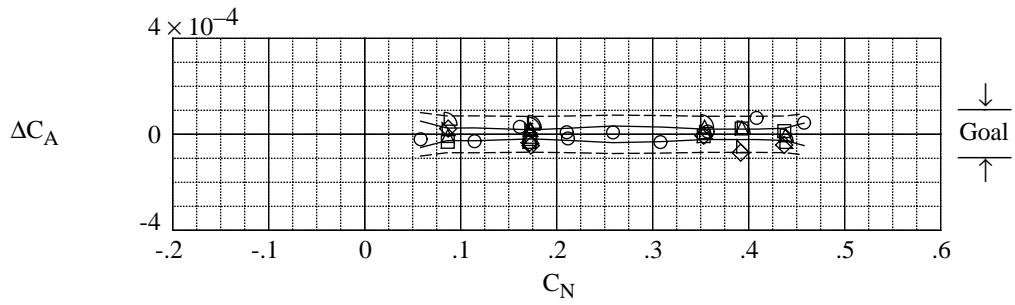
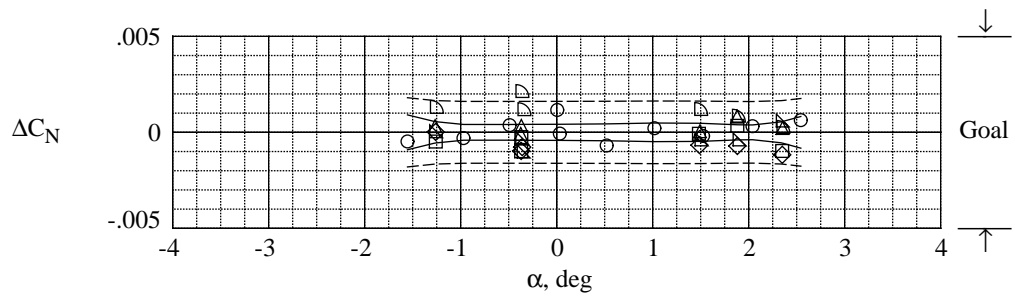
	Run	$R_{\bar{c}}$	M	q, psf
○	156	40.25×10^6	0.801	2666
□	158	40.21	.801	2662
◇	160	40.14	.799	2656
△	162	40.23	.800	2661
—	95% confidence interval			
- - -	95% prediction interval			



(d) Group 4.

Figure 7. Continued.

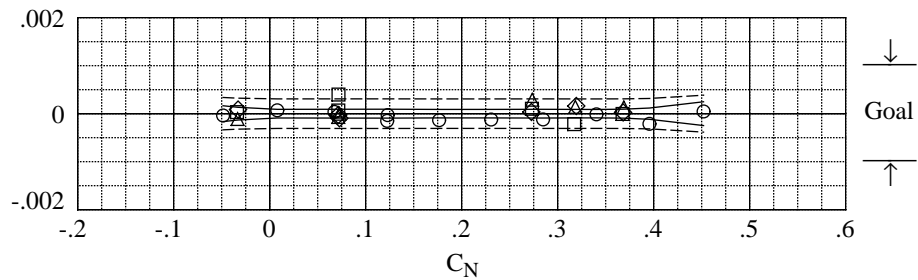
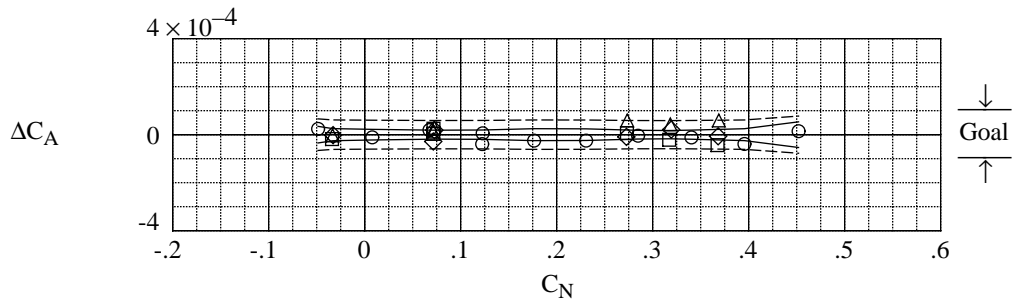
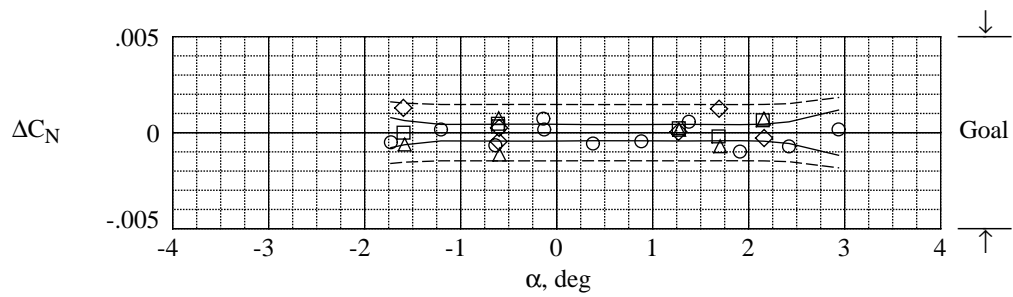
	Run	$R_{\bar{c}}$	M	q, psf
○	15	39.89×10^6	0.700	2426
□	17	39.90	.700	2426
◇	19	39.91	.699	2424
△	21	39.92	.700	2428
▽	23	39.91	.699	2422
▷	29	40.28	.701	2430
—	95% confidence interval			
- - -	95% prediction interval			



(e) Group 5.

Figure 7. Continued.

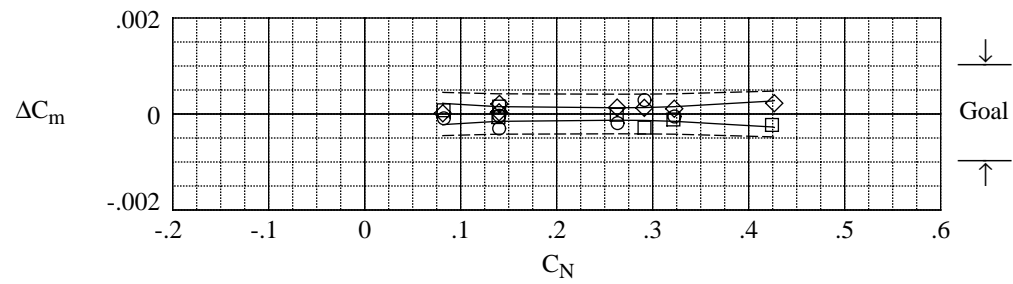
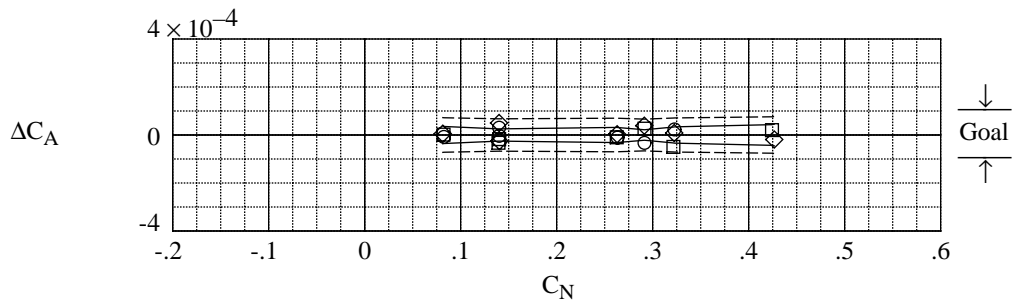
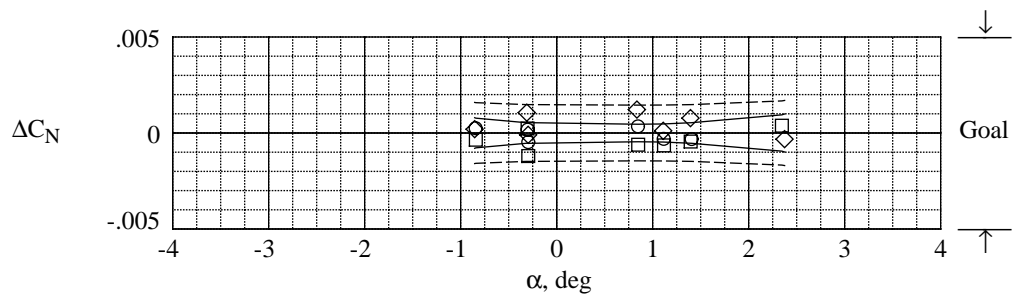
	Run	$R_{\bar{c}}$	M	q, psf
○	45	40.24×10^6	0.699	2423
□	47	40.25	.700	2428
◇	49	40.26	.700	2429
△	51	40.31	.700	2429
—	95% confidence interval			
- - -	95% prediction interval			



(f) Group 6.

Figure 7. Continued.

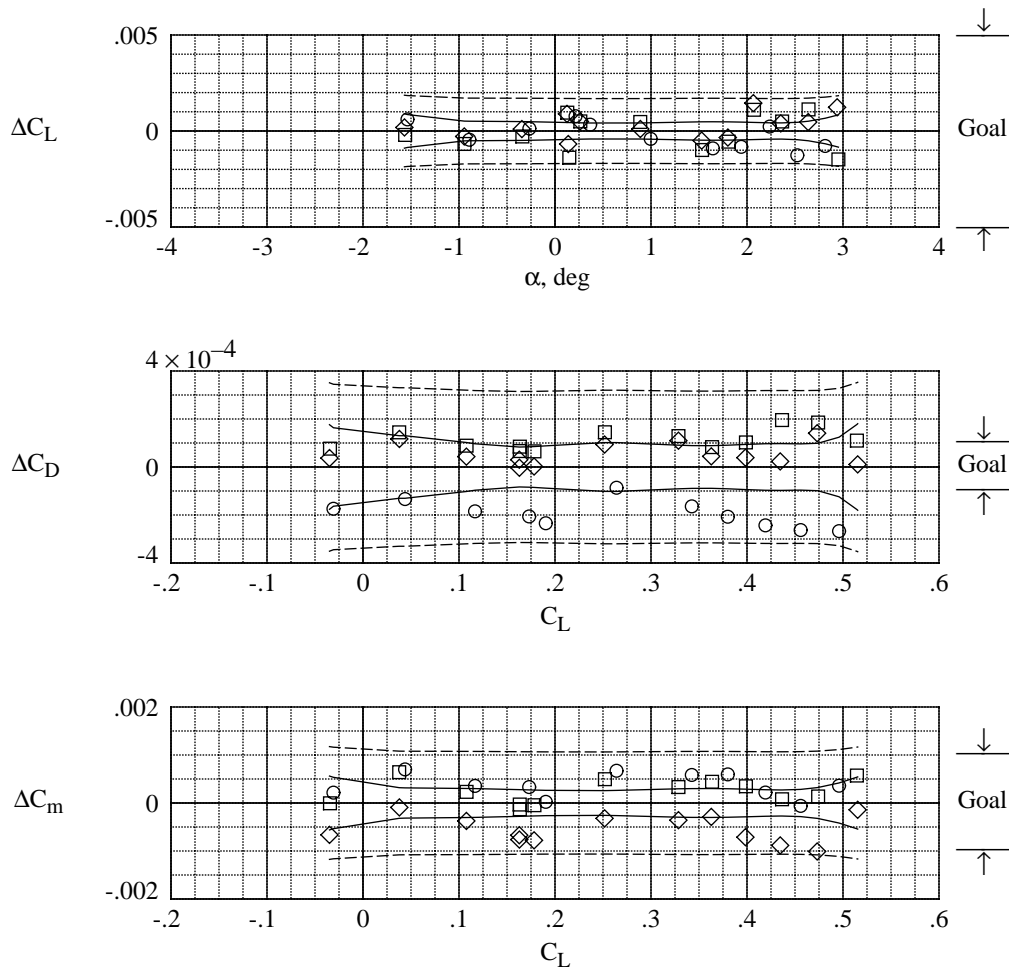
	Run	$R_{\bar{c}}$	M	q, psf
○	157	40.20×10^6	0.700	2424
□	159	40.16	.700	2423
◇	161	40.22	.702	2431
—	95% confidence interval			
- - -	95% prediction interval			



(g) Group 7.

Figure 7. Concluded.

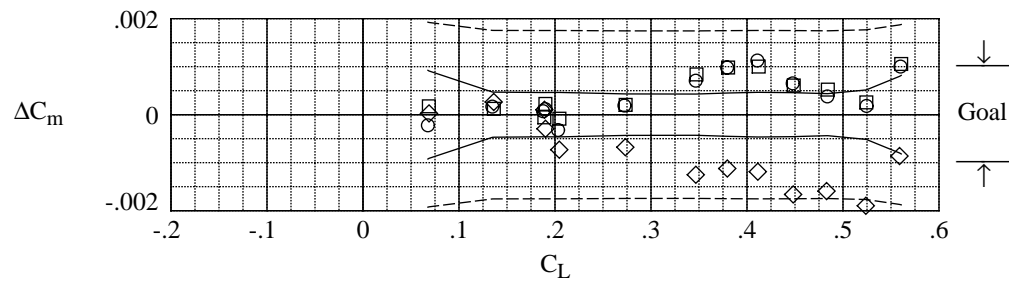
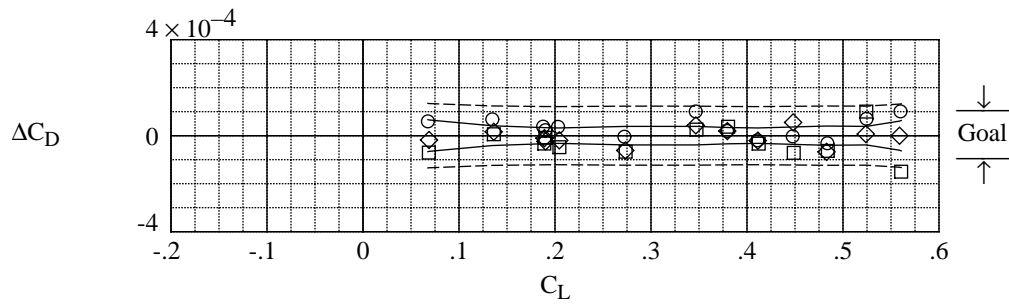
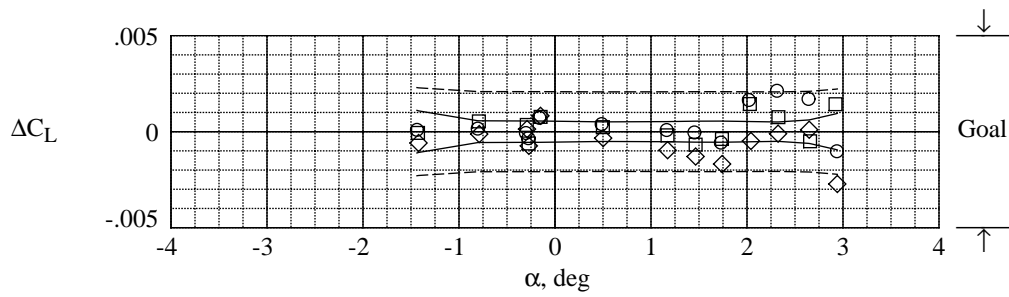
	Run	$R_{\bar{c}}$	M	q, psf
○	113	4.44×10^6	0.799	1235
□	117	4.45	.801	1239
◇	121	4.44	.801	1239
—	95% confidence interval			
- - -	95% prediction interval			



(a) Group 8.

Figure 8. Statistical results of C_L , C_D , and C_m short-term repeat data acquired in air mode.

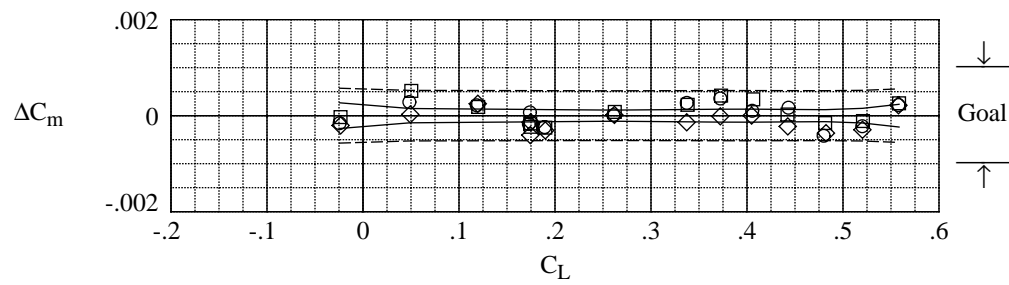
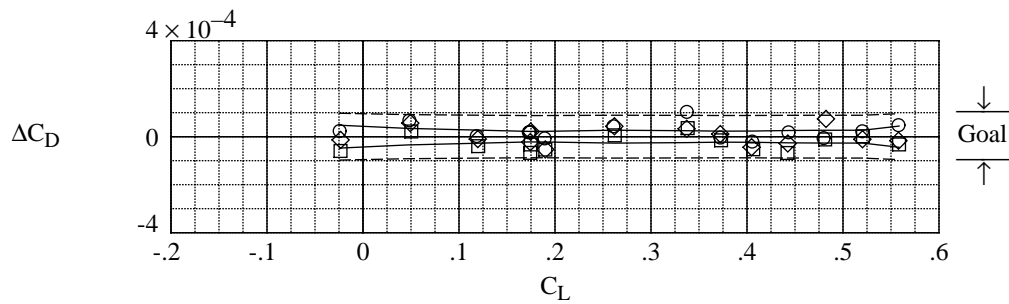
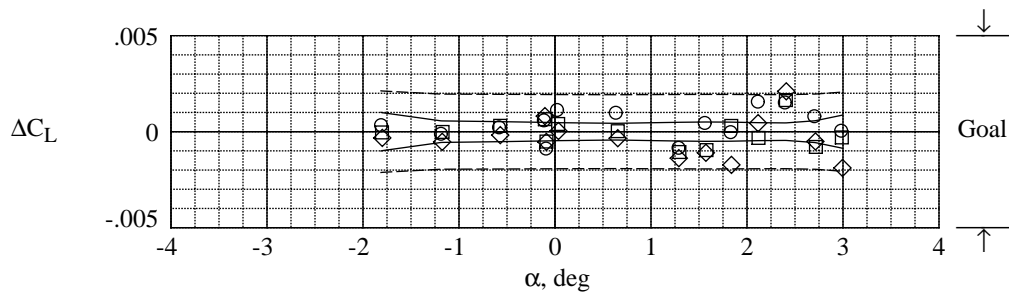
	Run	$R_{\bar{c}}$	M	q, psf
○	124	4.43×10^6	0.800	1237
□	128	4.45	.800	1236
◇	133	4.44	.800	1235
—	95% confidence interval			
- - -	95% prediction interval			



(b) Group 9.

Figure 8. Continued.

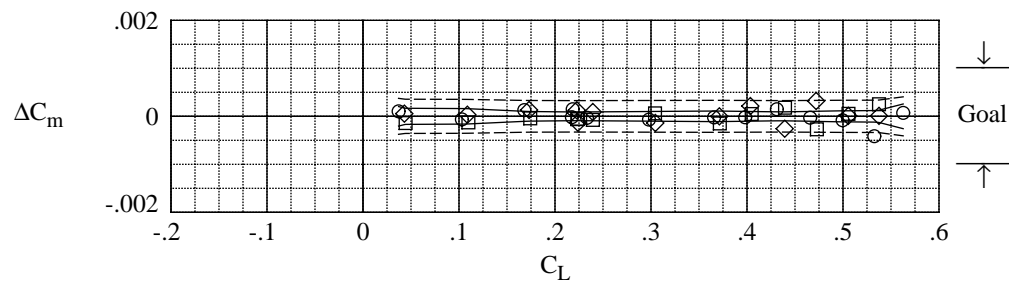
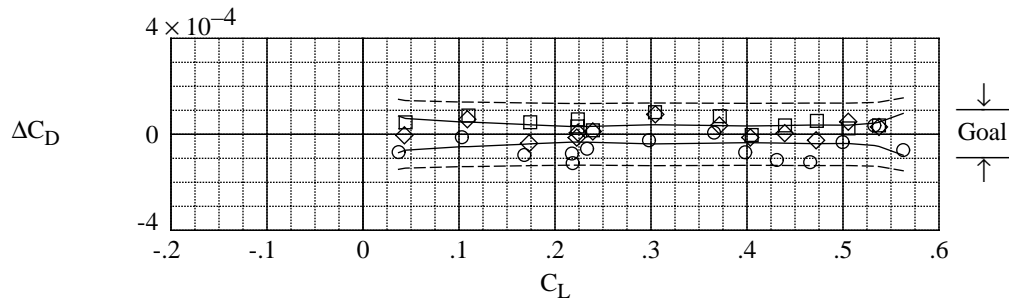
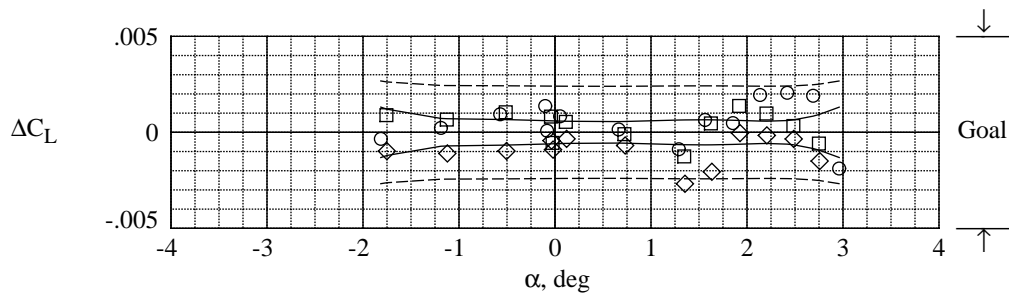
	Run	$R_{\bar{c}}$	M	q, psf
○	136	4.44×10^6	0.800	1237
□	140	4.47	.800	1236
◇	144	4.45	.800	1237
—	95% confidence interval			
- - -	95% prediction interval			



(c) Group 10.

Figure 8. Continued.

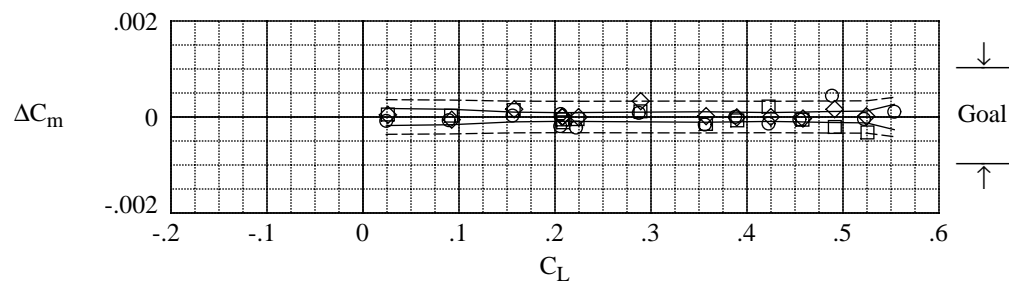
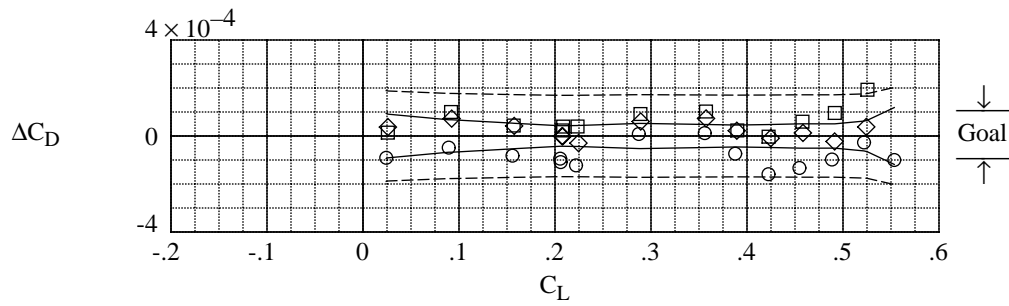
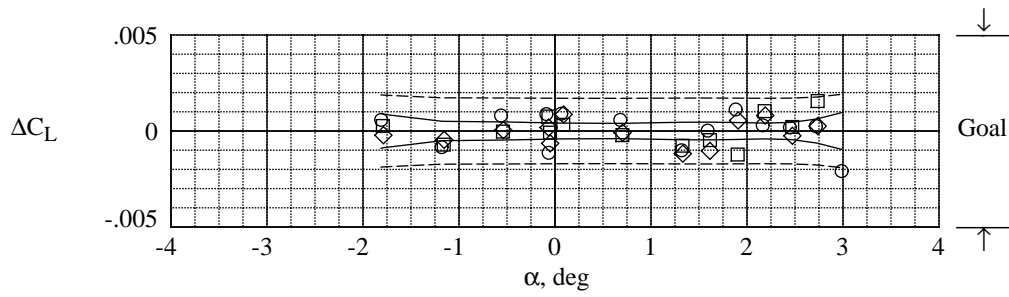
	Run	$R_{\bar{c}}$	M	q, psf
○	68	2.36×10^6	0.800	658
□	72	2.38	.800	662
◇	76	2.38	.800	662
—	95% confidence interval			
- - -	95% prediction interval			



(d) Group 11.

Figure 8. Continued.

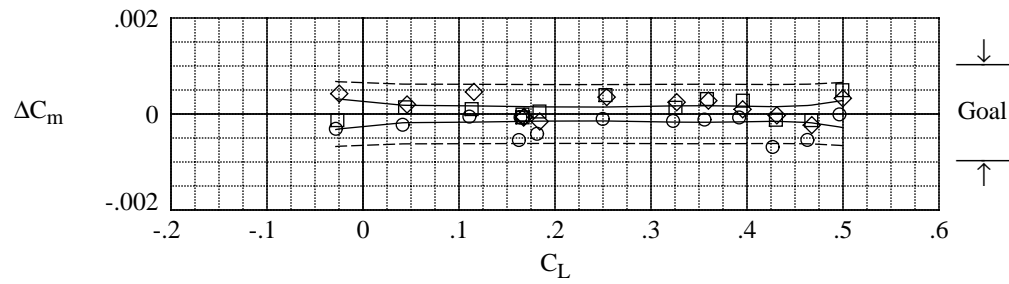
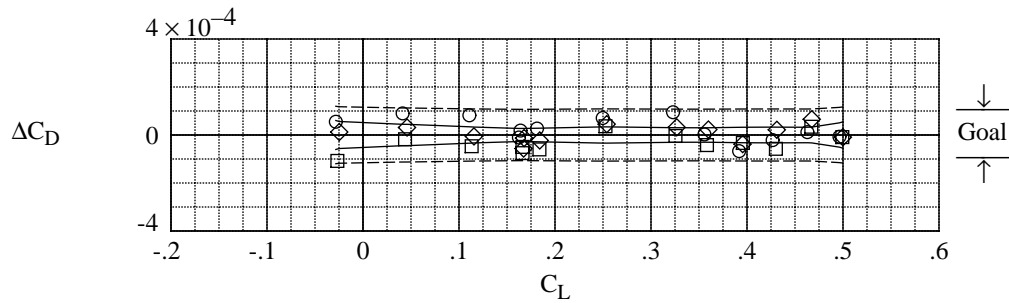
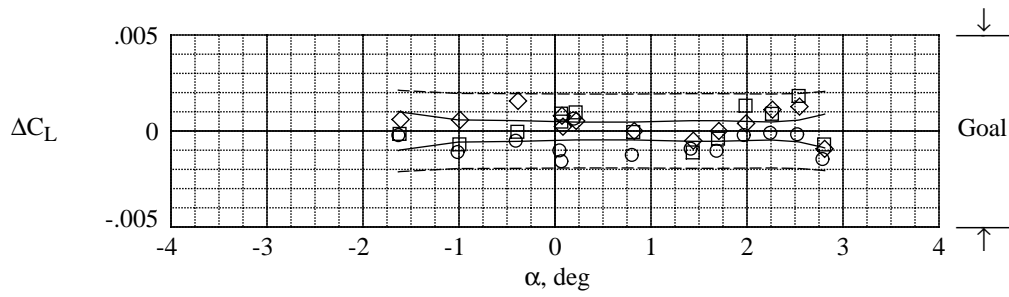
	Run	$R_{\bar{c}}$	M	q, psf
○	79	2.38×10^6	0.800	661
□	83	2.37	.800	660
◇	87	2.38	.800	662
—	95% confidence interval			
- - -	95% prediction interval			



(e) Group 12.

Figure 8. Continued.

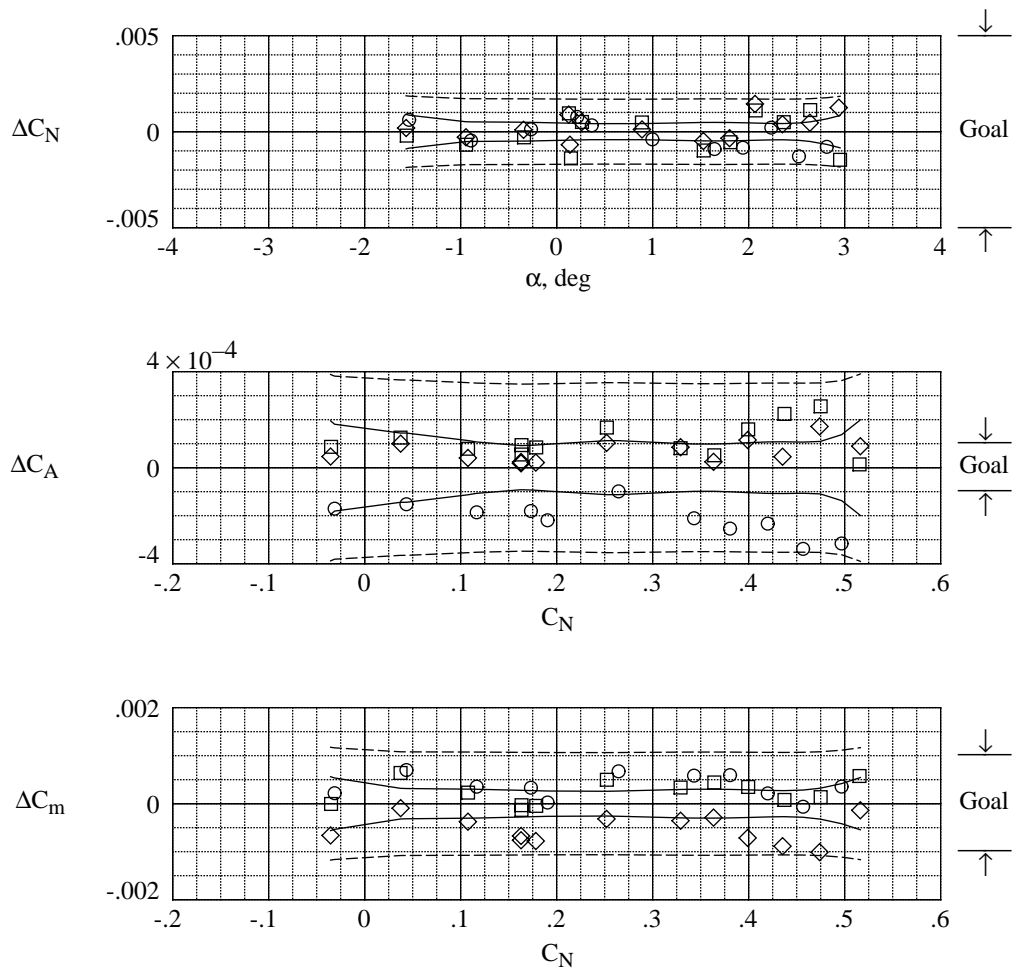
	Run	$R_{\bar{c}}$	M	q, psf
○	90	2.37×10^6	0.800	660
□	94	2.37	.801	660
◇	98	2.38	.801	663
—	95% confidence interval			
- - -	95% prediction interval			



(f) Group 13.

Figure 8. Concluded.

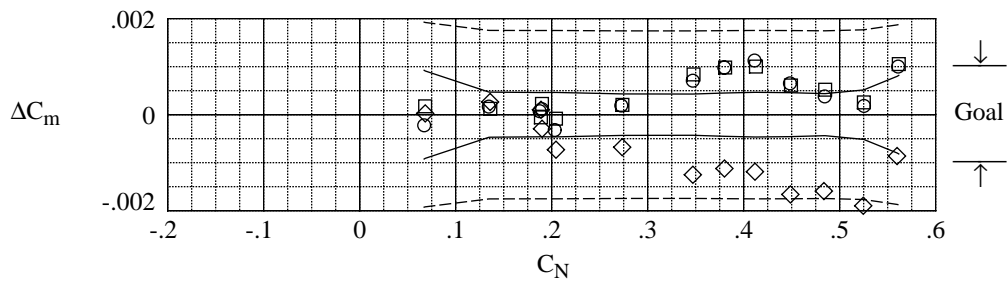
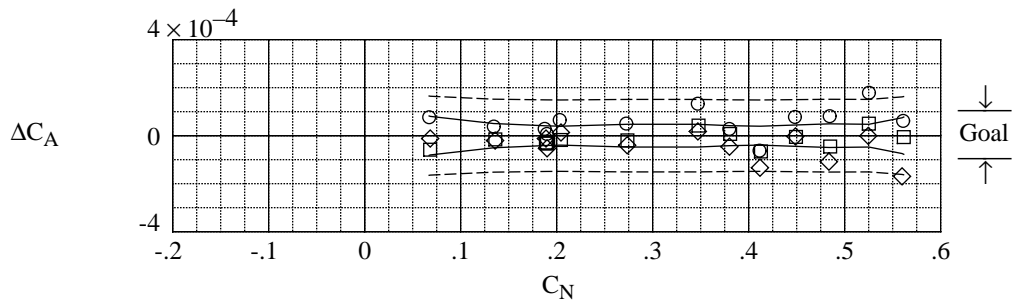
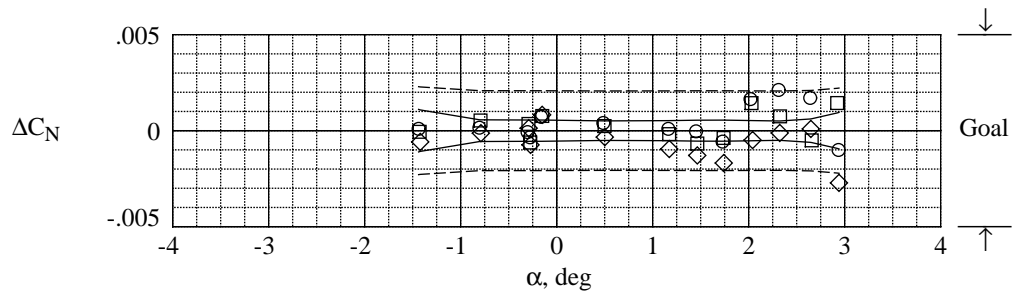
	Run	$R_{\bar{c}}$	M	q, psf
○	113	4.44×10^6	0.799	1235
□	117	4.45	.801	1239
◇	121	4.44	.801	1239
—	95% confidence interval			
- - -	95% prediction interval			



(a) Group 8.

Figure 9. Statistical results of C_N , C_A , and C_m short-term repeat data acquired in air mode.

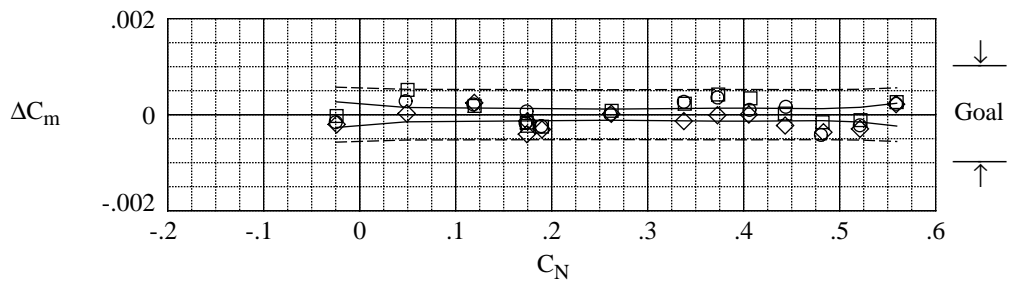
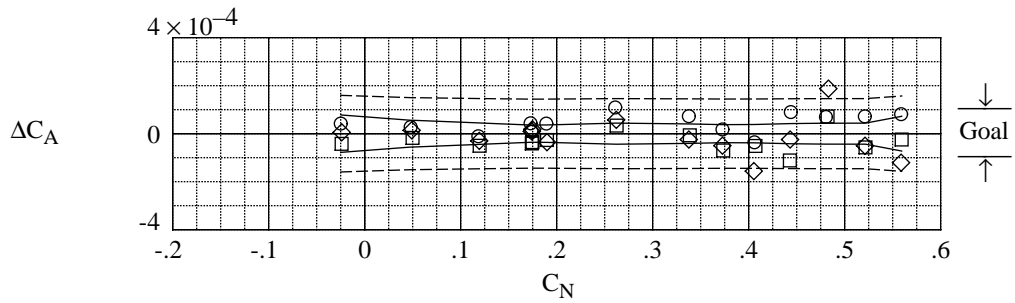
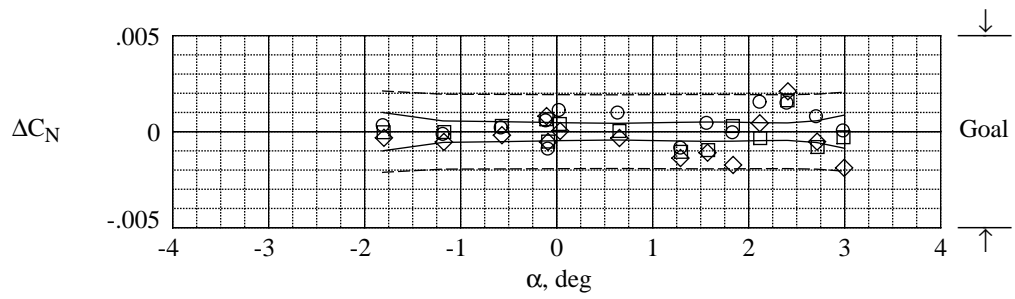
	Run	$R_{\bar{c}}$	M	q, psf
○	124	4.43×10^6	0.800	1237
□	128	4.45	.800	1236
◇	133	4.44	.800	1235
—	95% confidence interval			
- - -	95% prediction interval			



(b) Group 9.

Figure 9. Continued.

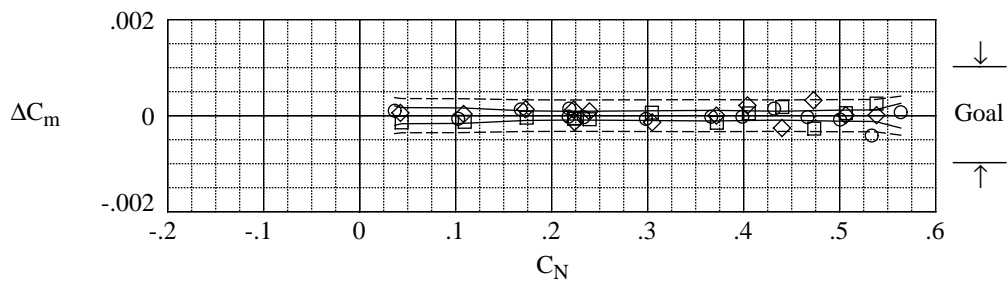
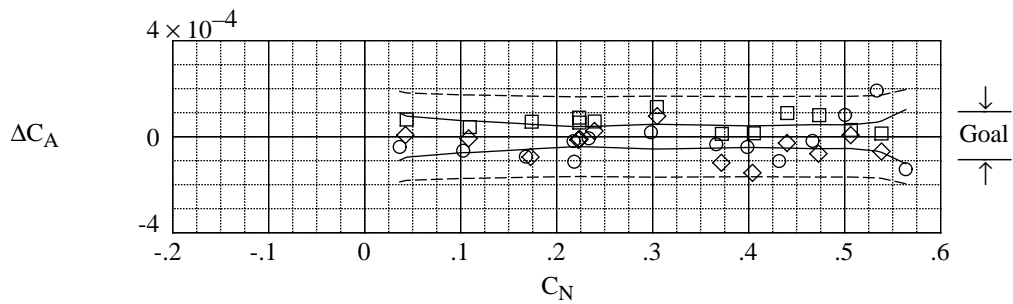
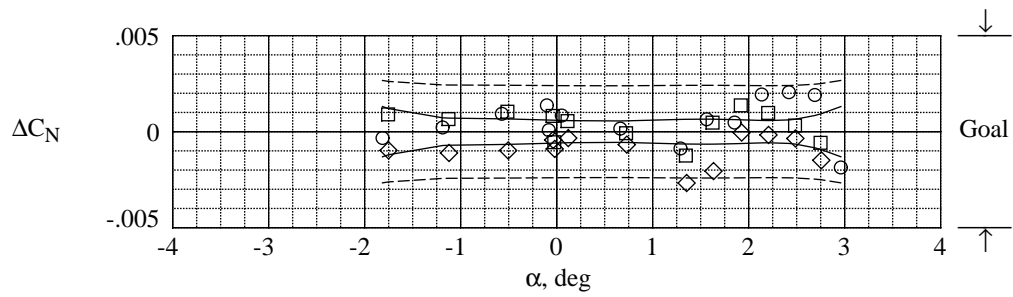
	Run	$R_{\bar{c}}$	M	q, psf
○	136	4.44×10^6	0.800	1237
□	140	4.47	.800	1236
◇	144	4.45	.800	1237
—	95% confidence interval			
- - -	95% prediction interval			



(c) Group 10.

Figure 9. Continued.

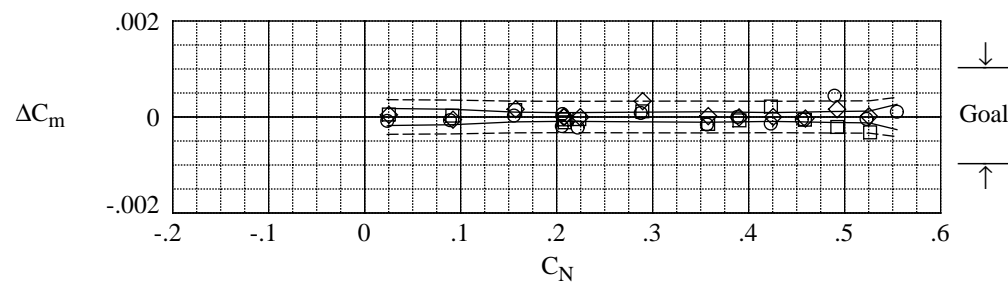
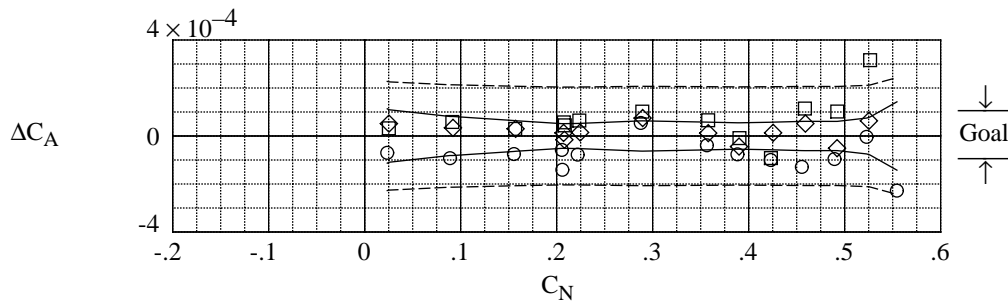
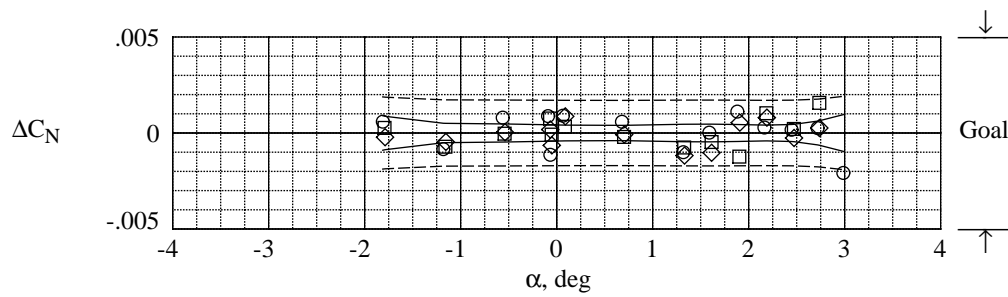
	Run	$R_{\bar{c}}$	M	q, psf
○	68	2.36×10^6	0.800	658
□	72	2.38	.800	662
◇	76	2.38	.800	662
—	95% confidence interval			
- - -	95% prediction interval			



(d) Group 11.

Figure 9. Continued.

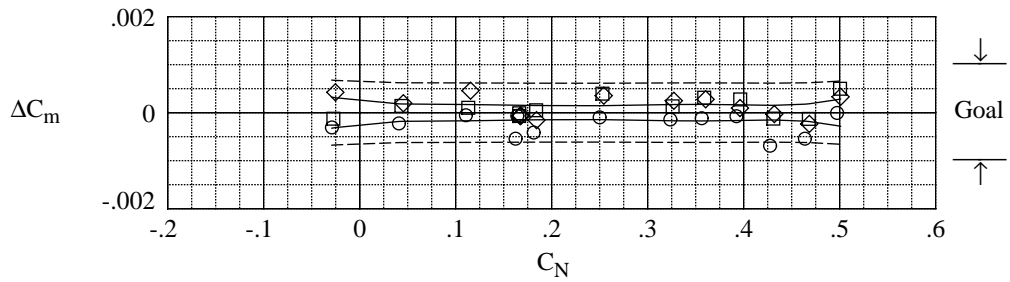
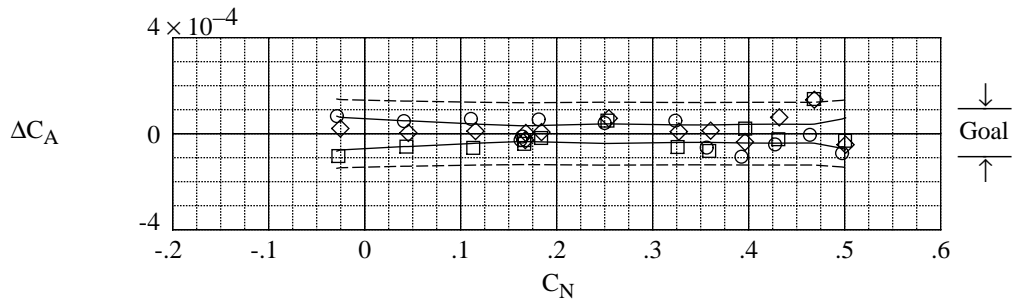
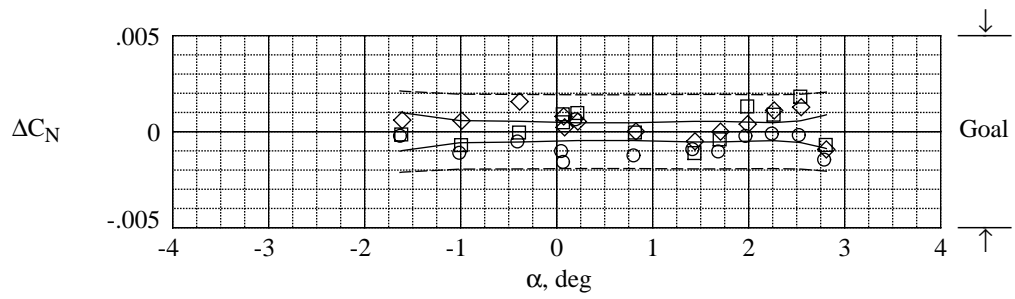
	Run	$R_{\bar{c}}$	M	q, psf
○	79	2.38×10^6	0.800	661
□	83	2.37	.800	660
◇	87	2.38	.800	662
—	95% confidence interval			
- - -	95% prediction interval			



(e) Group 12.

Figure 9. Continued.

	Run	$R_{\bar{c}}$	M	q, psf
○	90	2.37×10^6	0.800	660
□	94	2.37	.801	660
◇	98	2.38	.801	663
—	95% confidence interval			
- - -	95% prediction interval			



(f) Group 13.

Figure 9. Concluded.

	Configuration	$R_{\bar{c}}$	M	q, psf	Group
○	WBMNTH = -1 + Seal1	40.15×10^6	0.800	2660	2
□	WBMNTH = -1 + Seal3	40.14	.800	2659	3
—	95% confidence interval				
- - -	95% prediction interval				

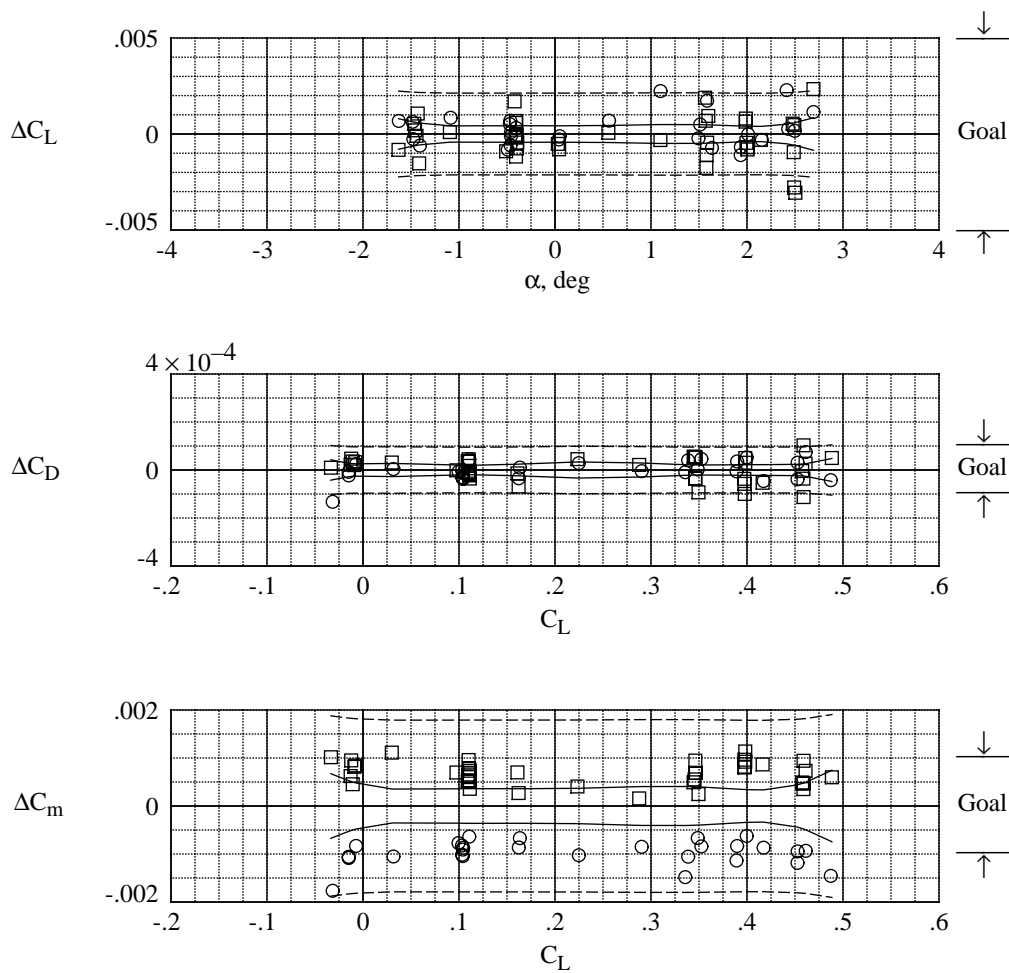


Figure 10. Statistical results of C_L , C_D , and C_m near-term repeat data acquired in cryogenic mode.

	Configuration	$R_{\bar{c}}$	M	q, psf	Group
○	WBMNTH = -1 + Seal1	40.15×10^6	0.800	2660	2
□	WBMNTH = -1 + Seal3	40.14	.800	2659	3
—	95% confidence interval				
- - -	95% prediction interval				

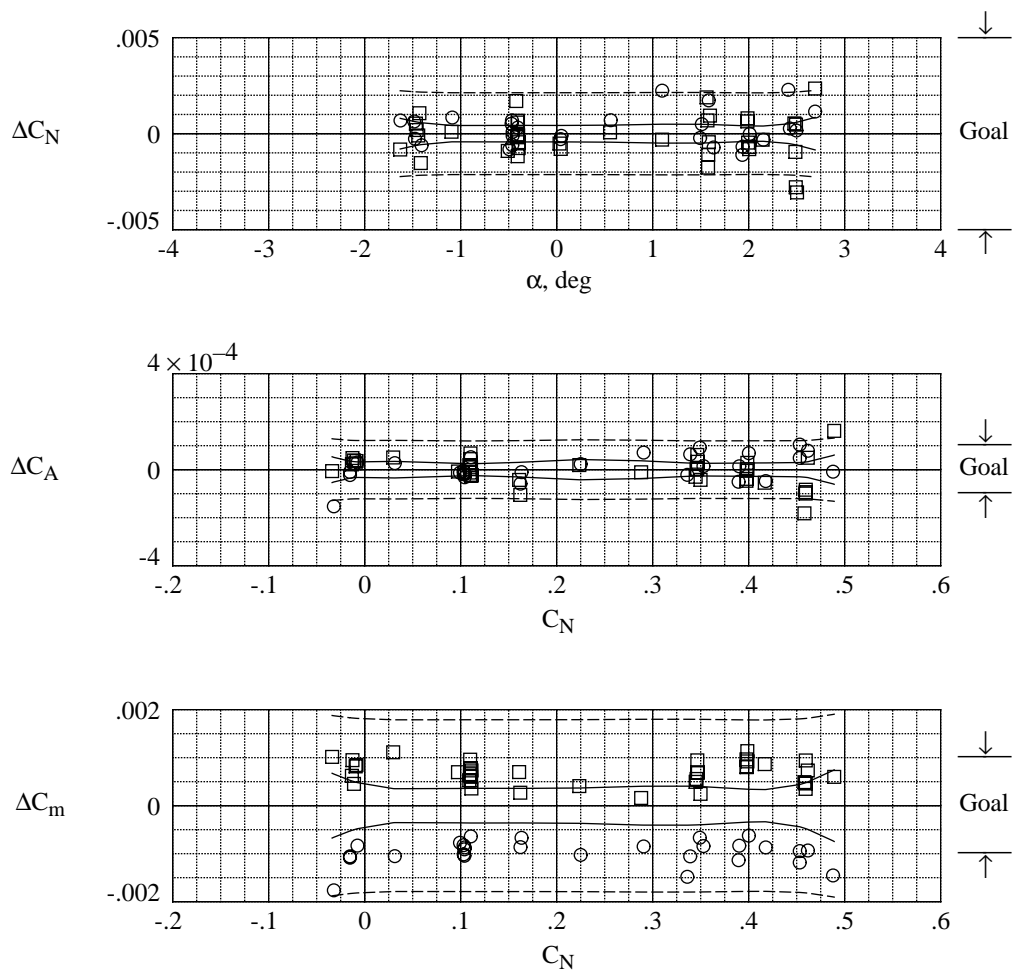


Figure 11. Statistical results of C_N , C_A , and C_m near-term repeat data acquired in cryogenic mode.

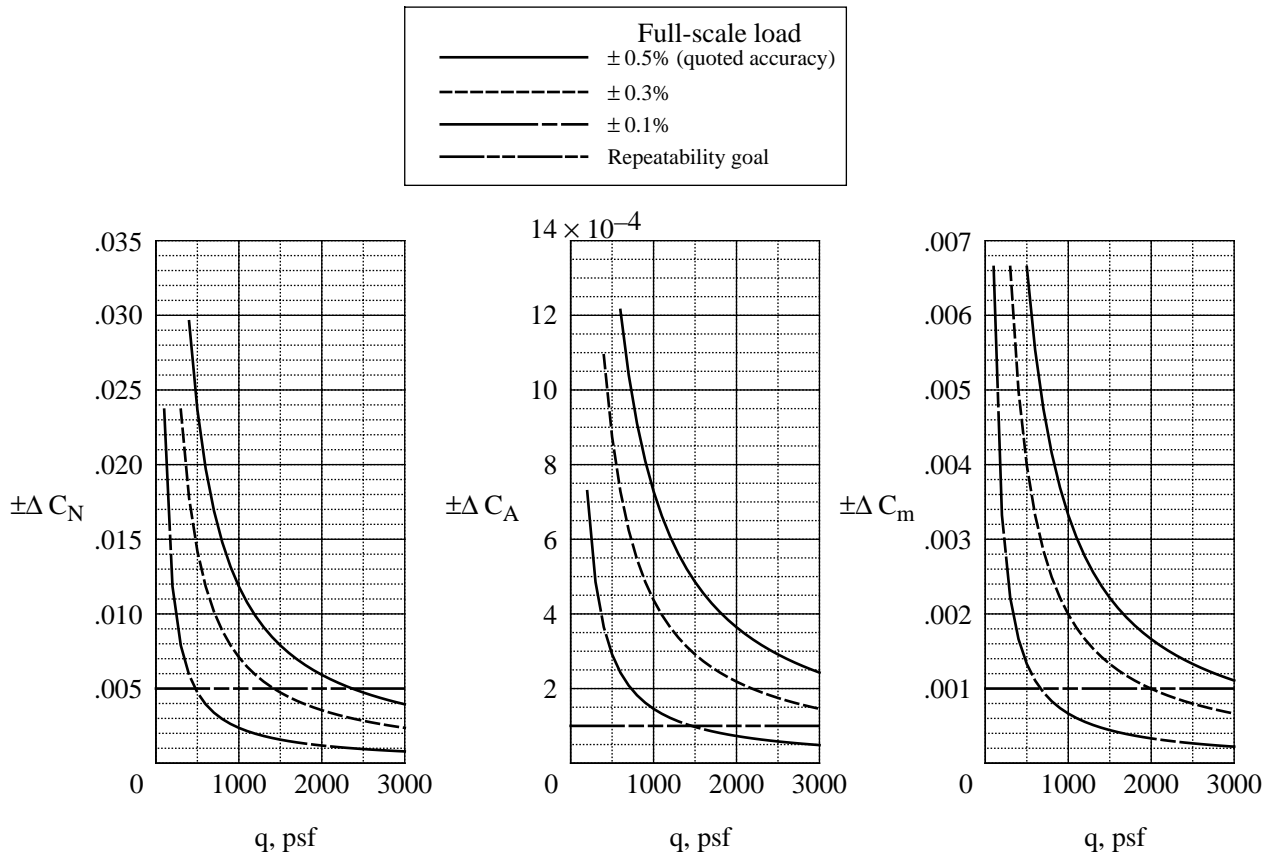
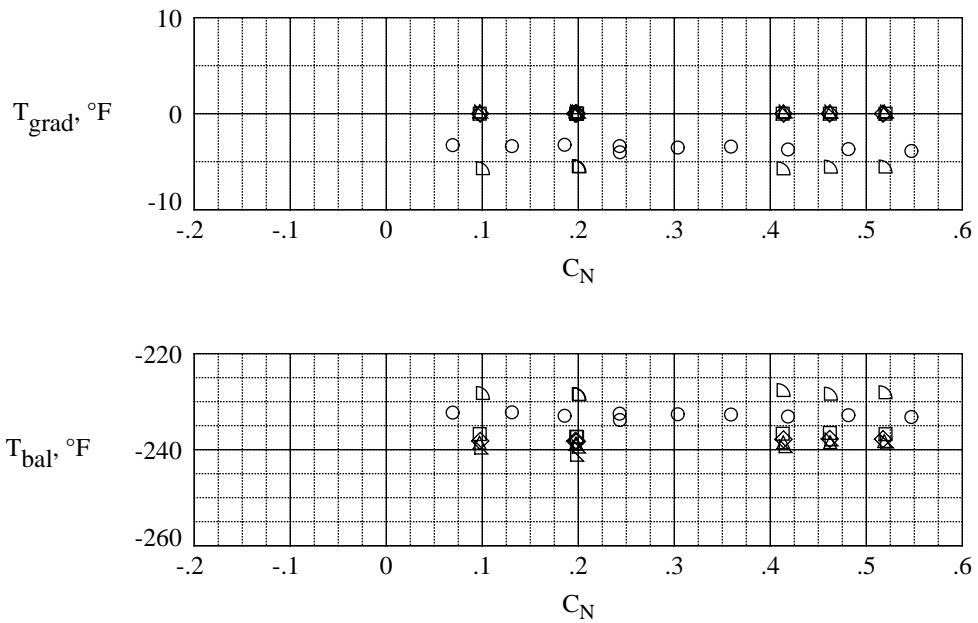


Figure 12. Balance accuracy bands in coefficient form based on full-scale loads given in table 1; quoted accuracy in terms of worst outlying point during calibration is ± 0.5 percent of full-scale load.

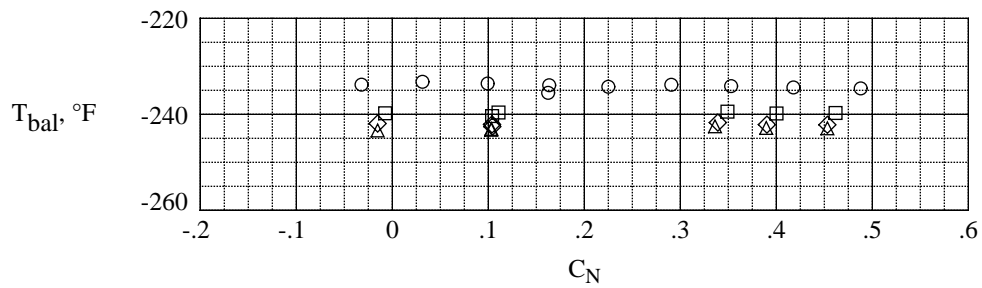
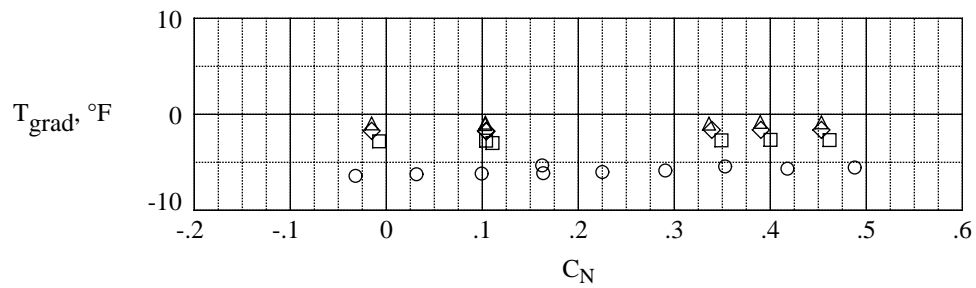
	Run	$R_{\bar{c}}$	M	q, psf	T_t , °F
○	14	39.92×10^6	0.800	2660	-249.8
□	16	39.93	.799	2658	-249.9
◇	18	39.95	.799	2658	-249.9
△	20	39.93	.800	2660	-249.9
▵	22	39.96	.800	2661	-249.9
▾	28	40.27	.800	2658	-251.1



(a) Group 1.

Figure 13. Variation of balance temperature and temperature gradient (front to rear).

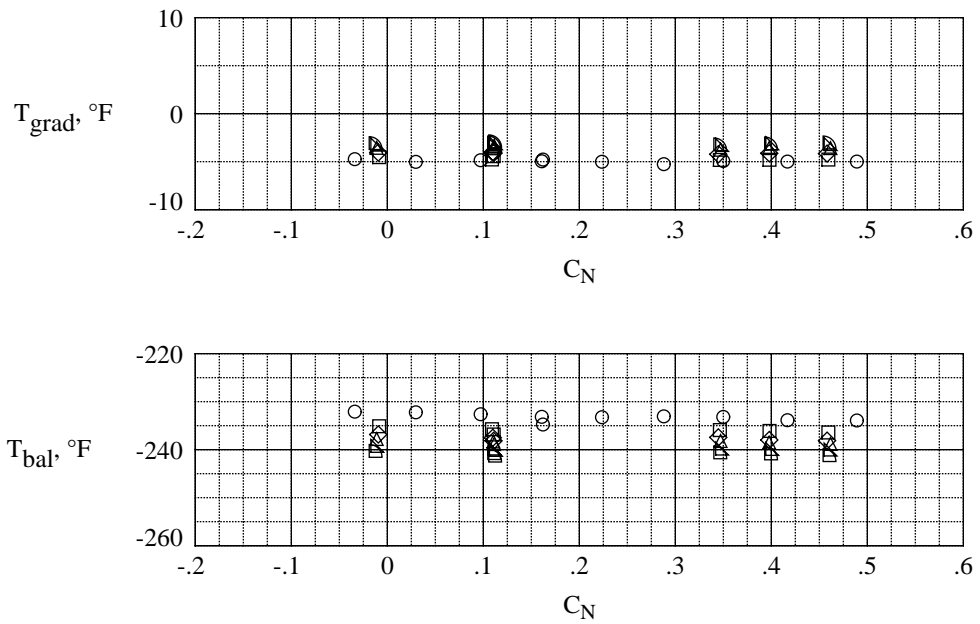
	Run	$R_{\bar{c}}$	M	q, psf	T_t , °F
○	44	40.17×10^6	0.800	2662	-250.6
□	46	40.18	.800	2664	-250.6
◇	48	40.11	.799	2656	-250.6
△	50	40.12	.799	2656	-250.6



(b) Group 2.

Figure 13. Continued.

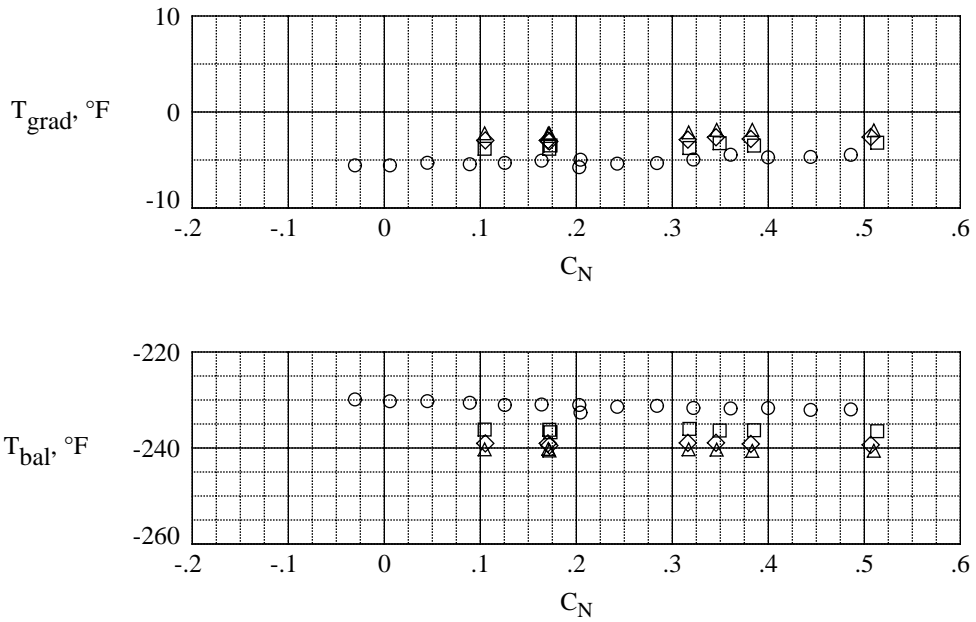
	Run	$R_{\bar{c}}$	M	q, psf	T_t , °F
○	147	40.12×10^6	0.800	2659	-250.5
□	148	40.17	.800	2659	-250.7
◇	149	40.14	.799	2658	-250.6
△	150	40.12	.800	2659	-250.5
▴	151	40.16	.800	2661	-250.6
▾	152	40.14	.800	2659	-250.6



(c) Group 3.

Figure 13. Continued.

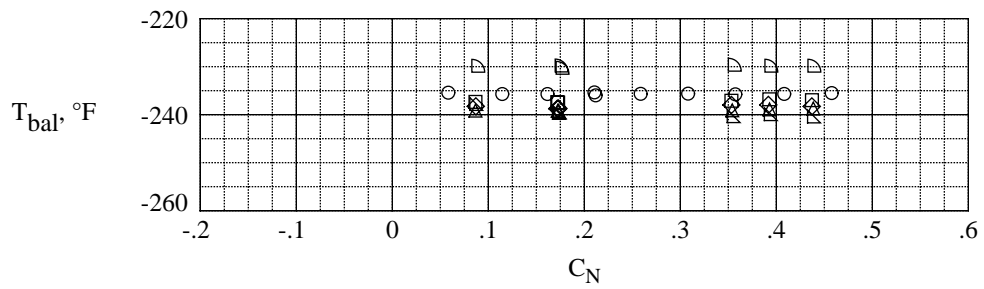
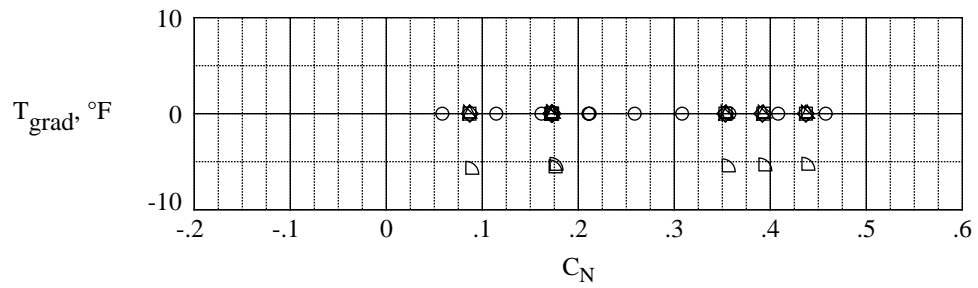
	Run	$R_{\bar{c}}$	M	q, psf	T_t , °F
○	156	40.25×10^6	0.801	2666	-250.8
□	158	40.21	.801	2662	-250.8
◇	160	40.14	.799	2656	-250.7
△	162	40.23	.800	2661	-250.8



(d) Group 4.

Figure 13. Continued.

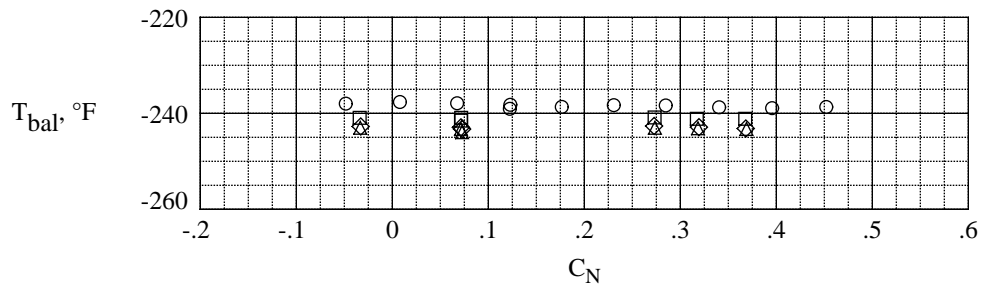
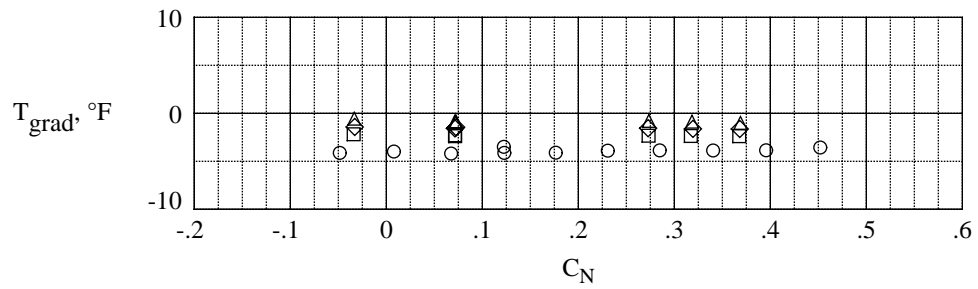
	Run	$R_{\bar{c}}$	M	q, psf	T_t , °F
○	15	39.89×10^6	0.700	2426	-249.6
□	17	39.90	.700	2426	-249.7
◇	19	39.91	.699	2424	-249.7
△	21	39.92	.700	2428	-249.7
▵	23	39.91	.699	2422	-249.8
▹	29	40.28	.701	2430	-250.9



(e) Group 5.

Figure 13. Continued.

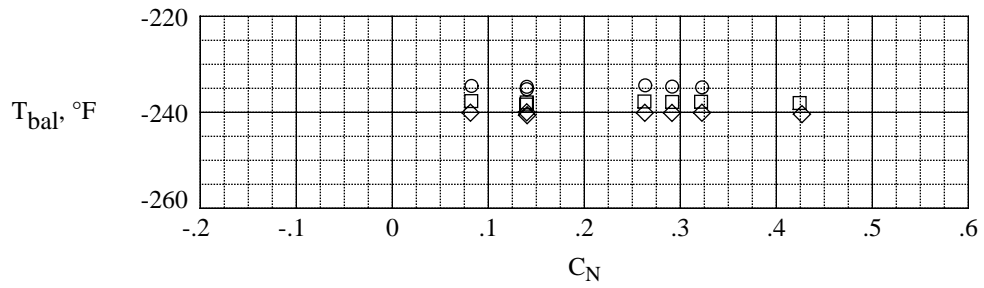
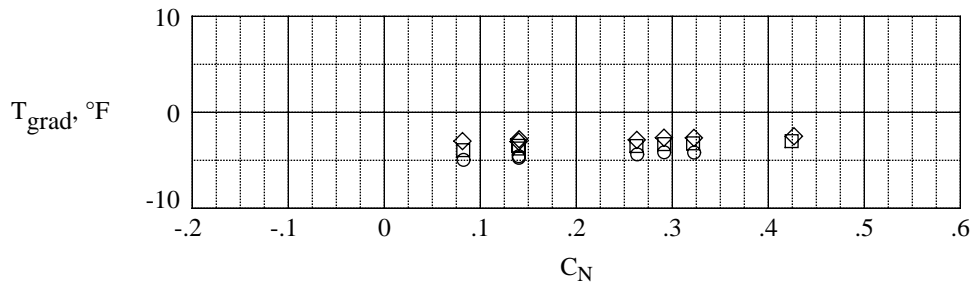
	Run	$R_{\bar{c}}$	M	q, psf	T_t , °F
○	45	40.24×10^6	0.699	2423	-250.9
□	47	40.25	.700	2428	-250.8
◇	49	40.26	.700	2429	-250.8
△	51	40.31	.700	2429	-251.0



(f) Group 6.

Figure 13. Continued.

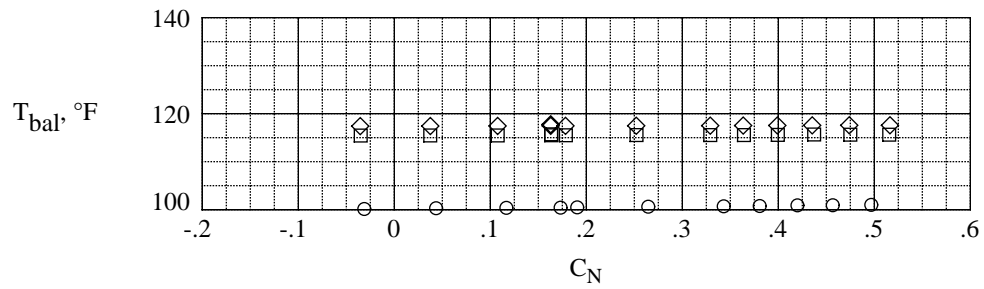
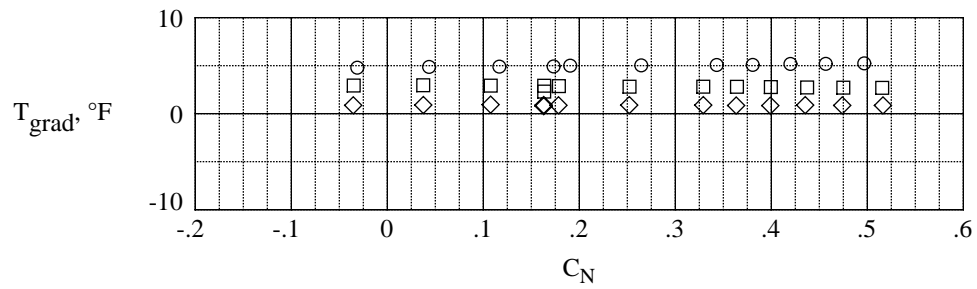
	Run	$R_{\bar{c}}$	M	q, psf	T_t , °F
○	157	40.20×10^6	0.700	2424	-250.8
□	159	40.16	.700	2423	-250.7
◇	161	40.22	.702	2431	-250.8



(g) Group 7.

Figure 13. Continued.

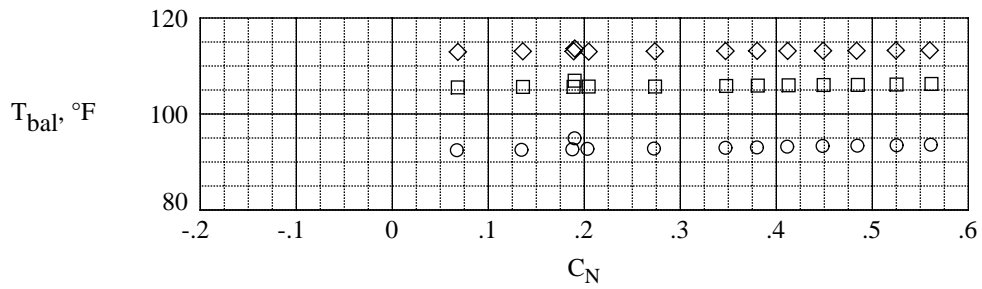
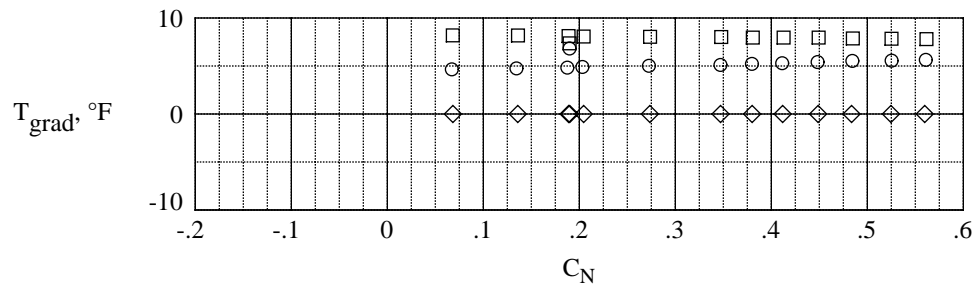
	Run	$R_{\bar{c}}$	M	q, psf	T_t , °F
○	113	4.44×10^6	0.799	1235	120.3
□	117	4.45	.801	1239	119.7
◇	121	4.44	.801	1239	121.6



(h) Group 8.

Figure 13. Continued.

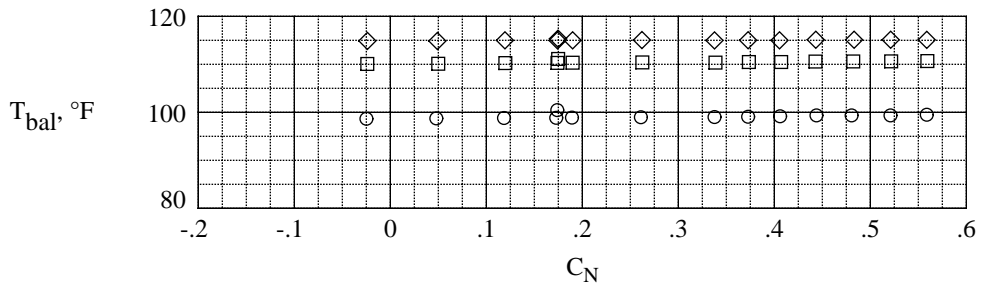
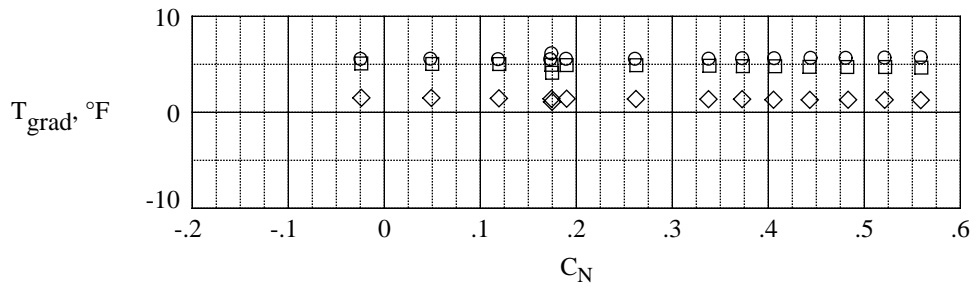
	Run	$R_{\bar{c}}$	M	q, psf	T_t , °F
○	124	4.43×10^6	0.800	1237	122.0
□	128	4.45	.800	1236	119.7
◇	133	4.44	.800	1235	



(i) Group 9.

Figure 13. Continued.

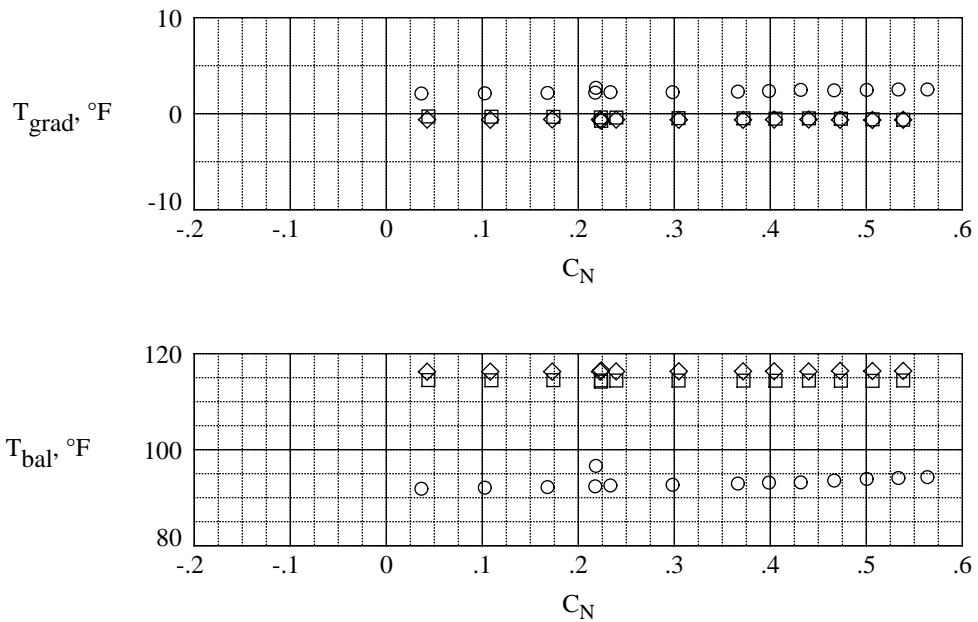
	Run	$R_{\bar{c}}$	M	q, psf	T_t , °F
○	136	4.44×10^6	0.800	1237	120.9
□	140	4.47	.800	1236	118.0
◇	144	4.45	.800	1237	120.2



(j) Group 10.

Figure 13. Continued.

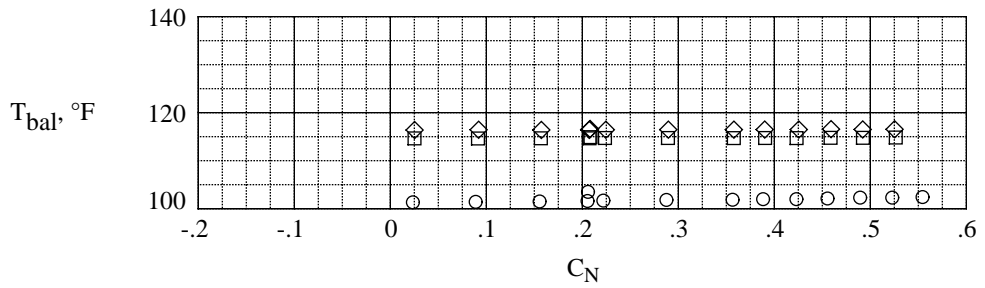
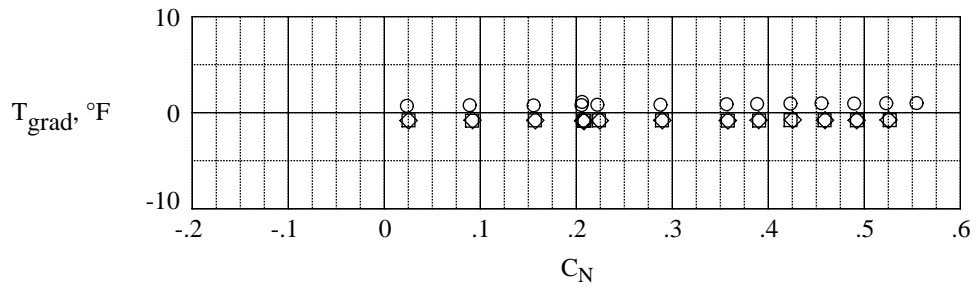
	Run	$R_{\bar{c}}$	M	q, psf	T_t , °F
○	68	2.36×10^6	0.800	658	121.4
□	72	2.38	.800	662	120.5
◇	76	2.38	.800	662	120.1



(k) Group 11.

Figure 13. Continued.

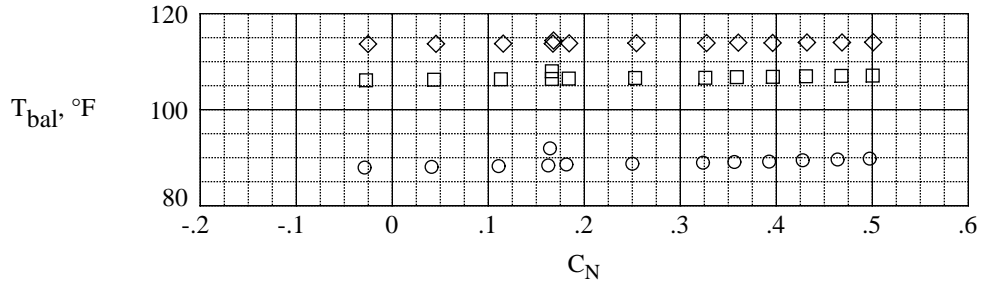
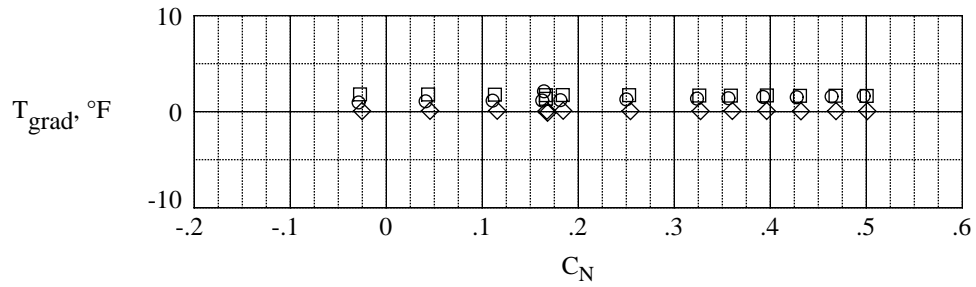
	Run	$R_{\bar{c}}$	M	q, psf	T_t , °F
○	79	2.38×10^6	0.800	661	119.8
□	83	2.37	.800	660	119.9
◇	87	2.38	.800	662	119.7



(l) Group 12.

Figure 13. Continued.

	Run	$R_{\bar{c}}$	M	q, psf	T_t , °F
○	90	2.37×10^6	0.800	660	121.7
□	94	2.37	.801	660	119.6
◇	98	2.38	.801	663	120.7



(m) Group 13.

Figure 13. Concluded.

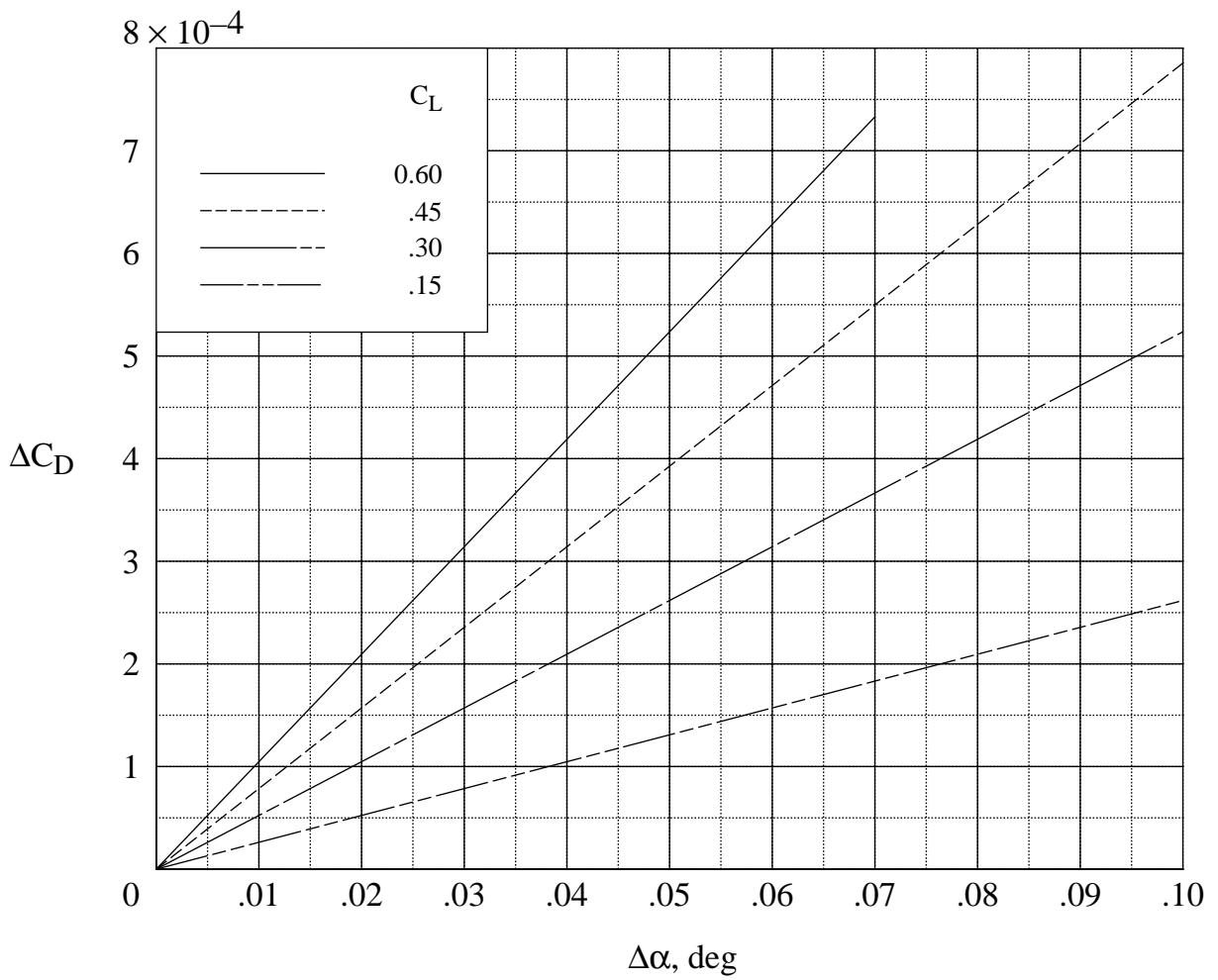
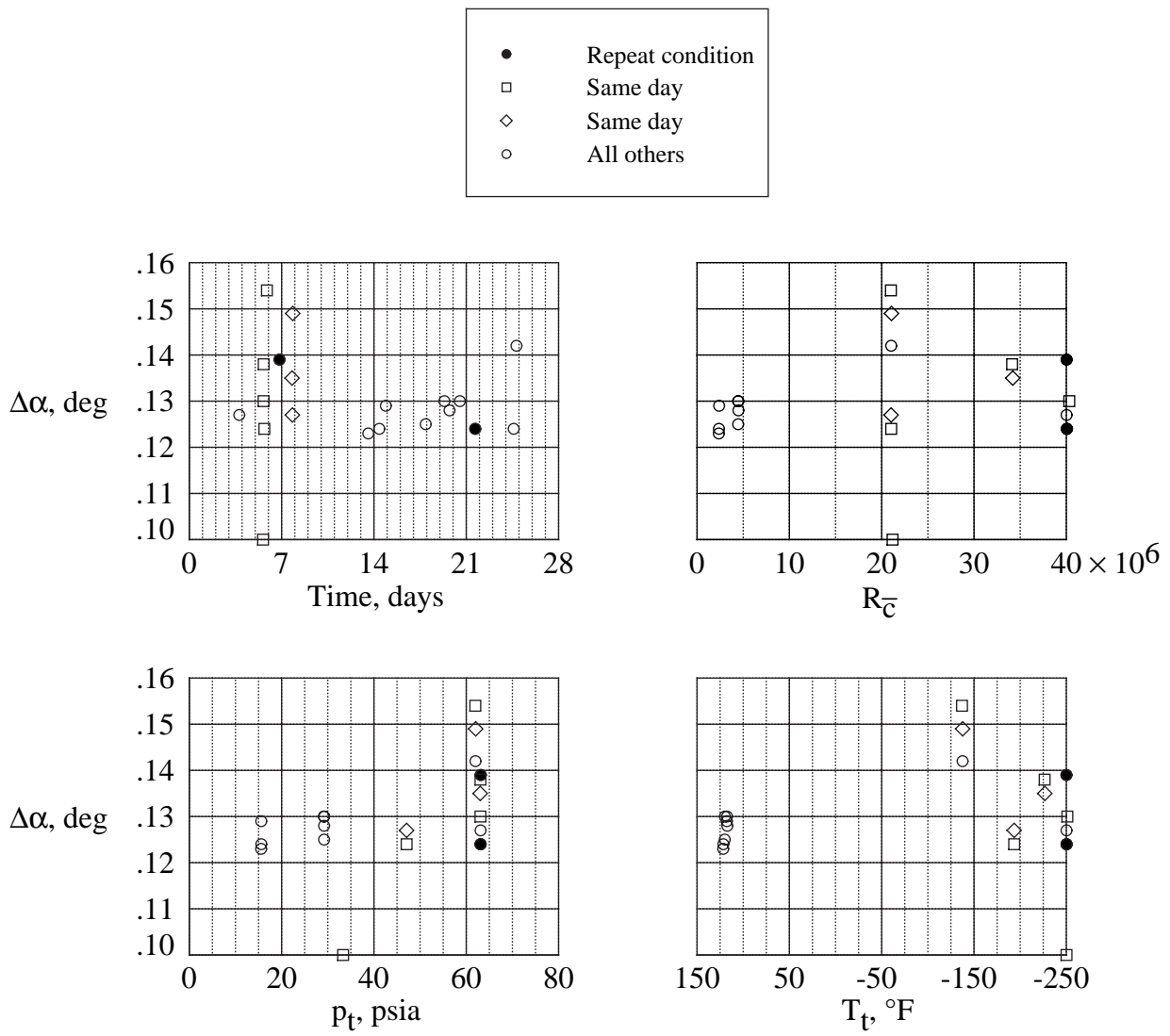
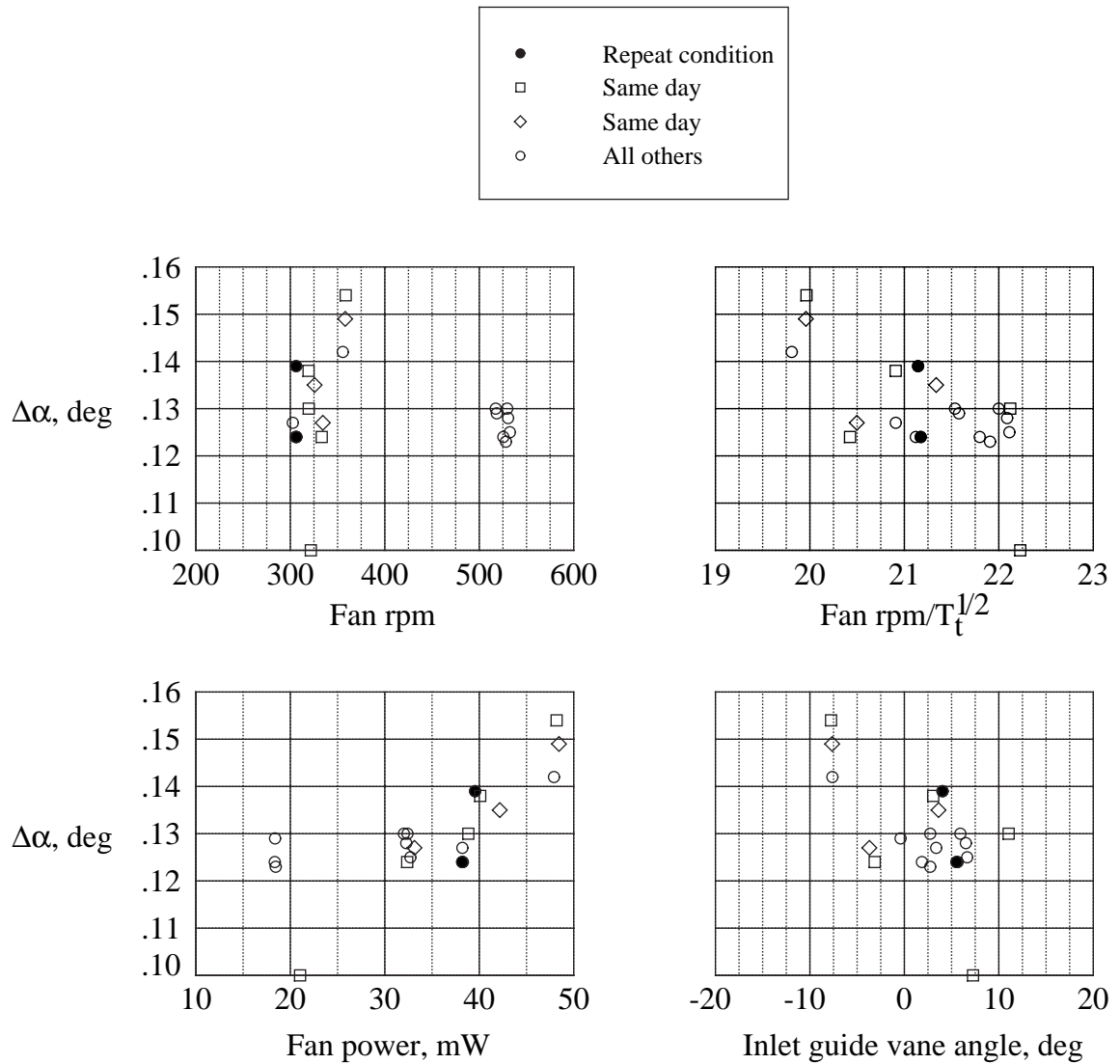


Figure 14. Effect of angle-of-attack errors on drag coefficient.



(a) Relationship to time, Reynolds number, total pressure, and total temperature.

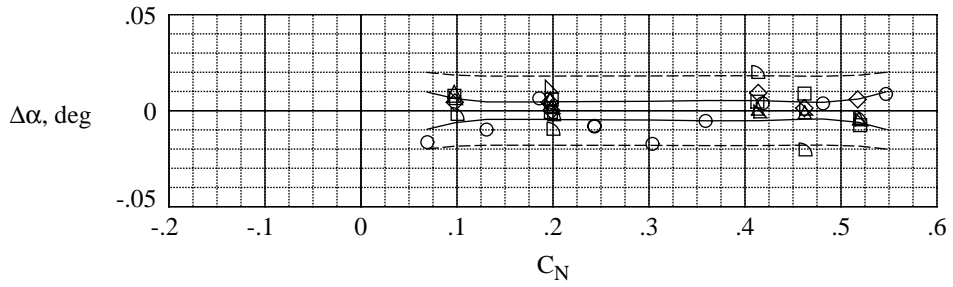
Figure 15. Variation of test-section flow angularity at $M = 0.80$ throughout investigation.



(b) Relationship to fan speed, fan tip speed compressibility factor, fan power, and inlet guide vane angle.

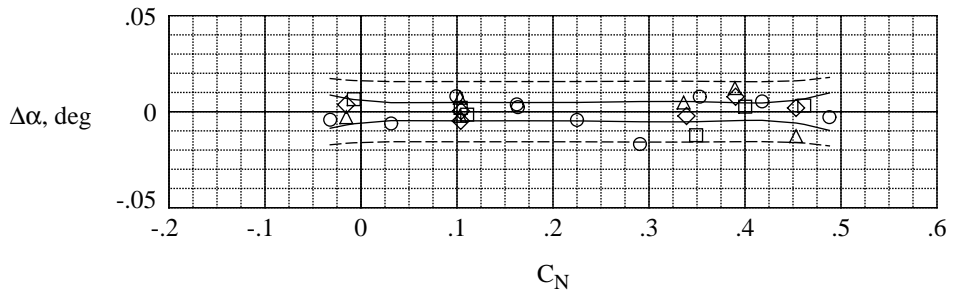
Figure 15. Concluded.

	Run	$R_{\bar{c}}$	M	q, psf
○	14	39.92×10^6	0.800	2660
□	16	39.93	.799	2658
◇	18	39.95	.799	2658
△	20	39.93	.800	2660
▵	22	39.96	.800	2661
▷	28	40.27	.800	2658
—	95% confidence interval			
- - -	95% prediction interval			



(a) Group 1.

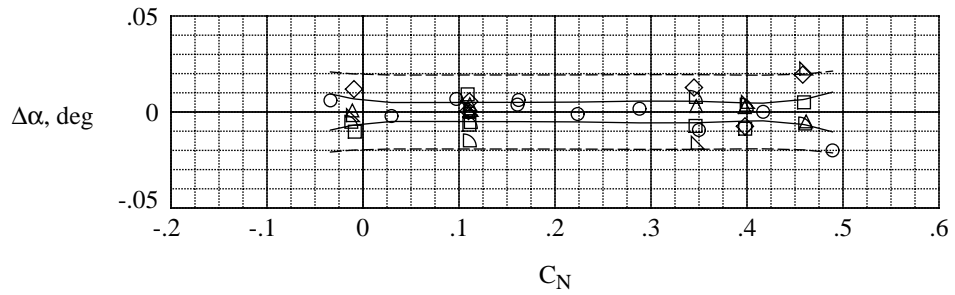
	Run	$R_{\bar{c}}$	M	q, psf
○	44	40.17×10^6	0.800	2662
□	46	40.18	.800	2664
◇	48	40.11	.799	2656
△	50	40.12	.799	2656
—	95% confidence interval			
- - -	95% prediction interval			



(b) Group 2.

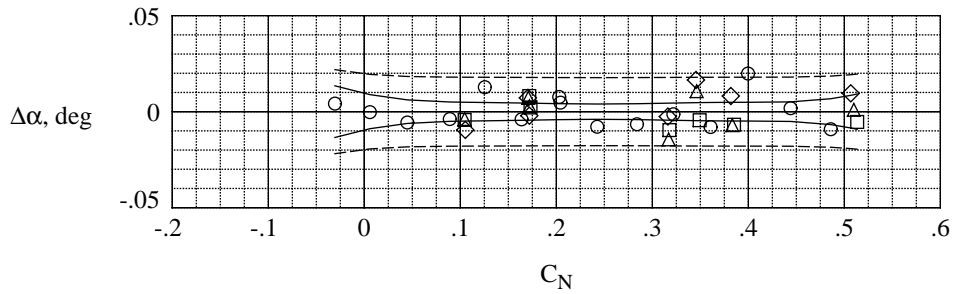
Figure 16. Statistical results of angle-of-attack short-term repeat data in cryogenic and air modes.

	Run	R_c	M	q, psf
○	147	40.12×10^6	0.800	2659
□	148	40.17	.800	2659
◇	149	40.14	.799	2658
△	150	40.12	.800	2659
▴	151	40.16	.800	2661
▾	152	40.14	.800	2659
—	95% confidence interval			
- - -	95% prediction interval			



(c) Group 3.

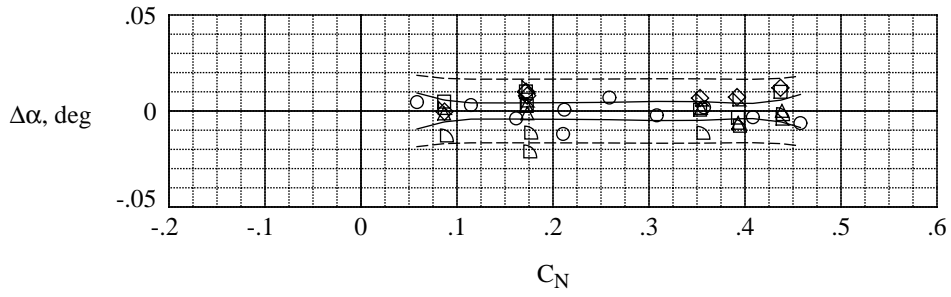
	Run	R_c	M	q, psf
○	156	40.25×10^6	0.801	2666
□	158	40.21	.801	2662
◇	160	40.14	.799	2656
△	162	40.23	.800	2661
—	95% confidence interval			
- - -	95% prediction interval			



(d) Group 4.

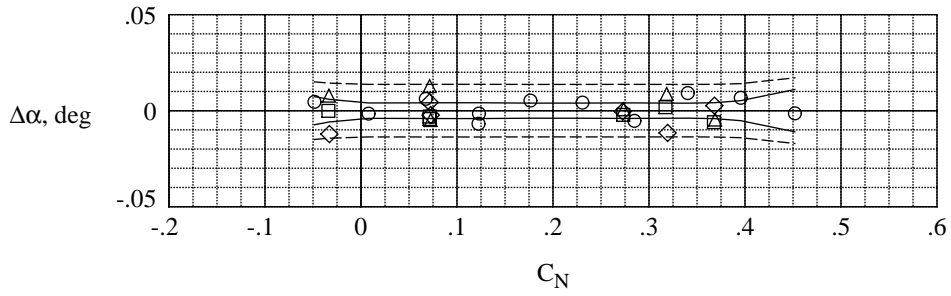
Figure 16. Continued.

	Run	$R_{\bar{c}}$	M	q, psf
○	15	39.89×10^6	0.700	2426
□	17	39.90	.700	2426
◇	19	39.91	.699	2424
△	21	39.92	.700	2428
▵	23	39.91	.699	2422
▾	29	40.28	.701	2430
—	95% confidence interval			
- - -	95% prediction interval			



(e) Group 5.

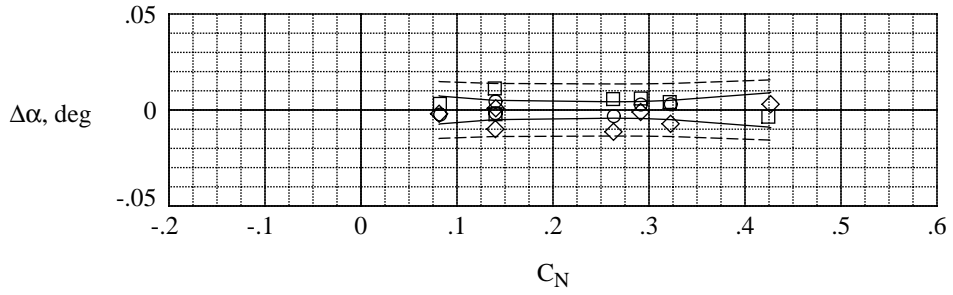
	Run	$R_{\bar{c}}$	M	q, psf
○	45	40.24×10^6	0.699	2423
□	47	40.25	.700	2428
◇	49	40.26	.700	2429
△	51	40.31	.700	2429
—	95% confidence interval			
- - -	95% prediction interval			



(f) Group 6.

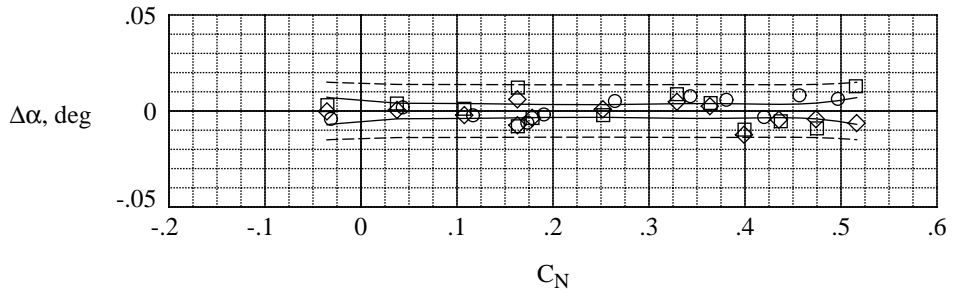
Figure 16. Continued.

	Run	$R_{\bar{c}}$	M	q, psf
○	157	40.20×10^6	0.700	2424
□	159	40.16	.700	2423
◇	161	40.22	.702	2431
—	95% confidence interval			
----	95% prediction interval			



(g) Group 7.

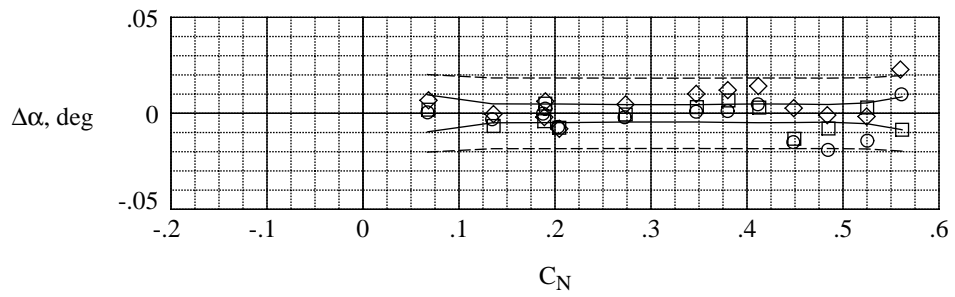
	Run	$R_{\bar{c}}$	M	q, psf
○	113	4.44×10^6	0.799	1235
□	117	4.45	.801	1239
◇	121	4.44	.801	1239
—	95% confidence interval			
----	95% prediction interval			



(h) Group 8.

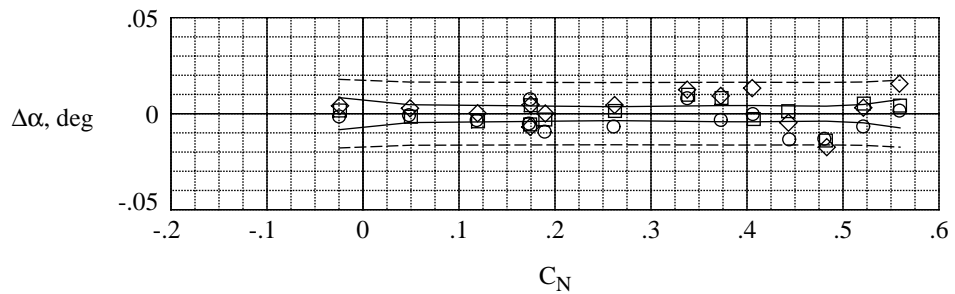
Figure 16. Continued.

	Run	$R_{\bar{c}}$	M	q, psf
○	124	4.43×10^6	0.800	1237
□	128	4.45	.800	1236
◇	133	4.44	.800	1235
—	95% confidence interval			
- - -	95% prediction interval			



(i) Group 9.

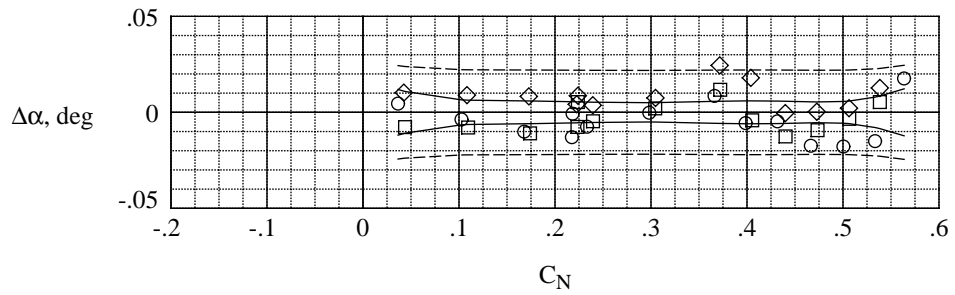
	Run	$R_{\bar{c}}$	M	q, psf
○	136	4.44×10^6	0.800	1237
□	140	4.47	.800	1236
◇	144	4.45	.800	1237
—	95% confidence interval			
- - -	95% prediction interval			



(j) Group 10.

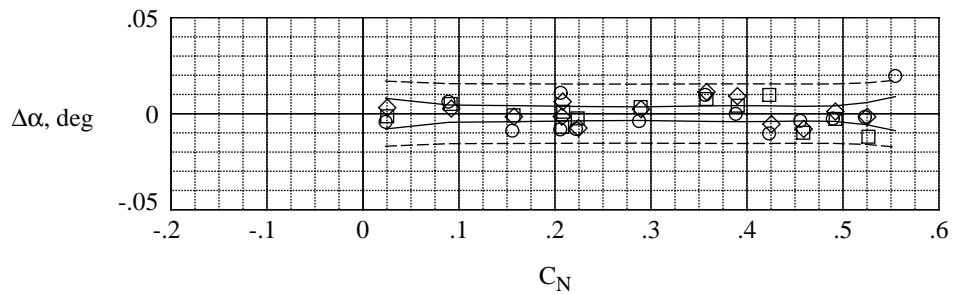
Figure 16. Continued.

	Run	$R_{\bar{c}}$	M	q, psf
○	68	2.36×10^6	0.800	658
□	72	2.38	.800	662
◇	76	2.38	.800	662
—	95% confidence interval			
- - -	95% prediction interval			



(k) Group 11.

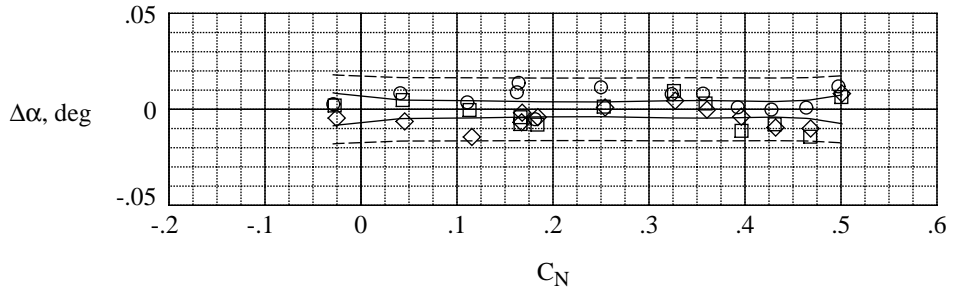
	Run	$R_{\bar{c}}$	M	q, psf
○	79	2.38×10^6	0.800	661
□	83	2.37	.800	660
◇	87	2.38	.800	662
—	95% confidence interval			
- - -	95% prediction interval			



(l) Group 12.

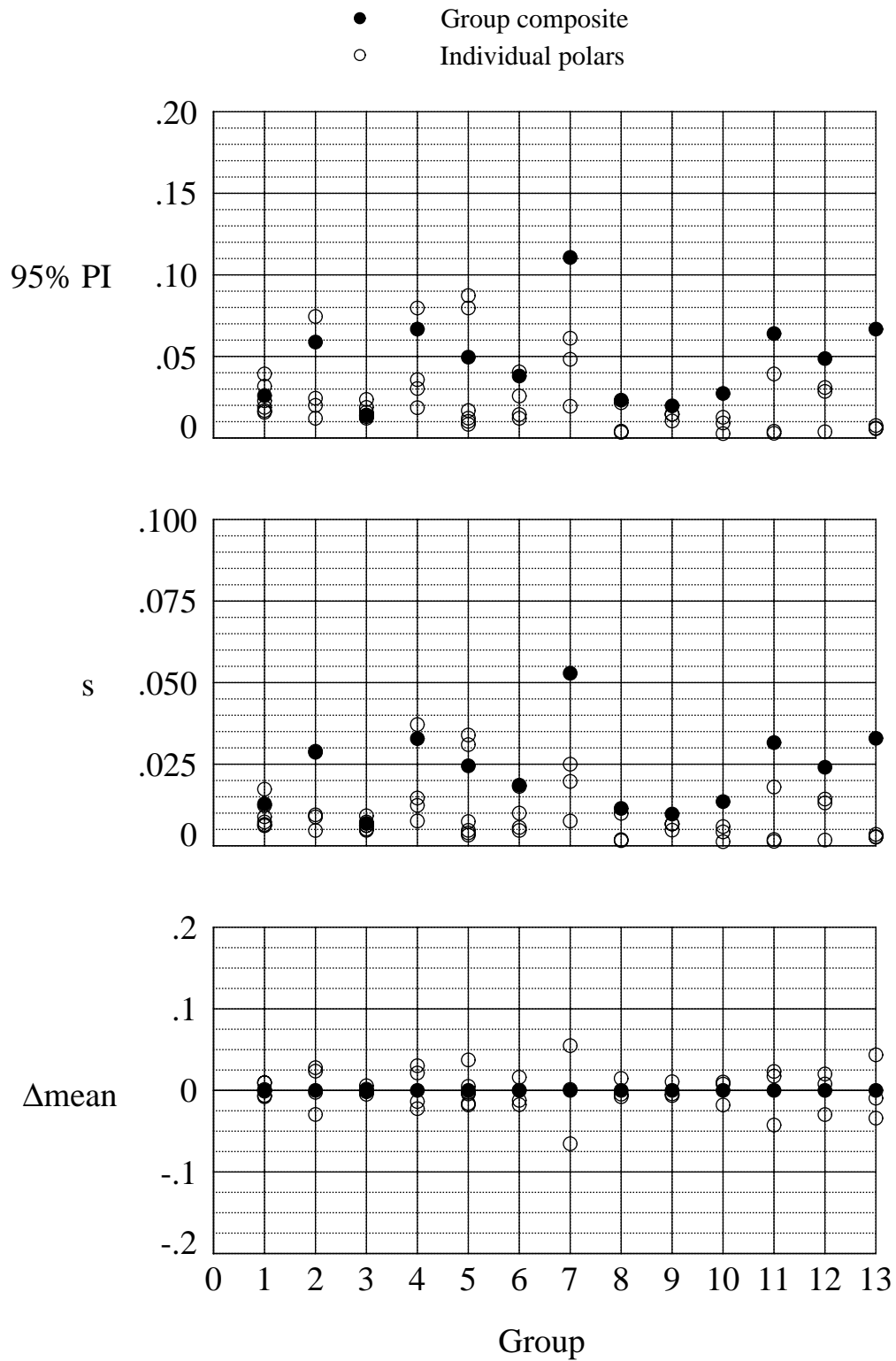
Figure 16. Continued.

	Run	R_c	M	q, psf
○	90	2.37×10^6	0.800	660
□	94	2.37	.801	660
◇	98	2.38	.801	663
—	95% confidence interval			
----	95% prediction interval			



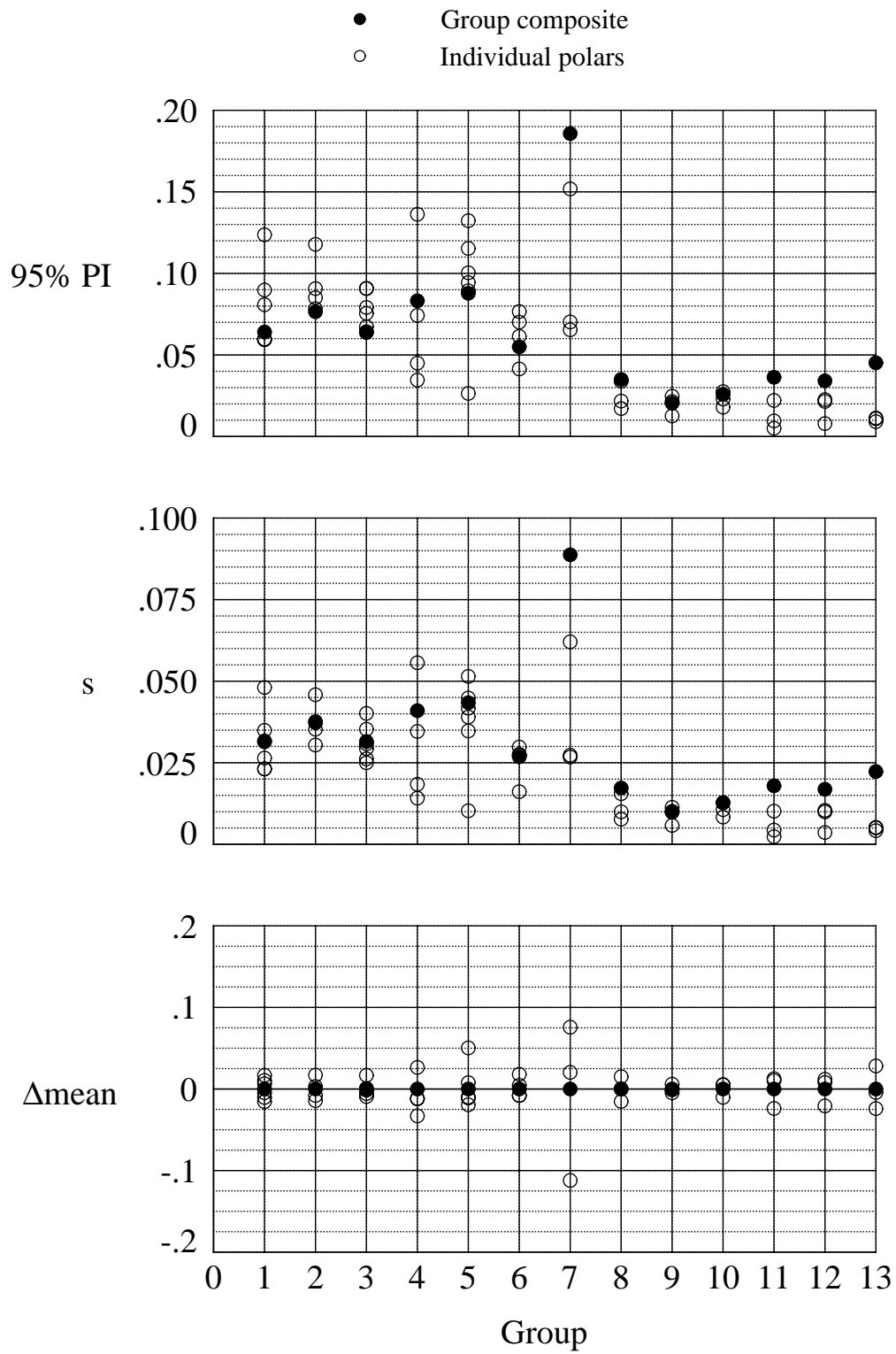
(m) Group 13.

Figure 16. Concluded.



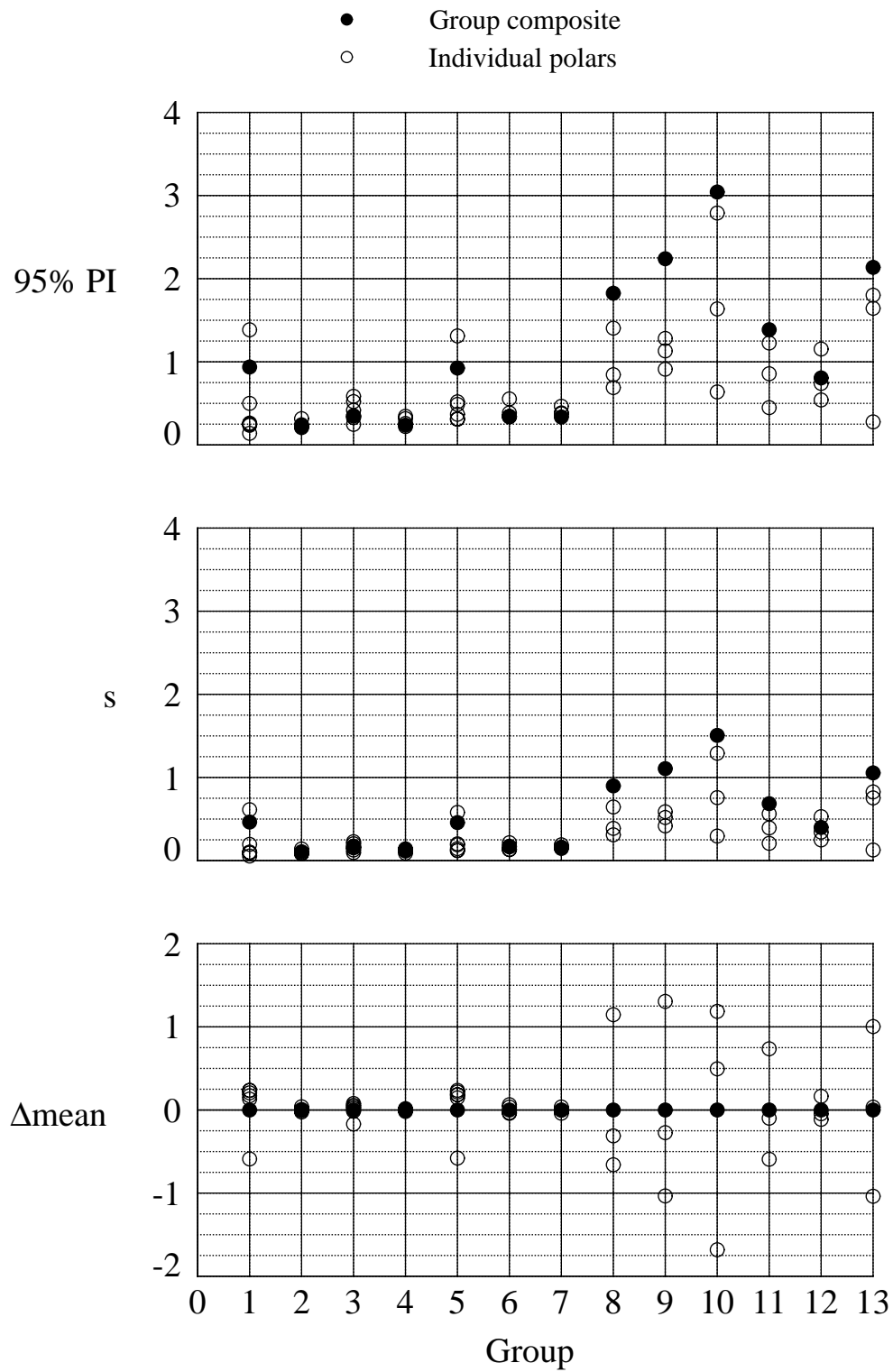
(a) p_t , psia.

Figure 17. Test condition repeatability for each polar within group; Δ mean = Polar mean – Group mean.



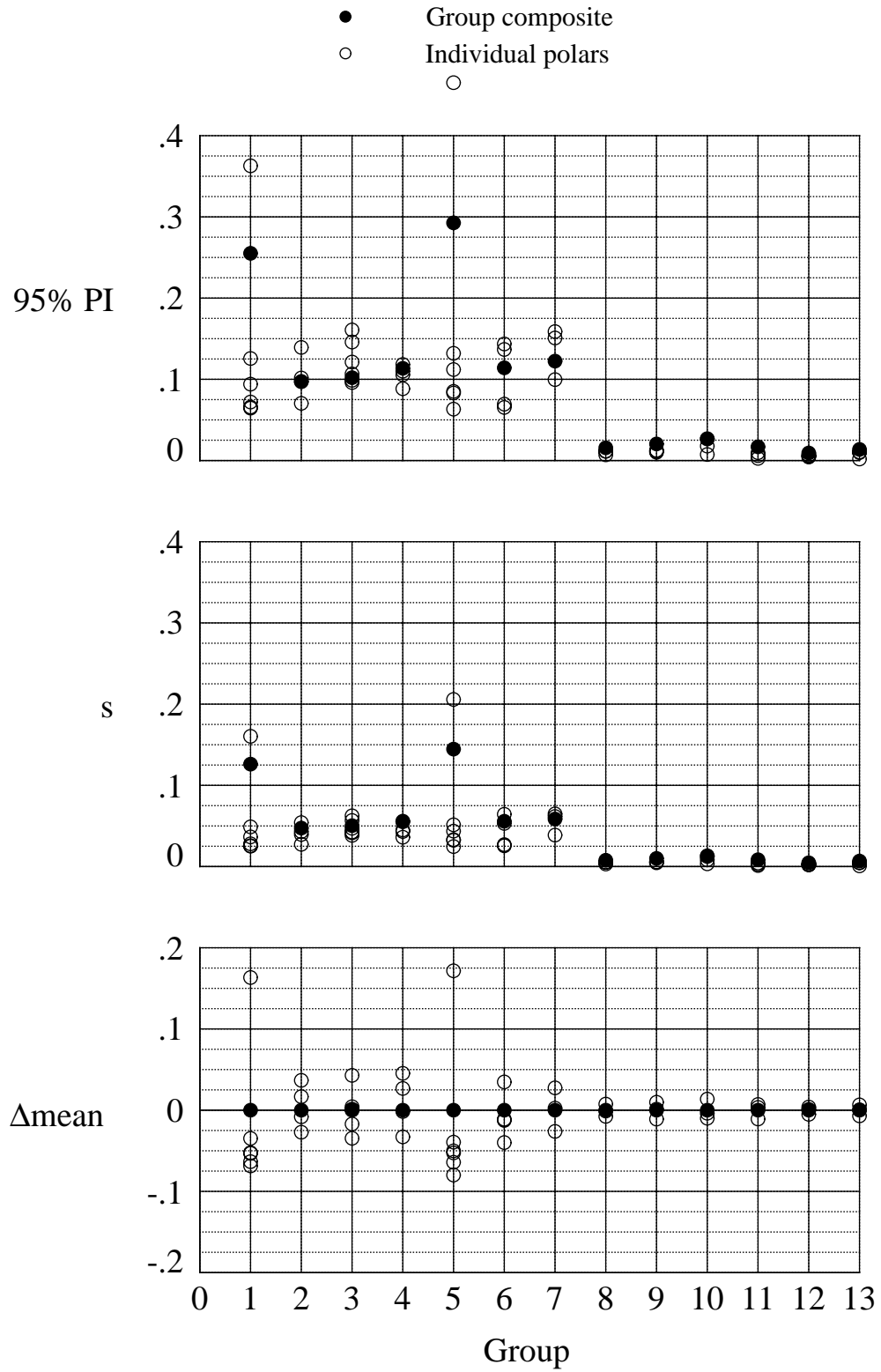
(b) p_s , psia.

Figure 17. Continued.



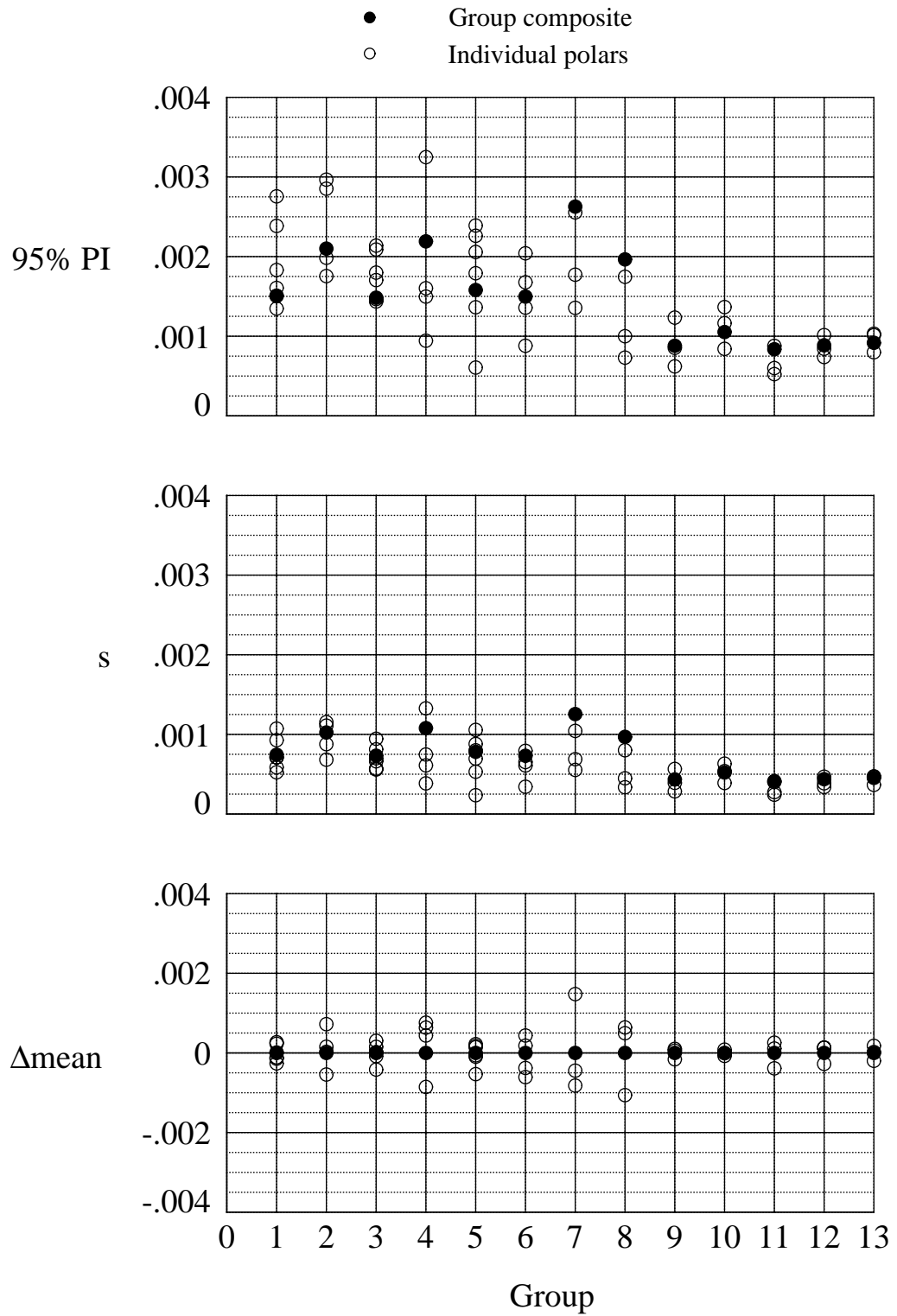
(c) T_p , °F.

Figure 17. Continued.



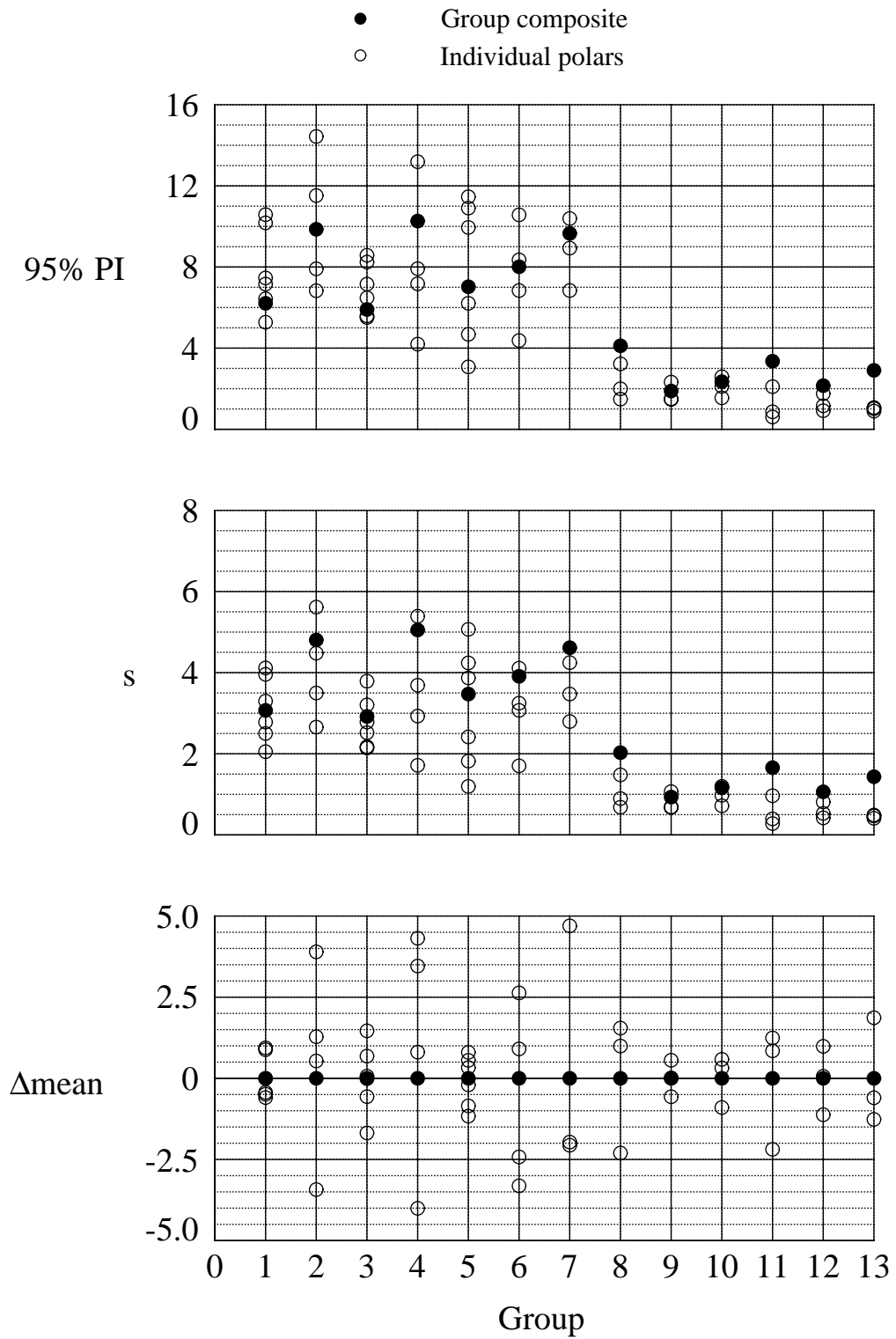
(d) $R_c, 10^6$.

Figure 17. Continued.



(e) Mach number.

Figure 17. Continued.



(f) q , psf.

Figure 17. Concluded.

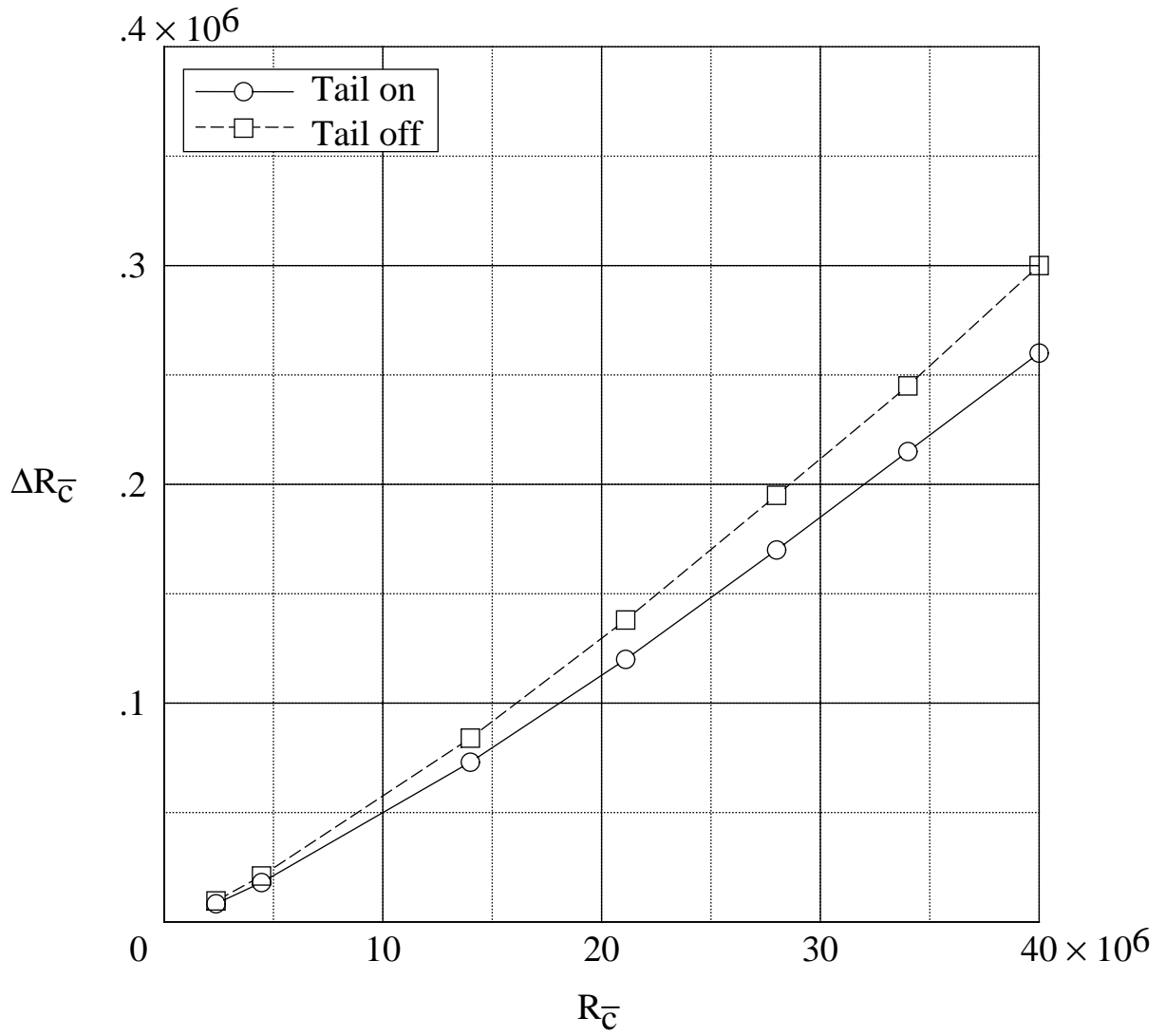


Figure 18. Reynolds number tolerance for $\Delta C_{D,sf} = 0.00001$ at $M = 0.80$.

REPORT DOCUMENTATION PAGE

Form Approved
OMB No. 0704-0188

Public reporting burden for this collection of information is estimated to average 1 hour per response, including the time for reviewing instructions, searching existing data sources, gathering and maintaining the data needed, and completing and reviewing the collection of information. Send comments regarding this burden estimate or any other aspect of this collection of information, including suggestions for reducing this burden, to Washington Headquarters Services, Directorate for Information Operations and Reports, 1215 Jefferson Davis Highway, Suite 1204, Arlington, VA 22202-4302, and to the Office of Management and Budget, Paperwork Reduction Project (0704-0188), Washington, DC 20503.

1. AGENCY USE ONLY <i>(Leave blank)</i>	2. REPORT DATE August 1995	3. REPORT TYPE AND DATES COVERED Technical Paper	
4. TITLE AND SUBTITLE A Longitudinal Aerodynamic Data Repeatability Study for a Commercial Transport Model Test in the National Transonic Facility		5. FUNDING NUMBERS WU 505-59-10-11	
6. AUTHOR(S) R. A. Wahls, J. B. Adcock, D. P. Witkowski, and F. L. Wright			
7. PERFORMING ORGANIZATION NAME(S) AND ADDRESS(ES) NASA Langley Research Center Hampton, VA 23681-0001		8. PERFORMING ORGANIZATION REPORT NUMBER L-17412	
9. SPONSORING/MONITORING AGENCY NAME(S) AND ADDRESS(ES) National Aeronautics and Space Administration Washington, DC 20546-0001		10. SPONSORING/MONITORING AGENCY REPORT NUMBER NASA TP-3522	
11. SUPPLEMENTARY NOTES Wahls and Adcock: Langley Research Center, Hampton, VA; Witkowski and Wright: Boeing Commercial Airplane Company, Seattle, WA.			
12a. DISTRIBUTION/AVAILABILITY STATEMENT Unclassified-Unlimited Subject Category 02 Availability: NASA CASI (301) 621-0390		12b. DISTRIBUTION CODE	
13. ABSTRACT <i>(Maximum 200 words)</i> A high Reynolds number investigation of a commercial transport model was conducted in the National Transonic Facility (NTF) at Langley Research Center. This investigation was part of a cooperative effort to test a 0.03-scale model of a Boeing 767 airplane in the NTF over a Mach number range of 0.70 to 0.86 and a Reynolds number range of 2.38 to 40.0×10^6 based on the mean aerodynamic chord. One of several specific objectives of the current investigation was to evaluate the level of data repeatability attainable in the NTF. Data repeatability studies were performed at a Mach number of 0.80 with Reynolds numbers of 2.38, 4.45, and 40.0×10^6 and also at a Mach number of 0.70 with a Reynolds number of 40.0×10^6 . Many test procedures and data corrections are addressed in this report, but the data presented do not include corrections for wall interference, model support interference, or model aeroelastic effects. Application of corrections for these three effects would not affect the results of this study because the corrections are systematic in nature and are more appropriately classified as sources of bias error. The repeatability of the longitudinal stability-axis force and moment data has been assessed. Coefficients of lift, drag, and pitching moment are shown to repeat well within the pretest goals of ± 0.005 , ± 0.0001 , and ± 0.001 , respectively, at a 95-percent confidence level over both short- and near-term periods.			
14. SUBJECT TERMS National Transonic Facility; Repeatability; Uncertainty; Commercial transports			15. NUMBER OF PAGES 91
			16. PRICE CODE A05
17. SECURITY CLASSIFICATION OF REPORT Unclassified	18. SECURITY CLASSIFICATION OF THIS PAGE Unclassified	19. SECURITY CLASSIFICATION OF ABSTRACT Unclassified	20. LIMITATION OF ABSTRACT